hexagon:2611.01247v1

A thermodynamic promenade through design theory

Fable and Teo

Abstract

The rescaled Hadamard matrices are the orthogonal matrices attaining the bound $||U||_1 \leq N\sqrt{N}$, and the local maximizers of the 1-norm, called almost Hadamard matrices, include matrices coming from block designs, such as the Fano plane and the Paley biplane. We look at such matrices from the point of view of statistical mechanics, where they can be frozen, as couplings of an array of Ising spins, or moving, as a particle on O_N. Besides the plain local maximizers there are twisted ones, coming from the Fano plane, which disprove the conjecture that S^tU, with $S = sgn(U)$, must be positive. The design arrays have crystalline states at any order, such as the hyperovals, the unitals and the Baer subplanes of the projective plane of order 4. On the moving side, we study the energy landscape around the Fano matrix, the known optimum at $N = 7$, we show that the projective plane of order 3 is optimal at $N = 13$, by an analogue of the bound of Barba, and we improve the best known value at $N = 11$. We also discuss the circulant case. In the complex case, we show with computer assistance that there is a circulant matrix of order 16 contradicting the almost Hadamard conjecture.

Contents

Introduction 1
1 Crossed wires, spins and rotators 4
2 Almost Hadamard matrices, local maxima 8
3 Block designs, plain and twisted 12
4 Frozen matrices, Ising spin arrays 19
5 Design arrays and their crystals 24
6 Moving matrices, heating and cooling 29
7 Sign matrices, the optimal crystals 32
8 Conference matrices, the upper bounds 37
9 Circulant matrices, the spin chains 43
10 Complex matrices, the dual model 48
References 56

Introduction

A Hadamard matrix is a square matrix $H \in M_N(\pm 1)$ whose rows are pairwise orthogonal. The matrix $U = H/\sqrt{N}$ is then orthogonal, and as observed in [2], the Cauchy-Schwarz inequality shows that such matrices are precisely the orthogonal matrices attaining the following bound:

$$||U||_1 = \sum_{ij} |U_{ij}| \leq N\sqrt{N}$$

Since such matrices can only exist at $N = 1, 2$ and $N \in 4\mathbb{N}$, this suggests looking at the maximizers of the 1-norm on O_N, and at its local maximizers. The corresponding matrices $H = \sqrt{N}U$ are called almost Hadamard, and their theory was developed in [3], [6], with the

main examples coming from the block designs, such as the Fano plane and the Paley biplane, and from the circulant matrices. See also Mohan [45], [46] for more, including the p-norm versions.

The starting point of this paper is the observation that all this is statistical mechanics in disguise. Indeed, consider the pairing between $U \in O_N$ and the sign matrices $S \in M_N(\pm 1)$:

$$\Phi(U, S) = Tr(S^t U) = \sum_{ij} U_{ij} S_{ij}$$

There are then 3 models around, each with its own heating and cooling:

(1) The matrix U can be frozen, with moving signs $S_{ij} = a_i b_j$. This is an Ising model with $2N$ spins and couplings U_{ij}, studied in [49] in the Hadamard case, and in [16] for planar rotators, as a deterministic model of a glass, in the spirit of Marinari, Parisi and Ritort [41], [42].

(2) The matrix U can move, with the signs following it, $S = sgn(U)$. This is a particle on O_N, with energy $-||U||_1$, the hard matrix model of Dong, Elser, Gyawali, Jee, Kent-Dobias, Mandaiya, Renz and Su [23], studied for $N \in 4\mathbb{N}$, where the crystals are the Hadamard matrices, as a model for the glass transition. See also Cugliandolo, Kurchan, Parisi and Ritort [20].

(3) Finally, the signs can move freely, with the matrix being their polar part, $U = Pol(S)$. This is an Ising model with N^2 spins and with energy $-Tr|S|$, where $|S| = \sqrt{S^t S}$.

Our purpose here is a promenade through these 3 models, with the matrices coming from block designs as a guide. The paper is a sequel to [16], [49], written in the same spirit, and Section 1 contains a brief account of them. Before heating or cooling anything, we must understand the local maximizers. With $S = sgn(U)$, the local maximizers studied in [2], [5], [6] are those where $X = S^t U$ is positive definite, the general criterion being from [4]. We have:

Theorem A. *Let $U \in O_N$ have nonzero entries, set $S = sgn(U)$, and assume that $X = S^t U$ is symmetric, with eigenvalues $\lambda_1 \leq \ldots \leq \lambda_N$.*

1. *U is a local maximizer of the 1-norm on O_N precisely when $\lambda_1 + \lambda_2 \geq 0$, and is a strict local maximizer precisely when $\lambda_1 + \lambda_2 > 0$.*

2. *Besides the plain case $\lambda_1 > 0$, where $U = Pol(S)$, there are neutral maximizers, with $\lambda_1 = 0$, for instance at $N = 5$, and twisted ones, with $\lambda_1 < 0$, for instance at $N = 7$.*

Here (1) is from [4], where $X \geq 0$ was conjectured for the local maximizers, and (2) shows that this is not the case, a reflection not being an infinitesimal move on O_N. The twisted maximizers are obtained from the polar part of S by a reflection, and live on the other component of O_N.

The simplest twisted maximizers come from designs. Let $M \in M_v(0, 1)$ be the incidence matrix of a symmetric (v, k, λ) design, set $n = k - \lambda$, and denote by $\mathbb{I}$ the all-one matrix. By [6] there are orthogonal matrices $U = aM + b\mathbb{I}$, one of them almost Hadamard. We have:

Theorem B. *Consider a symmetric (v, k, λ) design with $\lambda \geq 1$ and $v > 2k$, and set*

$$U_\pm = \frac{1}{\sqrt{n}} \left(M - \frac{k \pm \sqrt{n}}{v} \mathbb{I} \right)$$

1. *$U_\pm$ are orthogonal, with sign matrix $S = 2M - \mathbb{I}$, and with $||U_\pm||_1 = 2(v-1)\sqrt{n} \pm (v - 2k)$.*

2. *U_+ is the polar part of S, and is a plain local maximizer of the 1-norm.*

3. *U_- is a strict local maximizer precisely when $v = 4n - 1$, that is, for the Hadamard designs. In this case U_- is twisted, with $\lambda_1 = -1$.*

As an illustration, the Fano plane produces 2 local maximizers of the 1-norm on O_7, of norms $12\sqrt{2} \pm 1$, and the Paley biplane produces 2 local maximizers on O_{11}, of norms $20\sqrt{3} \pm 1$. The projective plane of order 3 produces only one.

Let us go now for our promenade. We first freeze the matrix U, and we consider the corresponding Ising array, with energy $-\Omega$, where $\Omega =< Ub, a >$, with $a, b \in \{\pm 1\}^N$. The law of Ω with respect to the uniform measure is the glow of U, in the terminology of [49], and the states with $\Omega = N$ are called crystalline. We have here:

Theorem C. *Let $U \in O_N$, and consider the variable $\Omega =< Ub, a >$, with $a, b \in \{\pm 1\}^N$.*

1. *The moments of order 2 and 4 of Ω are N and $3N^2 - 6N + 4||U||_4^4$.*
2. *We have $\Omega \leq N$, with equality precisely when $Ub = a$.*
3. *For the design matrix U_+ the states $a = -b = \pm\xi$, with ξ being the all-one vector, are crystalline, and these are the only crystalline states when n is not a square.*

Thus on the hot side the first invariant which distinguishes the arrays is the 4-norm, which is minimal precisely for the Hadamard matrices, and on the cold side the design arrays have a crystal at any order, with no arithmetic condition needed. When n is a square there are more crystalline states, which correspond to remarkable configurations of points: for the projective plane of order 4 we find the hyperovals, the unitals and the Baer subplanes, and for the projective space over $\mathbb{F}_2$ we find the ovoids, the lines and the pairs of skew lines. In physical terms, a design array has 2 kinds of junctions, ferromagnetic on the blocks and antiferromagnetic outside, and the 2 matrices of the Fano plane give 2 frustrated magnets, an antiferromagnet and a ferromagnet. We also show that for the Hadamard designs the free energy at high temperature is the universal one from [49], which is that of the random orthogonal model [42], and we compute the exact specific heat for the designs with $v \leq 23$, which has sharp maxima, well predicted by the crystallization temperature from [49].

Next, we let the matrix move. The cooling of the hard matrix model, at the orders where there is no Hadamard matrix, leads to the question of finding the optimal almost Hadamard matrices, and here the dual model is the efficient one:

Theorem D. *The following hold, with (2) coming from exhaustive computer searches.*

1. *The maximum of the 1-norm on O_N equals the maximum of $Tr|S|$ over the sign matrices $S \in M_N(\pm 1)$, with the maximizers corresponding to each other, U being a polar part of S, and S being the sign matrix of U.*
2. *This maximum is 11 at $N = 5$, then $8 + 2\sqrt{10}$ at $N = 6$, and $1 + 12\sqrt{2}$ at $N = 7$, where the maximizers are the matrices of the Fano plane.*
3. *For N odd this maximum is at most $(N-1)\sqrt{N-1} + \sqrt{2N-1}$, and for $N = 2(4)$ it is at most $(N-2)\sqrt{N-2} + 2\sqrt{2N-2}$, with equality at $N = 5, 13, 25, 41, 61$ and at $N = 6, 10, 14, 18, 26$. At $N = 13$ the maximizers are the matrices of the projective plane of order 3.*
4. *At $N = 11$ this maximum is at least 35.7006, which is more than the 1-norm $1 + 20\sqrt{3} = 35.6410$ of the matrix of the Paley biplane.*

Here (1) is a standard duality, and the values in (2) are known from the work of Holbrook, Johnston and Schoch [32], who computed them by using Schur norms and semidefinite programming. We recover them by an exhaustive search, which gives as well the numbers of maximizers, the second energy levels, and the whole density of states. The bounds in (3) are the analogues,

for the trace norm, of the bounds of Barba and of Ehlich and Wojtas for the maximal determinant problem of Hadamard [12], and have the same equality cases. They show that the best values known at $N = 10, 13, 14, 18$, from [6], [32], are optimal. In particular the matrix of the projective plane of order 3 is optimal at $N = 13$, and is the unique crystal there, up to the symmetries of the model. We also discuss the circulant matrices, which correspond to spin chains: at $N = 7, 11, 23$ the ground states are the Legendre sequences, but at $N = 15, 19$ the cyclic Hadamard designs are beaten. Finally, the matrix at $N = 11$ was found by a simulated annealing of the model with energy $-Tr|S|$, and improves the value 35.6991 from [32].

Finally, all the above makes sense over the complex numbers, with the signs replaced by planar rotators, $S \in M_N(\mathbb{T})$. The situation here is conjecturally very different: according to the almost Hadamard conjecture from [4], any local maximizer of the 1-norm on U_N must be a rescaled complex Hadamard matrix. See [15] for recent numerical evidence. In statistical mechanical terms, this conjecture says that the complex hard matrix model has no metastable states, and so no glass. We have here the following result:

Theorem E. *Let $L(U) = ||U||_1$ on U_N, and $M(S) = Tr|S|$ on the torus $M_N(\mathbb{T})$.*

1. *If U is a local maximizer of L then its phase matrix S is an invertible local maximizer of M, with $Pol(S) = U$. Conversely, if S is an invertible local maximizer of M, whose polar part U has nonzero entries, then U is a local maximizer of L.*

2. *At a critical point U of L with nonzero entries, such that $S^*U > 0$, the Hessians of L at U and of M at S have the same inertia.*

3. *At a given order N, all the local maximizers of L are rescaled complex Hadamard matrices if and only if all the invertible local maximizers of M, whose polar parts have nonzero entries, are complex Hadamard matrices.*

4. *The almost Hadamard conjecture can be shown, with computer assistance, to fail at $N = 16, 17, 18$, due to the existence of circulant counterexamples.*

The interest in the dual formulation comes from the fact that the unitarity constraint is gone, the variables being now N^2 free angles, and the model being of the same type as the Kuramoto models, where the absence of spurious local maxima is known in a number of situations, see for instance [19], [43]. In the dual picture the difference between the real and the complex case is the difference between Ising spins and planar rotators: the walls where an entry of U vanishes, called rubicons in [23], have codimension 1 in O_N, and codimension 2 in U_N. The design matrices U_+ are saddles on U_N, in agreement with [4]. For the circulant matrices the situation is different: at $N = 16$ there is a circulant matrix which is a local maximizer of the 1-norm on U_N, without being Hadamard, as we prove by a computation in interval arithmetic, and the same happens at $N = 17, 18$. These matrices are not explicit, but are located within 10^{-11} of numerical ones.

The paper is organized as follows. Section 1 is a survey of the models from [16], [49], Section 2 contains the general theory of the local maximizers, and Section 3 deals with the matrices coming from designs. In Sections 4 and 5 we study the Ising arrays, at high and at low temperature, in Sections 6 and 7 the hard matrix model and its dual, in Section 8 the conference matrices and the upper bounds, in Section 9 the circulant matrices, and in Section 10 the complex case. The computations are done by the programs accompanying this paper, which are mentioned at the places where they are used, their outputs being in the corresponding log files, and the program `pictures.py` computes the data for all the figures.

1 Crossed wires, spins and rotators

We first recall the 2 models which are behind the present paper, namely the planar rotators from [16] and the Ising spins from [49], both with couplings given by a Hadamard matrix. This

section is a survey, and can be skipped by the readers who are familiar with these 2 papers. For more on statistical mechanics, and on spin glasses, we refer to [44].

The switching game. Everything starts with a game, invented independently and for fun by Gale and Berlekamp, see [26]. A square board carries a lamp at each intersection of its rows and columns, and every row and every column has a switch, reversing all the lamps on it. Starting from some pattern of lit lamps, the player throws switches, and tries to light as many lamps as possible. With $H_{ij} = \pm 1$ recording the lamps, and with $a_i, b_j = \pm 1$ recording the switches, the number of lit lamps minus the number of dark ones is:

$$\Omega = \sum_{ij} H_{ij} a_i b_j =< Hb, a >$$

Our companion in this paper will be the Fano plane, shown in Figure 1. This is the smallest projective plane, having 7 points and 7 lines, with each line having 3 points, each point being on 3 lines, any 2 points being on exactly one line, and any 2 lines meeting in exactly one point. With the points labeled $0, \ldots, 6$, the lines are the sets $\{i+1, i+2, i+4\}$, modulo 7, and the incidence matrix M, having as entries $M_{ij} = 1$ when the j-th point is on the i-th line, and $M_{ij} = 0$ otherwise, is circulant.

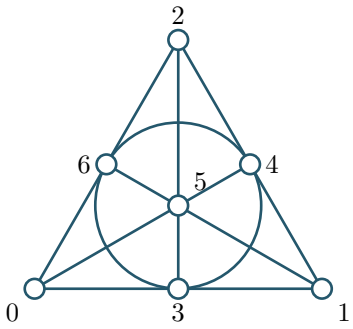

$$M = \begin{pmatrix} 0 & 1 & 1 & 0 & 1 & 0 & 0 \\ 0 & 0 & 1 & 1 & 0 & 1 & 0 \\ 0 & 0 & 0 & 1 & 1 & 0 & 1 \\ 1 & 0 & 0 & 0 & 1 & 1 & 0 \\ 0 & 1 & 0 & 0 & 0 & 1 & 1 \\ 1 & 0 & 1 & 0 & 0 & 0 & 1 \\ 1 & 1 & 0 & 1 & 0 & 0 & 0 \end{pmatrix}$$

Figure 1: The Fano plane, with its points $0, \ldots, 6$ and its 7 lines $\{i+1, i+2, i+4\}$, one of them being drawn as a circle, and its incidence matrix, whose rows correspond to the lines.

Figure 2 shows the board of the Fano plane, with a lamp for each of the 7 points and each of the 7 lines, lit when the point is on the line, that is, at the entries 1 of the above matrix. As computed by the program `pictures.py`, the best that one can do here is 33 lit lamps, out of 49.

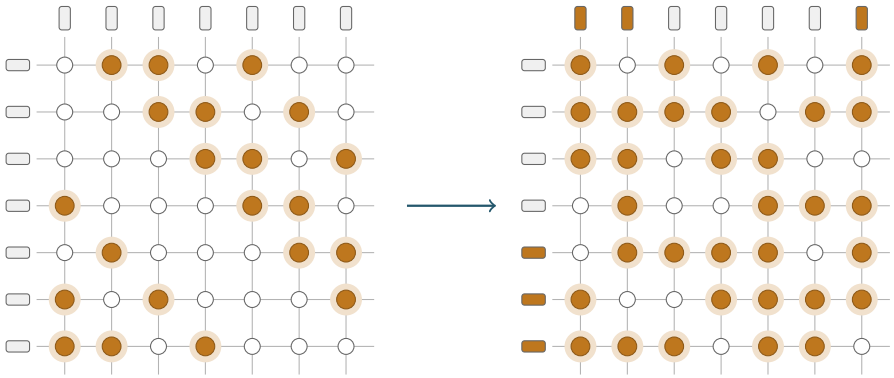

Figure 2: The board of the Fano plane, with 21 lit lamps, one for each point lying on a line, and one of the boards with 33 lit lamps which can be obtained from it, by throwing the switches drawn in gold.

The crossed wires. The physics comes by reading Ω as an energy. Take 2 layers of N parallel wires, the wires of one layer crossing those of the other one at right angles, put a spin a_i on the i-th row wire and a spin b_j on the j-th column wire, and couple the 2 spins at each crossing, with strength $H_{ij}/\sqrt{N}$. The energy of the system is then $E = -\Omega/\sqrt{N}$, the switching game is the search for the ground states, and the law of Ω, with the switches being thrown at random, called glow of H, is the density of states. When H is a Hadamard matrix, the coupling matrix $U = H/\sqrt{N}$ is orthogonal, and the coupling matrix of all the $2N$ spins is symmetric and orthogonal, with eigenvalues ± 1:

$$J = \begin{pmatrix} 0 & U \\ U^t & 0 \end{pmatrix}$$

This is the situation of the random orthogonal model of Marinari, Parisi and Ritort [42], which was introduced as a disordered version of their deterministic models [41], and which has a glass transition, the mean field equations being those of Parisi and Potters [51]. Thus, a Hadamard matrix is a deterministic, and very rigid, instance of a spin glass.

Planar rotators. In the complex case, studied in [16], the matrix $H \in M_N(\mathbb{T})$ is a complex Hadamard matrix, the spins are numbers of modulus 1, called planar rotators, and the energy is $-Re(\Omega)/\sqrt{N}$, with $\Omega =< Hb, a >$. This is the array of superconducting wires coupled by Josephson junctions proposed by Chandra, Ioffe and Sherrington [14], as a model of a glass without disorder, with the phases of the entries H_{ij} recording the magnetic field. The Fourier matrix corresponds to the uniform field, and a general complex Hadamard matrix corresponds to a flux pattern, the Hadamard equivalence being the gauge invariance. The main findings in [16] are that the moments of $|\Omega|^2$ are universal polynomials in N up to the order 3, the first correction, at order 4, being a sum of Wilson loops of charge 2, that the free energy at high temperature is universal, and that the ground states are the bistochastic forms of H, which exist by the theorem of Idel and Wolf [35].

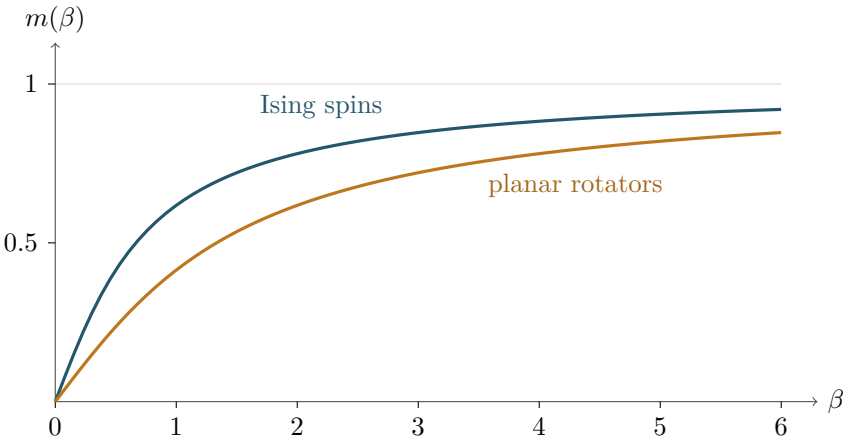

Figure 3: The predicted mean energy of a large Hadamard array, divided by its lower bound, as a function of the inverse temperature: Ising spins in blue, and planar rotators in gold. The 2 curves are the same, up to $\beta \to 2\beta$.

Ising spins. In the real case, studied in [49], the matrix $H \in M_N(\pm 1)$ is a usual Hadamard matrix, and the spins are signs. The moments of Ω are now universal polynomials up to the order 14, the first correction, at order 16, being given by the sums of products of 4 rows of H. The free energy at high temperature is universal too, and is that of the replica symmetric solution of the random orthogonal model [42]. Figure 3 shows the corresponding mean energy, divided by its lower bound, in both the real and the complex case. In the real case the predicted

entropy per row wire is $2\log 2 - \frac{1}{2}\log\frac{1+\sqrt{1+4\beta^2}}{2}$, which vanishes at $\beta = \sqrt{240}$, so this solution, called paramagnetic, must break down at low temperatures, as in the random energy model of Derrida [21]. What happens there depends on the matrix, and the main novelty is indeed at low temperatures, where the states with $\Omega = N\sqrt{N}$, called crystalline, may or may not exist. They exist precisely when H is equivalent to a regular matrix, with all the row and column sums equal to $\sqrt{N}$, so N must be a square, and their number controls the crystallization of the array, in the sense of the position of the specific heat maximum. Without crystalline states, as for 2 of the 5 Hadamard matrices of order 16, the array freezes smoothly, into frustrated ground states.

Beyond the Hadamard matrices. The above picture makes sense for any orthogonal, or unitary, coupling matrix U, the only change being that the junctions are no longer of equal strength. The question is then which matrices to use, and a natural answer is: those which are as close as possible to the Hadamard matrices, in the sense that their 1-norm is maximal, or locally maximal. This leads us into the almost Hadamard matrices, and into a second kind of statistical mechanics, where the matrix itself is the moving object, and where the cooling is the search for such maximizers. Figure 4 shows the 3 models which appear in this way, from the pairing $\Phi(U,S) = Tr(S^tU)$ of the Introduction.

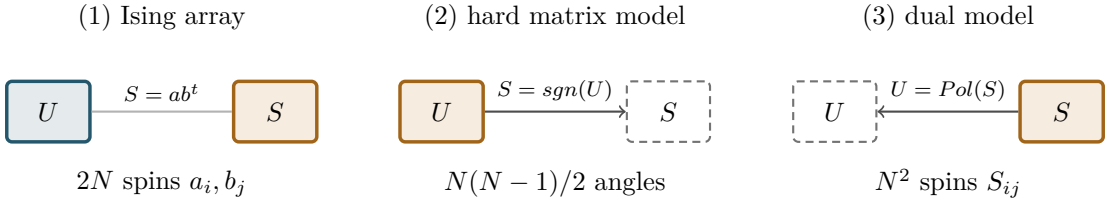

Figure 4: The 3 models coming from the pairing $\Phi(U,S) = Tr(S^tU)$, between orthogonal matrices and sign matrices. In blue the frozen variable, in gold the moving one, and dashed the one which follows. The energy is $-\Phi$, that is, $-<Ub,a>$, $-||U||_1$ and $-Tr|S|$.

In the complex case the same 3 models exist, with the signs replaced by rotators, and the situation is summarized by the following table, the last column being the present paper:

	[16]	[49]	here
spins	planar rotators	Ising spins	Ising spins, and matrices
couplings	complex Hadamard	real Hadamard	orthogonal, from designs
picture	Josephson array	switching game	2 kinds of junctions
hot side	Wilson loops	products of 4 rows	4-norm
cold side	bistochastic forms	regular matrices	aligned states, optima

Let us record now the results from [16], [49] that we will use in what follows. We agree to say that a convergence of functions of β holds coefficientwise when it holds for each coefficient of the Taylor series at $\beta = 0$. The result is as follows:

Theorem 1.1. *Let H be a Hadamard matrix of order N, real or complex, and let $\Omega =< Hb, a >$, with a, b being uniform and independent, signs in the real case, and numbers of modulus 1 in the complex case. Consider the function $\Phi_0(x) = \sqrt{1+4x} - 1 - \log\frac{1+\sqrt{1+4x}}{2}$.*

1. *In the complex case, $\frac{1}{N}\log E(e^{\beta Re(\Omega)/\sqrt{N}}) \to \Phi_0(\beta^2/4)$, coefficientwise, uniformly in H.*
2. *In the real case, $\frac{1}{N}\log E(e^{\beta\Omega/\sqrt{N}}) \to \frac{1}{2}\Phi_0(\beta^2)$, coefficientwise, uniformly in H.*
3. *We have $|\Omega| \leq N\sqrt{N}$, with equality precisely at the bistochastic forms of H, which always exist in the complex case, and which exist in the real case precisely when H is equivalent to a regular Hadamard matrix.*

Proof. The first 2 assertions are from [16], [49], the idea being that the cumulants of Ω are sums over connected graphs, that the Hadamard condition allows one to remove the vertices of degree 2, and that the graphs which reduce completely are counted by comparing with a Haar random matrix. As for (3), this follows from the Cauchy-Schwarz inequality, the existence result in the complex case being the theorem of Idel and Wolf [35]. □

2 Almost Hadamard matrices, local maxima

We are interested in the orthogonal matrices $U \in O_N$, and in their 1-norm, $||U||_1 = \sum_{ij} |U_{ij}|$. The starting point is the following observation, from [2]:

Proposition 2.1. *For $U \in O_N$ we have $||U||_1 \leq N\sqrt{N}$, with equality precisely when the matrix $H = \sqrt{N}U$ is Hadamard.*

Proof. This follows from the Cauchy-Schwarz inequality, $||U||_1 \leq N||U||_2 = N\sqrt{N}$, with the equality case holding when the numbers $|U_{ij}|$ are all equal, so when $H \in M_N(\pm 1)$. □

Since the Hadamard matrices are quite rare, it is natural to relax the maximality condition into a local one. We are led in this way to the following notion, from [6]:

Definition 2.2. *A matrix $H \in M_N(\mathbb{R})$ is called almost Hadamard if $U = H/\sqrt{N}$ is orthogonal, and is a local maximizer of the 1-norm on O_N. When U is a global maximizer, we say that H is optimal.*

It is known from [2], [6] that a local maximizer cannot have zero entries, the proof being by rotating 2 rows, and by looking at the derivatives of the 1-norm at the left and at the right. Thus we can talk about the sign matrix $S = sgn(U)$, which belongs to $M_N(\pm 1)$, and the 1-norm is given around U by a linear formula, as follows:

$$||V||_1 = Tr(S^tV)$$

This formula holds for any matrix V having the same sign matrix as U, so on a neighborhood of U. In order to study the local maximizers, the idea is to use the fact that this neighborhood consists of the matrices Ue^A, with A antisymmetric and small. We have:

Proposition 2.3. *Let $U \in O_N$ have nonzero entries, and set $S = sgn(U)$, $X = S^tU$.*

1. *U is a critical point of the 1-norm on O_N precisely when X is symmetric.*
2. *In this case, for any antisymmetric matrix A, the second derivative at $t = 0$ of the function $||Ue^{tA}||_1$ is $-\sum_{k<l}(\lambda_k + \lambda_l)A_{kl}^2$, where $\lambda_1, \ldots, \lambda_N$ are the eigenvalues of X, and A_{kl} are the entries of A with respect to an orthonormal eigenbasis of X.*

Proof. For t small we have $||Ue^{tA}||_1 = Tr(Xe^{tA})$, with derivatives at $t = 0$ as follows:

$$Tr(XA) \quad , \quad Tr(XA^2)$$

(1) The first derivative vanishes for any antisymmetric A precisely when X is orthogonal to the antisymmetric matrices, with respect to the usual scalar product of matrices, so when X is symmetric.

(2) In an orthonormal eigenbasis of X we have $(A^2)_{kk} = -\sum_l A_{kl}^2$, and so:

$$Tr(XA^2) = -\sum_{kl} \lambda_k A_{kl}^2 = -\sum_{k<l} (\lambda_k + \lambda_l) A_{kl}^2$$

Thus we are led to the conclusions in the statement. □

As a consequence, as observed in [4], in order to have a local maximizer, what is needed is the positivity of the sums $\lambda_k + \lambda_l$ with $k \neq l$, and not the positivity of the eigenvalues themselves. With the eigenvalues in increasing order, $\lambda_1 \leq \ldots \leq \lambda_N$, the condition is $\lambda_1 + \lambda_2 > 0$, and this allows the first eigenvalue to be zero, or even negative. So, let us formulate:

Definition 2.4. *Let $U \in O_N$ have nonzero entries, with $X = S^tU$ symmetric, having eigenvalues $\lambda_1 \leq \ldots \leq \lambda_N$ satisfying $\lambda_1 + \lambda_2 > 0$. We say that U is:*

1. *Plain, if $\lambda_1 > 0$.*
2. *Neutral, if $\lambda_1 = 0$.*
3. *Twisted, if $\lambda_1 < 0$.*

Figure 5 shows the spectrum of X in each of these 3 cases, and in a case where the condition fails, for matrices that we will meet in what follows. In each case the matrix X is symmetric, so U is a critical point of the 1-norm, and what matters is the position of the 2 smallest eigenvalues with respect to 0.

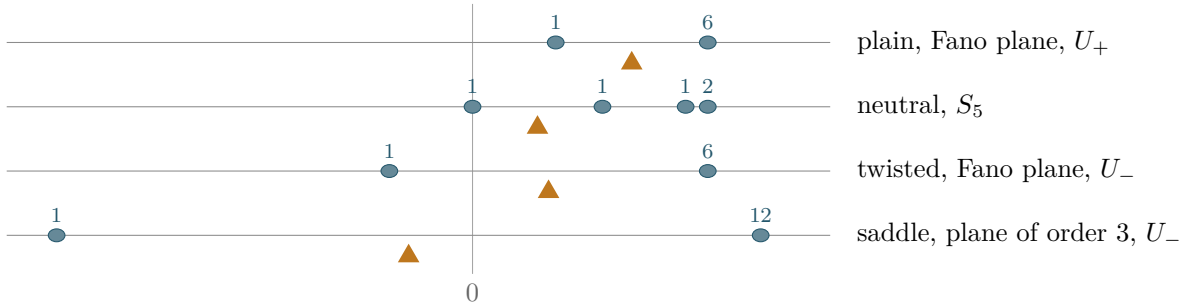

Figure 5: The eigenvalues of $X = S^tU$, with their multiplicities, in 4 situations. The triangle marks the mean of the 2 smallest eigenvalues, and we have a local maximizer when it is on the right of 0.

The plain case is the one studied in [2], [5], [6], where $X > 0$. Since we have $S = UX$, in this case S is invertible, and U is its polar part, $U = Pol(S) = S|S|^{-1}$. In general, the above matrices can be described in terms of S alone. Consider indeed a sign matrix $S \in M_N(\pm 1)$, with singular values $\sigma_1 \geq \ldots \geq \sigma_N \geq 0$, and assume that we have $\sigma_{N-1} > \sigma_N$. Starting from a singular value decomposition $S = WDV^t$, with $D = diag(\sigma_1, \ldots, \sigma_N)$, we can construct 2 orthogonal matrices, as follows:

$$U_\pm = W\, diag(1, \ldots, 1, \pm 1)\, V^t$$

When $\sigma_N > 0$ the matrix U_+ is the polar part of S, and $U_- = U_+(1 - 2\eta\eta^t)$ is obtained from it by a reflection, with η being the last column of V, which is well-defined up to a sign. When $\sigma_N = 0$ the pair $\{U_+, U_-\}$ is well-defined, and consists of the 2 orthogonal matrices which coincide with the partial isometry $S|S|^{-1}$ on the orthogonal complement of η. We have:

Proposition 2.5. *The matrices from Definition 2.4 having a given sign matrix S are as follows:*

1. *In the plain case, the only candidate is $Pol(S)$, with S being invertible.*
2. *In the neutral case we must have $\sigma_{N-1} > \sigma_N = 0$, and the candidates are $U_\pm$.*
3. *In the twisted case we must have $\sigma_{N-1} > \sigma_N > 0$, and the only candidate is U_-.*

In each case, a candidate is indeed such a matrix precisely when its sign matrix is S, and its 1-norm is then $\sigma_1 + \ldots + \sigma_{N-1} \pm \sigma_N$, with the sign being that of λ_1.

Proof. Assume that U is as in Definition 2.4. From $S = UX$ we get $S^tS = X^2$, so the numbers $|\lambda_i|$ are the singular values of S. In the plain case we have $X > 0$, so $X = |S|$ and $U = Pol(S)$. In the other cases $\lambda_1 + \lambda_2 > 0$ gives $\lambda_2 > |\lambda_1|$, so we have $\lambda_i = \sigma_{N+1-i}$ for $i \geq 2$, then $\lambda_1 = -\sigma_N$, and finally $\sigma_{N-1} > \sigma_N$. Thus $X = V\,diag(\sigma_1, \ldots, \sigma_{N-1}, -\sigma_N)V^t$, and by using $S = UX$ we obtain that U maps the columns of V to those of W, up to a sign for the last one, which is -1 when $\sigma_N > 0$. Thus $U = U_-$ in the twisted case, and $U = U_\pm$ in the neutral case. Conversely, if one of the candidates has S as sign matrix, then $X = S^tU$ is symmetric, with eigenvalues $\sigma_1, \ldots, \sigma_{N-1}, \pm\sigma_N$, and we are in the situation of Definition 2.4. Finally, we have $||U||_1 = Tr(S^tU) = Tr(X)$, which gives the last assertion. □

The situation is illustrated in Figure 6. The orthogonal matrices having a given sign matrix S form a region of O_N, which can meet both components, and on which the 1-norm is the linear function $Tr(S^tU)$. The matrices U_+, U_- lie in different components, being exchanged by a reflection, and each of them is a critical point of this function, provided that it belongs to the region.

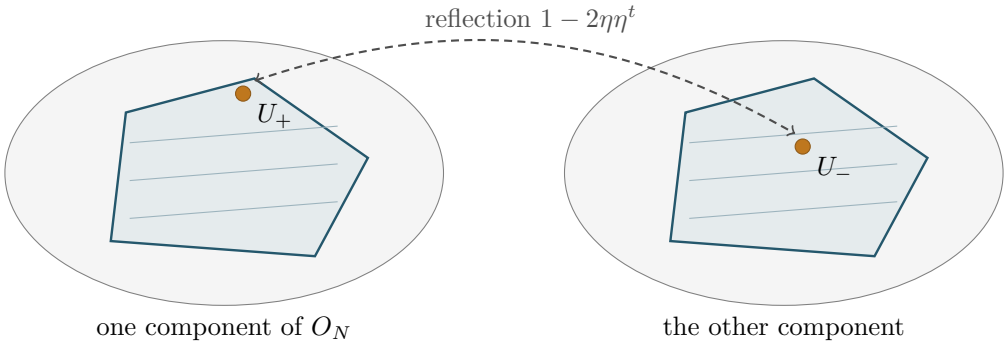

Figure 6: The orthogonal matrices having a given sign matrix S, in blue, in a case where they meet both components of O_N, and contain the matrices $U_\pm$, with the level sets of the 1-norm, and with the 2 critical points $U_\pm$, whose 1-norms are $\sigma_1 + \ldots + \sigma_{N-1} \pm \sigma_N$. The plain maximizer U_+ always wins, but U_- can be a local maximizer too.

The above result makes it possible to search for the local maximizers by computer, by going through the sign matrices. The program `census.py` does this, exhaustively at $N = 3, 4, 5, 6$, with the first row and column of S being normalized to be positive, and on random samples of 2^{22} sign matrices at $N = 7, 8, 9$. The numbers of sign matrices which carry plain, neutral and twisted local maximizers are as follows:

N	sign matrices	plain	neutral	twisted
3	16	6	0	0
4	512	78	0	0
5	65536	7560	1800	0
6	33554432	3407760	415800	0
7	4194304	143157	14255	4913
8	4194304	50773	4023	1923
9	4194304	16939	741	491

Thus, according to this census, which is exhaustive up to $N = 6$, and which relies on floating point computations, with a tolerance of 10^{-9}, the neutral case first appears at $N = 5$, and the twisted case at $N = 7$. As a first example, the following sign matrix has rank 4, and both the corresponding matrices $U_\pm \in O_5$ are neutral local maximizers, as verified by the program

`optimal.py`:

$$S_5 = \begin{pmatrix} + & + & + & + & + \\ + & - & + & - & + \\ + & + & - & + & - \\ + & + & + & - & - \\ + & - & - & - & - \end{pmatrix}$$

The singular values of this matrix are $\sqrt{8}, \sqrt{8}, (\sqrt{17} \pm 1)/2, 0$, so the 1-norm of the matrices $U_\pm$ is $4\sqrt{2} + \sqrt{17} = 9.7799$. This is to be compared with the maximum of the 1-norm on O_5, which is 11, as we will see in Section 7. We will see as well, in Section 3, that the simplest example of a twisted local maximizer comes from the Fano plane. As for the best twisted maximizers found by the above search, these have $||U||_1/N^{3/2} = 0.8774, 0.9085, 0.9091$ at $N = 7, 8, 9$, with the corresponding sign matrices being listed in the log file. At $N = 7$ this is the matrix U_- associated to the following sign matrix, whose smallest singular value is 0.2003:

$$T_7 = \begin{pmatrix} - & + & - & + & + & - & - \\ - & - & - & - & + & + & + \\ - & + & + & - & - & - & + \\ + & + & - & - & - & + & - \\ - & - & - & - & - & + & - \\ - & + & - & + & + & + & + \\ + & - & + & + & - & + & - \end{pmatrix}$$

Let us also mention that at $N = 5, 6$ the neutral matrices come in pairs, U_+ and U_- having both S as sign matrix, while from $N = 7$ on this is not always the case. Summarizing, we have:

Theorem 2.6. *The local maximizers of the 1-norm on O_N are as follows:*

1. *Any local maximizer U has nonzero entries, and the matrix $X = S^tU$ is symmetric.*
2. *Conversely, if U has nonzero entries, with X symmetric, then U is a local maximizer precisely when $\lambda_1 + \lambda_2 \geq 0$, and is a strict local maximizer precisely when $\lambda_1 + \lambda_2 > 0$.*
3. *The plain matrices, the neutral matrices and the twisted matrices are all strict local maximizers, and neutral and twisted matrices exist, at $N = 5$ and $N = 7$ respectively.*

Proof. (1) The first assertion is from [2], [6], and the second one follows from Proposition 2.3.

(2) This is from [4], the idea being as follows. The orthogonal matrices which are close to U are of the form UR with $R \in SO_N$ close to 1, and they have S as sign matrix, so $||UR||_1 = Tr(XR)$. Now R is a product of rotations of angles θ_j in mutually orthogonal planes, with orthonormal bases (u_j, v_j), and since X is symmetric we obtain:

$$Tr(X) - Tr(XR) = \sum_j (1 - \cos\theta_j)\left(< Xu_j, u_j > + < Xv_j, v_j >\right)$$

Each of the quantities on the right is at least $\lambda_1 + \lambda_2$, with equality for the plane of the first 2 eigenvectors of X, and this gives the result. Indeed, when $\lambda_1 + \lambda_2 = 0$ the 1-norm is constant on the rotations of U in this latter plane, and when $\lambda_1 + \lambda_2 < 0$ it increases. See also Bernal and Lawrence [8] for the matrices of maximal trace over the rotations.

(3) The first assertion follows from (2). The neutral case at $N = 5$ is illustrated by the above matrix S_5, and the twisted case at $N = 7$ comes from the above table, or from Theorem 3.4 below. □

As a comment, the Hessian of the 1-norm at a critical point is the quadratic form $A \to Tr(XA^2)$ on the antisymmetric matrices, which can be negative definite without X being positive, and conceptually, the reflection which exchanges the matrices U_+ and U_- is not connected

to the identity. Observe also that in the boundary case $\lambda_1 + \lambda_2 = 0$ we have local maximizers which are not strict, and we will see in Section 3 that this happens for the Menon designs. Finally, it was conjectured in [4] that the conditions in (2) should imply $X \geq 0$, and the twisted matrices show that this is not the case.

3 Block designs, plain and twisted

We discuss now the orthogonal matrices coming from block designs, following [6], with some simplifications, and with a new feature, coming from Theorem 2.6. Let us first recall the basic definitions from design theory. For more on all this, we refer to [18], [56].

Definition 3.1. *A symmetric (v, k, λ) design is a collection of v subsets of a set with v elements, called blocks, each having k elements, such that any 2 distinct blocks have exactly λ elements in common. The incidence matrix $M \in M_v(0, 1)$ is given by $M_{ij} = 1$ when the j-th element belongs to the i-th block, and the number $n = k - \lambda$ is called the order.*

It is well-known that any 2 distinct elements belong then to exactly λ blocks, and that we have $\lambda(v-1) = k(k-1)$. In terms of the incidence matrix, and with $\mathbb{I}$ being the all-one matrix, the axioms and their consequences read:

$$MM^t = M^tM = n + \lambda\mathbb{I} \quad , \quad M\mathbb{I} = \mathbb{I}M = k\mathbb{I}$$

The basic examples are the projective planes of order q, with parameters $(q^2+q+1, q+1, 1)$, the first one being the Fano plane, with parameters $(7, 3, 1)$, and the Hadamard designs, with parameters $(4n-1, 2n-1, n-1)$, which are in correspondence with the Hadamard matrices of order $4n$. The Fano plane is also a Hadamard design, and the next Hadamard design is the Paley biplane, with parameters $(11, 5, 2)$, the name coming from the fact that any 2 points lie on exactly 2 blocks. By replacing the blocks with their complements we obtain a design with parameters $(v, v-k, v-2k+\lambda)$, having the same order, so we can always assume $v > 2k$. Finally, we have the trivial design, with parameters $(v, 1, 0)$ and with $M = 1$. The correspondence with the Hadamard matrices is as follows: if M is the incidence matrix of a Hadamard design, then by adding to the sign matrix $2M - \mathbb{I}$ a first row and a first column of 1 entries we obtain a Hadamard matrix of order $4n$, and conversely. For the Fano plane and for the Paley biplane this gives the following matrices, where $\pm$ stand for ± 1, the first one being equivalent to the Walsh matrix of order 8, and the second one being the Paley matrix of order 12:

$$H_8 = \begin{pmatrix} + & + & + & + & + & + & + & + \\ + & - & + & + & - & + & - & - \\ + & - & - & + & + & - & + & - \\ + & - & - & - & + & + & - & + \\ + & + & - & - & - & + & + & - \\ + & - & + & - & - & - & + & + \\ + & + & - & + & - & - & - & + \\ + & + & + & - & + & - & - & - \end{pmatrix} \qquad H_{12} = \begin{pmatrix} + & + & + & + & + & + & + & + & + & + & + & + \\ + & - & + & - & + & + & + & - & - & - & + & - \\ + & - & - & + & - & + & + & + & - & - & - & + \\ + & + & - & - & + & - & + & + & + & - & - & - \\ + & - & + & - & - & + & - & + & + & + & - & - \\ + & - & - & + & - & - & + & - & + & + & + & - \\ + & - & - & - & + & - & - & + & - & + & + & + \\ + & + & - & - & - & + & - & - & + & - & + & + \\ + & + & + & - & - & - & + & - & - & + & - & + \\ + & + & + & + & - & - & - & + & - & - & + & - \\ + & - & + & + & + & - & - & - & + & - & - & + \\ + & + & - & + & + & + & - & - & - & + & - & - \end{pmatrix}$$

Most of the designs that we will use are cyclic. This means that the points are the elements of $\mathbb{Z}_v$, and that the blocks are the translates $D + i$ of a set $D \subset \mathbb{Z}_v$ having k elements, called difference set, such that any nonzero element of $\mathbb{Z}_v$ can be written in exactly λ ways as a difference of 2 elements of D. For the Fano plane we can take $D = \{1, 2, 4\}$, as in Section 1, and for the Paley designs, where $v = 3(4)$ is prime, D is the set of the nonzero squares modulo v. Figure 7 shows the 8 difference sets that we will use, listed in `designs.py`.

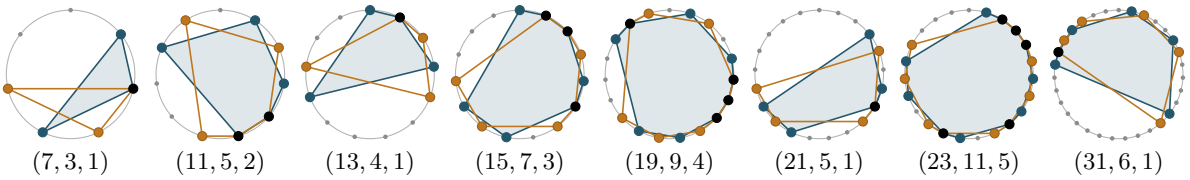

Figure 7: The 8 cyclic designs of this paper, with the points of $\mathbb{Z}_v$ on a circle, the block D in blue, and the block $D+1$ in gold, the λ common points being in black. From left: the Fano plane, the Paley biplane, the projective plane of order 3, the projective space over $\mathbb{F}_2$, a Paley design, the projective plane of order 4, a Paley design, and the projective plane of order 5.

The incidence matrices of the cyclic designs are circulant, each row being obtained from the previous one by a shift, and this makes the axioms easy to read: any 2 rows have exactly λ common entries equal to 1. Figure 8 shows 4 of these matrices.

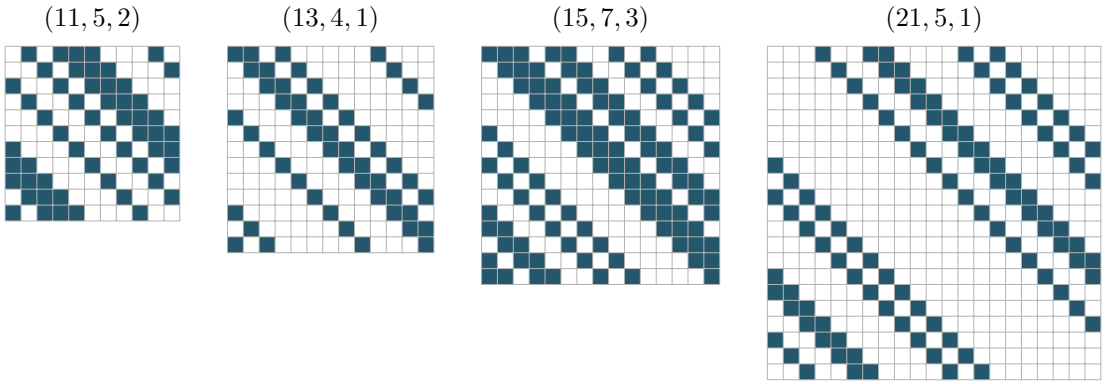

Figure 8: The incidence matrices of the Paley biplane, of the projective plane of order 3, of the projective space over $\mathbb{F}_2$, and of the projective plane of order 4, with the entries 1 in blue. Each row is a block, and any 2 rows have $\lambda = 2, 1, 3, 1$ common entries.

Among these designs, 2 deserve a portrait of their own. The first one is the Paley biplane, shown in Figure 9. The 11 blocks are the pentagons obtained by rotating the pentagon of the squares $\{1, 3, 4, 5, 9\}$, and the axioms can be read on the picture: the points 0 and 1 lie on exactly 2 blocks, and these 2 blocks have no other common point. This is where the name comes from: any 2 points lie on 2 blocks, instead of one, as in a projective plane.

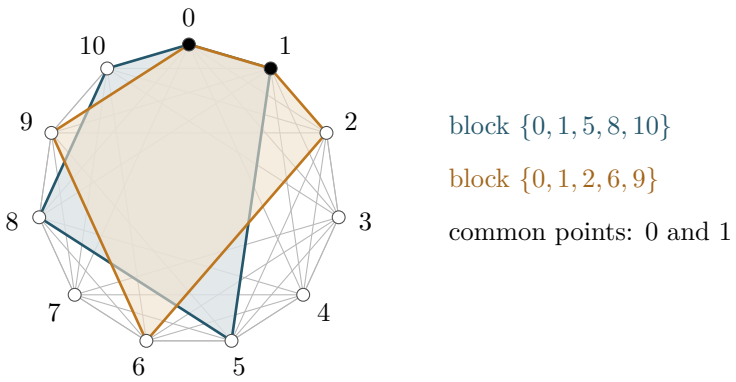

Figure 9: The Paley biplane: the 11 points are the elements of $\mathbb{Z}_{11}$, and the 11 blocks are the pentagons obtained by rotating the pentagon of the squares $\{1, 3, 4, 5, 9\}$. The points 0 and 1 lie on exactly 2 blocks, in blue and in gold, and these 2 blocks have exactly 2 common points.

While there are infinitely many projective planes, only finitely many biplanes are known, the biggest ones having 13 points on each block, and whether there are infinitely many of them is an old open question [18]. The automorphism group of this design has order 660, as computed by the program `portraits.py`, which finds as well 168 automorphisms for the Fano plane, and 5616 automorphisms for the projective plane of order 3.

The second one is the projective plane of order 3, which will play a special role in Section 8, as the unique crystal of the hard matrix model at $N = 13$. In its cyclic form this plane is not easy to see, and Figure 10 shows its affine form: the 9 points of the plane over $\mathbb{F}_3$, the 12 lines, which come in 4 parallel classes, and 4 more points at infinity, one for each class, which form the last line. The program `portraits.py` checks that this is the same design as the cyclic one.

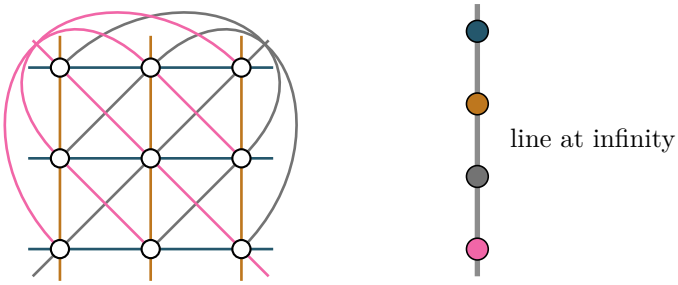

Figure 10: The projective plane of order 3: the 9 points of the affine plane over $\mathbb{F}_3$, with its 12 lines, which form 4 parallel classes, drawn in 4 colors, and 4 points at infinity, one for each class, which form the last line. Each line has 4 points: 3 affine ones, and the point at infinity of its class.

Let us go back now to the general theory. The parameters of a symmetric design are not arbitrary, and the inequality below, which compares v with $4n$, will decide which of the matrices coming from the design are local maximizers of the 1-norm. We will need:

Proposition 3.2. *For a symmetric (v, k, λ) design with $v > 2k$ we have*

$$(v - 2k)^2 = v^2 - 4n(v - 1)$$

and so $v \geq 4n - 1$. Moreover, the following hold:

1. *$v - 2k = 1$ happens precisely when $v = 4n - 1$, that is, for the Hadamard designs.*
2. *$v - 2k < 2\sqrt{n}$ happens precisely when $v = 4n - 1$ too.*
3. *$v - 2k = 2\sqrt{n}$ happens precisely when $v = 4n$.*

Proof. With $\lambda = k - n$ the formula $\lambda(v - 1) = k(k - 1)$ reads $k(v - k) = n(v - 1)$, and this gives the formula in the statement. Now since $v - 2k \geq 1$ we obtain $(v - 2n)^2 \geq (2n - 1)^2$, and so $v \geq 4n - 1$, because $v > 2k \geq 2n$, with equality precisely when $v - 2k = 1$. In this case we have $k = 2n - 1$ and $\lambda = n - 1$, which proves (1). As for (2,3), these follow from the fact that $v - 2k < 2\sqrt{n}$ is equivalent to $v^2 - 4nv < 0$, so to $v < 4n$, and similarly for the equality. □

In relation now with the orthogonal matrices, the idea, from [6], is to look for such matrices in the linear span of M and $\mathbb{I}$. This leads to a quadratic equation, which has 2 solutions, and up to a sign, we obtain in this way the following 2 matrices:

$$U_\pm = \frac{1}{\sqrt{n}}\left(M - \frac{k \pm \sqrt{n}}{v}\,\mathbb{I}\right)$$

To be more precise, we have the following result, where $P = \mathbb{I}/v$ is the projection onto the all-one vector ξ, and where the last assertion makes the link with the notations from Section 2:

Proposition 3.3. *For a symmetric (v, k, λ) design with $\lambda \geq 1$ and $v > 2k$, the above matrices $U_\pm$ are orthogonal, with $U_\pm\xi = \mp\xi$, their entries are positive on the blocks, and negative outside the blocks, and with $S = 2M - \mathbb{I}$ we have the formula*

$$S^tU_\pm = 2\sqrt{n}\,(1 - P) \pm (v - 2k)P$$

so the singular values of S are $2\sqrt{n}$, with multiplicity $v - 1$, and $v - 2k$. In particular U_+ is the polar part of S, and $U_- = U_+(1 - 2P)$ is its twisted version.

Proof. With $c = (k \pm \sqrt{n})/v$ we have $c^2v - 2ck + \lambda = 0$, because $k^2 - \lambda v = n$, and so:

$$(M - c\mathbb{I})(M - c\mathbb{I})^t = n + (\lambda - 2ck + c^2v)\mathbb{I} = n$$

Thus $U_\pm$ are orthogonal, and the formula $U_\pm\xi = \mp\xi$ is clear. The entries are $(1 - c)/\sqrt{n}$ on the blocks, and $-c/\sqrt{n}$ outside, and we have $0 < c < 1$, because $\sqrt{n} < k$ and $k + \sqrt{n} < 2k < v$. Thus the sign matrix is $S = 2M - \mathbb{I}$. Finally, we have:

$$\sqrt{n}\,S^tU_\pm = (2M^t - \mathbb{I})(M - c\mathbb{I}) = 2n + (2\lambda - k + c(v - 2k))\mathbb{I}$$

On the orthogonal complement of ξ this operator is $2n$, and on ξ its eigenvalue is $2n + 2\lambda v - kv + (k \pm \sqrt{n})(v - 2k) = \pm\sqrt{n}(v - 2k)$, by using $\lambda(v - 1) = k(k - 1)$. This gives the result. □

As an illustration, for the Fano plane the entries of U_+ are $(4 - \sqrt{2})/(7\sqrt{2})$ on the lines and $-(3 + \sqrt{2})/(7\sqrt{2})$ outside the lines, and we recover the matrix from [6]. As for U_-, the entries here are $(4 + \sqrt{2})/(7\sqrt{2})$ and $-(3 - \sqrt{2})/(7\sqrt{2})$. For the trivial design the above formulae still make sense, with $U_+ = 1 - 2P$ being, up to a sign, the basic almost Hadamard matrix $K_N/\sqrt{N}$ from [6], and with $U_- = 1$ having zero entries. In matrix form, the 2 matrices of the Fano plane are as follows, with $x = 4 \mp \sqrt{2}$ and $y = 3 \pm \sqrt{2}$, the matrix U_+ being the one from [6], and the matrix on the right being the matrix $U_+ = 1 - 2P$ of the trivial design, at $v = 5$:

$$U_\pm = \frac{1}{7\sqrt{2}}\begin{pmatrix} -y & x & x & -y & x & -y & -y\\ -y & -y & x & x & -y & x & -y\\ -y & -y & -y & x & x & -y & x\\ x & -y & -y & -y & x & x & -y\\ -y & x & -y & -y & -y & x & x\\ x & -y & x & -y & -y & -y & x\\ x & x & -y & x & -y & -y & -y \end{pmatrix} \qquad 1 - 2P = \frac{1}{5}\begin{pmatrix} 3 & -2 & -2 & -2 & -2\\ -2 & 3 & -2 & -2 & -2\\ -2 & -2 & 3 & -2 & -2\\ -2 & -2 & -2 & 3 & -2\\ -2 & -2 & -2 & -2 & 3 \end{pmatrix}$$

The program `designs.py` constructs the matrices $U_\pm$ for 8 designs coming from cyclic difference sets, and verifies all the above, as well as the local maximality, by using random rotations, and the softest rotation, in the plane of the first 2 eigenvectors of S^tU. The results are as follows, with the 1-norms being divided by $v^{3/2}$:

design	n	$\|\|U_+\|\|_1$	$\|\|U_-\|\|_1$	$\|\|U_+\|\|_4^4$	U_-
$(7, 3, 1)$	2	0.9703	0.8623	1.2047	local maximizer
$(11, 5, 2)$	3	0.9769	0.9221	1.1673	local maximizer
$(13, 4, 1)$	3	0.9935	0.7802	1.0558	saddle
$(15, 7, 3)$	4	0.9812	0.9467	1.1400	local maximizer
$(19, 9, 4)$	5	0.9841	0.9599	1.1202	local maximizer
$(21, 5, 1)$	4	0.9456	0.7170	1.5556	saddle
$(23, 11, 5)$	6	0.9862	0.9680	1.1054	local maximizer
$(31, 6, 1)$	5	0.8874	0.6672	2.3178	saddle

Figure 11 shows the matrices $U_\pm$ of the Fano plane and of the Paley biplane, drawn by `pictures.py`. For the Paley biplane the entries are, in absolute value, $0.224, 0.353$ for U_+, and $0.406, 0.172$ for U_-.

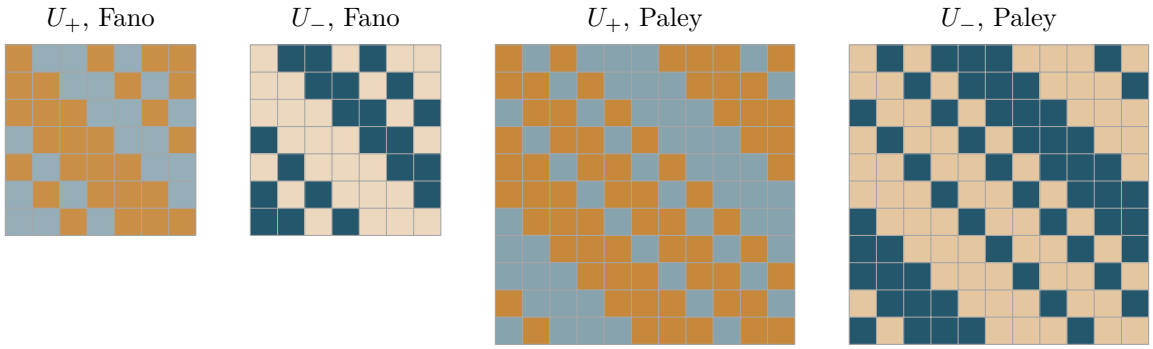

Figure 11: The matrices U_+ and U_- of the Fano plane and of the Paley biplane, with the positive entries in blue, on the blocks, the negative entries in gold, and the color being proportional to the absolute value. For the Fano plane the entries are, in absolute value, $0.261, 0.446$ for U_+, and $0.547, 0.160$ for U_-.

The 1-norms from the above table are shown in Figure 12. We can see that the matrices U_+ are all far above the average over the orthogonal group, the best one being that of the projective plane of order 3, while the matrices U_- are above this average only for the Hadamard designs.

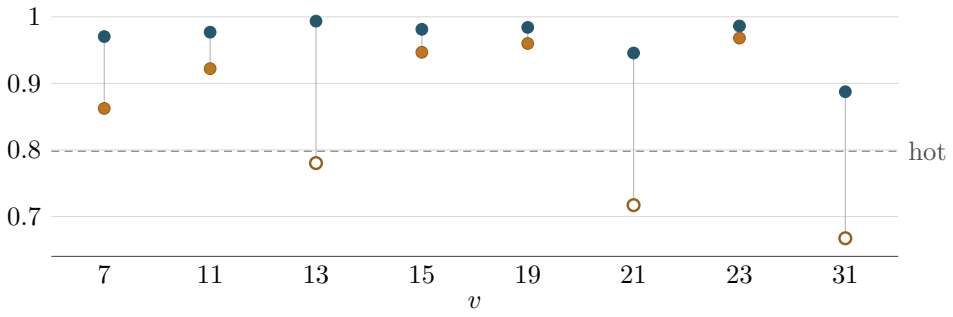

Figure 12: The values of $||U_\pm||_1/v^{3/2}$ for the 8 designs of the table: U_+ in blue, and U_- in gold, filled when it is a local maximizer, which happens for the Hadamard designs, and hollow when it is a saddle. The dashed line is the average $\sqrt{2/\pi}$ over the orthogonal group, at $v \to \infty$.

Here the designs with $\lambda = 1$ are the projective planes of order $3, 4, 5$, and the other ones are Hadamard designs, with $(15, 7, 3)$ coming from the points and planes of the projective space over $\mathbb{F}_2$, and with the last 2 ones being of Paley type. We have included the 4-norms, to be used in Section 4. The above table is explained by the following result:

Theorem 3.4. *Consider a symmetric (v, k, λ) design with $\lambda \geq 1$ and $v > 2k$.*

1. *U_+ is a plain local maximizer of the 1-norm on O_v, and $||U_+||_1 = 2(v-1)\sqrt{n} + v - 2k$.*
2. *When $v = 4n - 1$ the matrix U_- is a twisted local maximizer, with $\lambda_1 = -1$, and with $||U_-||_1 = 4(2n-1)\sqrt{n} - 1$.*
3. *When $v = 4n$ the matrix $\sqrt{v}\, U_+$ is Hadamard, and U_- is a non-strict local maximizer.*
4. *When $v > 4n$ the matrix U_- is not a local maximizer.*

Proof. We use Proposition 3.3, which gives the eigenvalues of $X = S^tU_\pm$, namely $2\sqrt{n}$ with multiplicity $v-1$, and $\pm(v-2k)$, and so the 1-norms, $||U_\pm||_1 = Tr(X)$.

(1) This is clear, because for U_+ we have $X > 0$. This result is from [6].

(2,4) For U_- we have $\lambda_1 = -(v-2k)$ and $\lambda_2 = 2\sqrt{n}$, and the results follow from Theorem 2.6 and from Proposition 3.2, which tells us that $\lambda_1 + \lambda_2 > 0$ happens precisely when $v = 4n-1$, with $v - 2k = 1$ in this case, and that $\lambda_1 + \lambda_2 < 0$ happens when $v > 4n$.

(3) Here $n = m^2$ is a square, by Proposition 3.2, with $v - 2k = 2m$, so $k = 2m^2 - m$, and the entries of U_+ are $\pm 1/(2m)$. These are the Menon designs, see [18]. The simplest example is the design with parameters $(16, 6, 2)$ whose points are the 16 cells of a 4×4 board, the block associated to a cell being formed by the 6 other cells lying on the same row or on the same column. Any 2 such blocks have 2 common cells, and the corresponding Hadamard matrix $2M - \mathbb{I}$ is regular, with all the row and column sums equal to -4. As for U_-, here $\lambda_1 + \lambda_2 = 2\sqrt{n} - (v-2k) = 0$, and Theorem 2.6 applies. □

In other words, the case $v = 4n$ is the one where our construction produces the crystals themselves, namely the regular Hadamard matrices, which were the main characters of [49]. The Menon design on the board, and its Hadamard matrix, are shown in Figure 13.

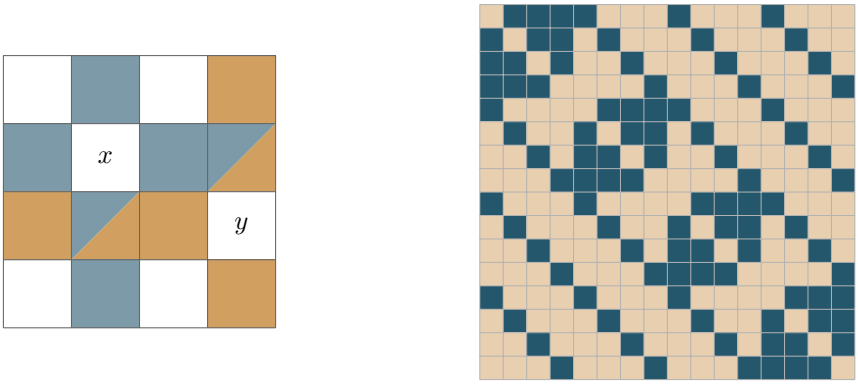

Figure 13: The Menon design on the 4×4 board, also known as the Kummer configuration: the blocks of the cells x and y, in blue and in gold, have 2 common cells. On the right, the corresponding Hadamard matrix of order 16, with the entries 1 in blue, and the entries -1 in light gold.

The above design on the board is a famous object: this is the Kummer configuration, formed by the 16 nodes of a Kummer quartic surface and by the 16 planes which touch this surface along conics, each plane containing 6 nodes, and any 2 nodes lying on exactly 2 planes [33]. There is some physics here, because the wave surface of Fresnel, which describes the propagation of light in a biaxial crystal, is a Kummer surface. It has 4 real nodes, found by Hamilton, where the 2 sheets of the surface meet, and which are responsible for the conical refraction, and 12 complex ones, see [22]. Figure 14 shows a principal section of the wave surface, together with a second portrait of our design: in the Clebsch graph, which has 16 vertices, each of them having 5 neighbors, the blocks are the vertices taken with their neighbors, and `portraits.py` checks that the design obtained in this way is isomorphic to the one on the board.

The Clebsch graph is an instance of a general construction, which is worth recording. Recall that a graph with v vertices is called strongly regular, with parameters (v, k, λ, μ), when each vertex has k neighbors, 2 adjacent vertices have λ common neighbors, and 2 distinct non-adjacent vertices have μ common neighbors. Basic examples include the pentagon, the Petersen graph, the Clebsch graph, with parameters $(16, 5, 0, 2)$, and the Paley graphs, with parameters $(q, (q-1)/2, (q-5)/4, (q-1)/4)$, that we will meet in Section 8.

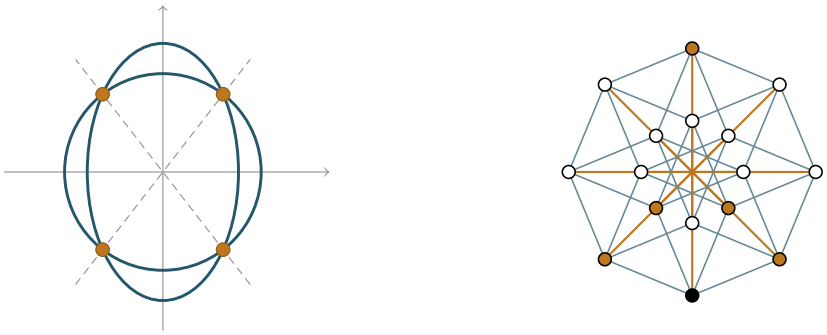

wave surface, with its 4 real nodes

Clebsch graph, with a block

Figure 14: On the left, the section of the wave surface of Fresnel by a principal plane, which is the union of a circle and of an ellipse, meeting at 4 of the 16 nodes of the surface. On the right, the Clebsch graph, drawn on the 16 vertices of a hypercube, with the edges of the hypercube in blue and its 8 diagonals in gold: a vertex, in black, and its 5 neighbors, in gold, form a block of the Kummer configuration.

In terms of the adjacency matrix A, the strong regularity condition reads $A^2 = k + \lambda A + \mu(\mathbb{I} - 1 - A)$, and for certain values of $\lambda - \mu$ such graphs produce designs, as follows:

Proposition 3.5. *Let A be the adjacency matrix of a strongly regular graph, with parameters (v, k, λ, μ).*

1. *When $\lambda = \mu$, the neighborhoods of the vertices form a symmetric (v, k, λ) design, with $M = A$.*

2. *When $\lambda = \mu - 2$, the vertices taken with their neighbors form a symmetric $(v, k + 1, \mu)$ design, with incidence matrix $M = A + 1$.*

In both cases M is symmetric, and so are the corresponding matrices $U_\pm$.

Proof. When $\lambda = \mu$ the above formula gives $A^2 = k - \lambda + \lambda\mathbb{I}$, and when $\lambda = \mu - 2$ this gives $(A + 1)^2 = k + 1 - \mu + \mu\mathbb{I}$, as desired. □

On 16 vertices we have the following examples, verified by `detours.py`. First we have the graph of the moves of a rook on the 4×4 board, with parameters $(16, 6, 2, 2)$, whose design is by definition the one on the board. Then we have the Shrikhande graph, which has the same parameters. Finally, we have the Clebsch graph, with parameters $(16, 5, 0, 2)$, to which (2) applies, and whose complement, with parameters $(16, 10, 6, 6)$, produces the complementary design. The 3 designs with $k = 6$ are isomorphic, and the symmetric matrix $2M - \mathbb{I}$ coming from the rook graph is a Hadamard matrix with -1 on the diagonal, equivalent to the Walsh matrix of order 16, its rows forming a group under the entrywise product, after normalization.

As a first comment, for the Hadamard designs both the quantities $||U_\pm||_1/v^{3/2}$ converge to 1 with $n \to \infty$. For the projective planes we have $||U_+||_1 = q^2 - q - 1 + 2q(q + 1)\sqrt{q}$, as in [6], and so $||U_+||_1/v^{3/2} \simeq 2/\sqrt{q}$, the best plane being the one of order 3. Observe also that the matrix U_- of the Fano plane provides us with an explicit counterexample to the necessity of the condition $X > 0$, which can be verified by hand: we have here $X = 2\sqrt{2}(1 - P) - P$, and for any antisymmetric matrix A we have $Tr(XA^2) = -2\sqrt{2}\,||A||_2^2 + (2\sqrt{2} + 1)||A\xi||^2/7$, which is negative for $A \neq 0$, because $||A||_2^2 \geq 2||A\xi||^2/7$. Figure 15, computed by `pictures.py`, shows what happens along the softest rotation, in the plane of the 2 eigenvectors of X having the smallest eigenvalues, where the second derivative of the 1-norm is $-(\lambda_1 + \lambda_2)$, by Proposition 2.3. For the matrices U_- we have $\lambda_1 = -(v - 2k)$, with eigenvector ξ, and the other eigenvalues are all equal to $2\sqrt{n}$, so any rotation mixing ξ with a vector orthogonal to it is a softest one,

and $\lambda_1 + \lambda_2 = 2\sqrt{n} - (v - 2k)$ equals $2\sqrt{2} - 1$, $2\sqrt{3} - 1$ and $2\sqrt{3} - 5$ for the 3 designs in the figure.

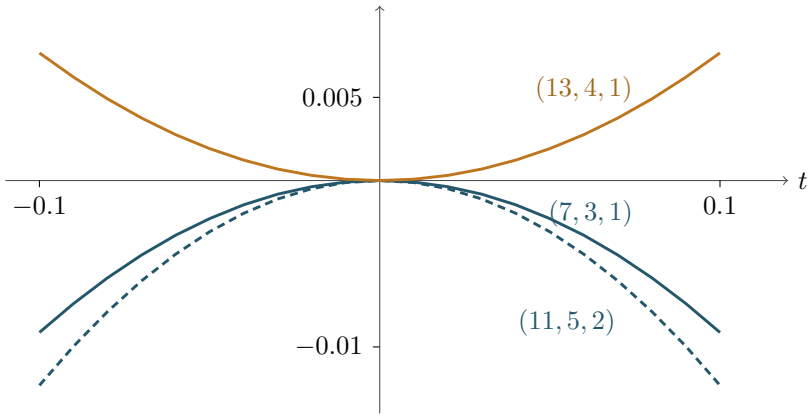

Figure 15: The variation of the 1-norm of $U_- e^{tA}$, with A being the generator of the softest rotation: the twisted matrices of the Fano plane and of the Paley biplane are local maximizers, while the one of the projective plane of order 3 is a saddle.

Observe also that, unlike the plain maximizers, the twisted ones are not stable under tensor products. For the plain ones the stability is known from [6], the matrix X of a tensor product being the tensor product of the matrices X of the factors. But for the matrix U_- of the Fano plane, tensored with the rescaled Hadamard matrix of order 2, we obtain in this way $X = (2\sqrt{2}(1 - P) - P) \otimes \sqrt{2}$, whose smallest eigenvalue $-\sqrt{2}$ has multiplicity 2. Thus this orthogonal matrix of order 14 is a critical point of the 1-norm, which is not a local maximizer, as verified by `detours.py`.

4 Frozen matrices, Ising spin arrays

We discuss now the first model from the Introduction, where the orthogonal matrix is frozen, and plays the role of a coupling matrix. The definition is as follows, in analogy with [49], where the matrix was a rescaled Hadamard one:

Definition 4.1. *The Ising array of a matrix $U \in O_N$ is the system having $2N$ spins, $a_1, \ldots, a_N$ and $b_1, \ldots, b_N$, each of them being ± 1, with energy $-\Omega$, where:*

$$\Omega(a, b) = < Ub, a > = \sum_{ij} U_{ij} a_i b_j$$

The law of Ω, with a, b being uniform and independent, is called the glow of U.

In the picture of [49] the spins a_i live on N row wires and the spins b_j on N column wires, and they interact at the crossings, with couplings U_{ij}. In terms of the pairing from the Introduction we have $\Omega = \Phi(U, S)$, where $S = (a_i b_j)$ is a sign matrix of rank 1.

When U is not a rescaled Hadamard matrix, the junctions at the crossings are no longer of equal strength. For the design matrices $U_\pm$ there are 2 kinds of junctions: ferromagnetic ones, having positive couplings, at the crossings ij with the j-th point lying on the i-th block, and antiferromagnetic ones, having negative couplings, at the other crossings. Figure 16 shows the Fano array. For U_+ there are 21 ferromagnetic junctions of strength 0.261 and 28 antiferromagnetic junctions of strength 0.446, so the array is mainly an antiferromagnet. For U_- the strengths are 0.547 and 0.160, and the array is mainly a ferromagnet. Both magnets are frustrated: as we will see in Section 5, in the ground states the 2 layers are aligned, against each

other for U_+ and with each other for U_-, and this satisfies all the junctions of the dominant kind, and violates all the other ones. In the language of the Josephson arrays from [14], [16], such a system would be an array having both usual junctions and π-junctions.

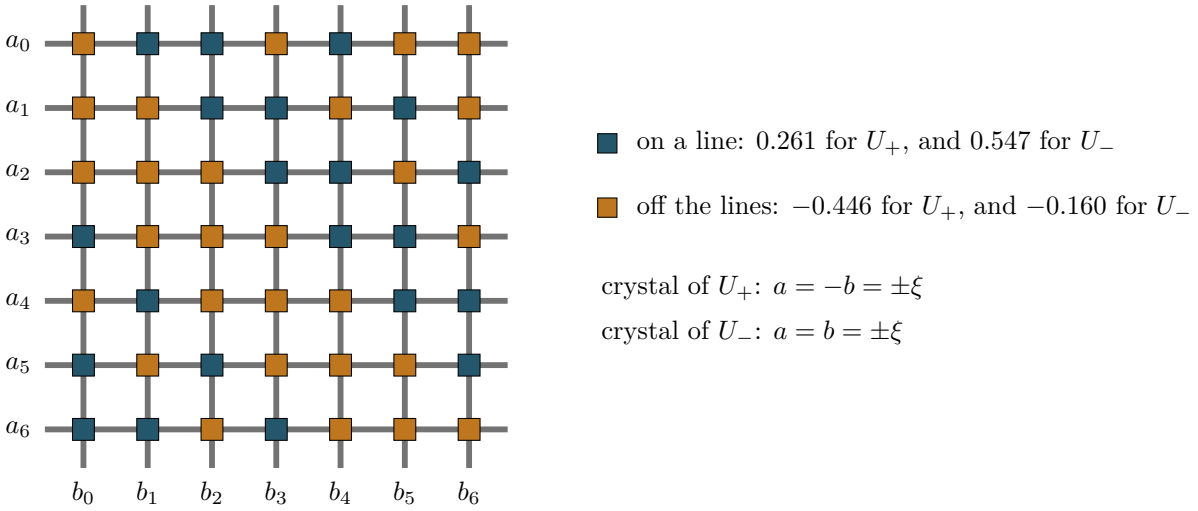

Figure 16: The Fano array: 7 row wires, one for each line, and 7 column wires, one for each point, with a ferromagnetic junction when the point is on the line, in blue, and an antiferromagnetic one otherwise, in gold. The same wiring carries 2 magnets, with the strengths of U_+ or of U_-.

The wiring of the ferromagnetic junctions of the Fano array is a famous graph too. This is the Heawood graph, which has 14 vertices, namely the 7 points and the 7 lines, and 21 edges, one for each point lying on a line, and which contains no cycle of length less than 6. Heawood found it while studying the coloring of maps [30]: the graph can be drawn on a torus, where it bounds 7 hexagonal countries, each of them touching the 6 other ones, so that 7 colors can be needed for coloring a map on a torus. Figure 17 shows both pictures, the checks being done by `portraits.py`. As for the antiferromagnetic junctions, these form the complementary wiring, each point being connected to the 4 lines which do not contain it.

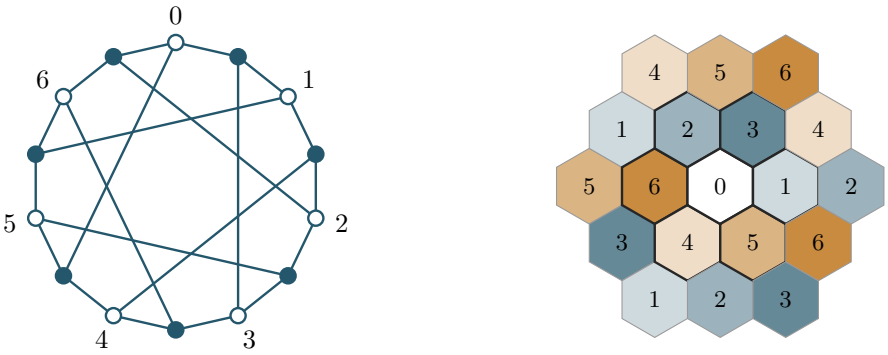

Figure 17: The Heawood graph, in 2 ways. On the left, as the wiring of the ferromagnetic junctions of the Fano array, with the 7 points in white, and the 7 lines in blue. On the right, drawn on a torus, the picture being periodic: the 14 vertices are the corners of 7 hexagonal countries, numbered $0, \ldots, 6$, each of which touches the 6 other ones.

The Heawood graph is the case of the Fano plane of a general construction. Any symmetric design has a wiring graph, having as vertices the v points and the v blocks, with a point being joined to a block when it lies on it, and with vk edges, which are the ferromagnetic junctions of the array. In terms of this graph, the design array becomes a familiar system:

Proposition 4.2. *For a symmetric (v, k, λ) design, with wiring graph X, the following hold:*

1. *The eigenvalues of X are $\pm k$, and $\pm\sqrt{n}$, with multiplicity $v-1$ each.*
2. *The quantity $\sqrt{n}\,\Omega(a,b)$, for the array of $U_\pm$, is the sum of the products $a_i b_j$ over the edges of X, minus $c_\pm(\sum_i a_i)(\sum_j b_j)$, where $c_\pm = (k \pm \sqrt{n})/v$.*

Proof. The adjacency matrix of X has M, M^t as off-diagonal blocks, and 0 on the diagonal blocks, so its square has diagonal blocks $MM^t = M^tM = n + \lambda\mathbb{I}$, with eigenvalues k^2, and n with multiplicity $v-1$. Since the spectrum of a bipartite graph is symmetric, this gives (1). As for (2), this is clear from the formula $U_\pm = (M - c_\pm\mathbb{I})/\sqrt{n}$. □

In other words, the design array is an Ising ferromagnet on the wiring graph, with coupling $1/\sqrt{n}$, together with a mean field interaction between the total magnetizations of the 2 layers, which is antiferromagnetic, of strength $c_\pm/\sqrt{n}$. For the Fano plane we obtain the Ising model on the Heawood graph, with the mean field having strength 0.446 for U_+, and 0.160 for U_-. When all the spins are aligned the graph contributes with $vk/\sqrt{n}$ to Ω, and the mean field with $-(k \pm \sqrt{n})v/\sqrt{n}$, the total being $\mp v$. Thus for U_- the ferromagnet wins, for U_+ the mean field wins, and we recover the 2 crystals from Figure 16. Observe also that $\sqrt{n}$ is the smallest possible value for the second eigenvalue of a bipartite k-regular graph with $2v$ vertices, as one can see by computing the trace of MM^t, so the wiring graphs of the designs are optimal expanders, and in particular Ramanujan graphs. As for the girth, this is 6 for the projective planes, as for the Heawood graph, and 4 for the other designs.

The Hadamard designs have a second physical life, in astronomy. An X-ray telescope cannot use lenses, and uses instead a mask with open and closed cells, placed in front of the detector, the image of the sky being reconstructed by correlating the shadow of the mask with the mask itself. For this to work the periodic autocorrelation of the mask must be flat, and this is precisely the axiom of a design: any 2 distinct translates of the set of open cells must have the same number of common cells. The uniformly redundant arrays of Fenimore and Cannon [25] are of this type, and are built from the squares modulo 2 primes r, s with $r - s = 2$, in the spirit of the Paley construction. The cell (i, j), with i taken modulo r and j taken modulo s, is closed when $i = 0$, open when $j = 0$ and $i \neq 0$, and is otherwise open precisely when i, j are both squares, or both nonsquares. Figure 18 shows the mask with $r = 13$, $s = 11$.

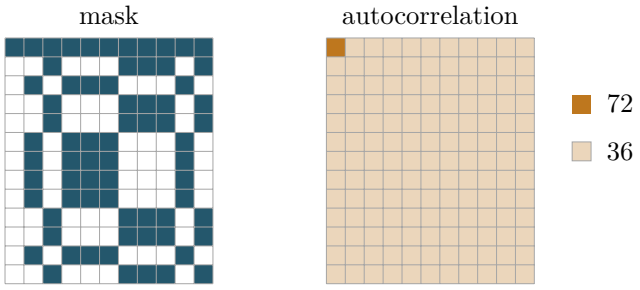

Figure 18: A coded aperture mask of size 13×11, with the closed cells in blue, and its periodic autocorrelation, that is, the number of open cells that the mask has in common with each of its translates: this is 72 for the mask itself, and 36 for all the other translates.

As computed by `portraits.py`, this mask has 72 open cells out of 143, any 2 distinct translates of it have 36 common open cells, and the closed cells form a Hadamard design, with parameters $(143, 71, 35)$. Thus Theorem 3.4 applies, and the mask produces 2 almost Hadamard matrices of order 143, a plain one and a twisted one, the values of $||U_\pm||_1/v^{3/2}$ being 0.9971 and 0.9959.

There is more to be said here, about the decoding. With $M' = \mathbb{I} - M$ being the incidence matrix of the open cells, a sky x casts on the detector the shadow $y = M'x$, and the problem is that of recovering x from y, without amplifying the noise. The answer is given by the sign matrix:

Proposition 4.3. *For a Hadamard design, with $M' = \mathbb{I} - M$ and $S = 2M - \mathbb{I}$, the following hold:*

1. *$M'S^t = -2n$, so the inverse of M' is the matrix $-S^t/(2n)$.*
2. *$S = 2\sqrt{n}\,U_+ + (2\sqrt{n} - 1)P$, where $P = \mathbb{I}/v$ is the projection onto the all-one vector.*

Proof. (1) By using $MM^t = n + \lambda\mathbb{I}$ and $M\mathbb{I} = \mathbb{I}M = k\mathbb{I}$ we obtain $M'S^t = (3k - v - 2\lambda)\mathbb{I} - 2n$, and the coefficient of $\mathbb{I}$ vanishes when $v = 4n - 1$, $k = 2n - 1$, $\lambda = n - 1$.

(2) This follows from Proposition 3.3, which gives $S = U_+(2\sqrt{n}(1 - P) + P)$ in the present case, where $v - 2k = 1$, together with $U_+P = -P$. □

Thus the sky is recovered by correlating the picture with the mask itself, with the open cells counted positively, and the closed ones negatively, which is the balanced decoding from [25]. Up to the term involving P, which only shifts the background, the decoder is the transpose of the almost Hadamard matrix U_+, rescaled by $-1/\sqrt{n}$. This matrix being orthogonal, the noise is not amplified, and this is why such masks are used. For the mask in Figure 18 all this is verified by `detours.py`, the singular values of S being 12, with multiplicity 142, and 1.

With this picture in mind, let us go back to an arbitrary orthogonal matrix $U \in O_N$. At high temperature the partition function $E(e^{\beta\Omega})$ is controlled by the first moments of the glow, exactly as in the Hadamard case, and these moments can be computed as follows:

Proposition 4.4. *The glow of an orthogonal matrix $U \in O_N$ is symmetric, its moment of order 2 is N, and its moment of order 4 is $3N^2 - 6N + 4||U||_4^4$, where $||U||_4^4 = \sum_{ij} U_{ij}^4$.*

Proof. The symmetry comes from $\Omega(-a, b) = -\Omega(a, b)$. For the moments we use the following formulae, valid for any vector $x \in \mathbb{R}^N$, with the averages being taken over $a \in \{\pm 1\}^N$:

$$E(< x, a >^2) = \sum_i x_i^2 \quad , \quad E(< x, a >^4) = 3\Big(\sum_i x_i^2\Big)^2 - 2\sum_i x_i^4$$

With $x = Ub$ we have $\sum_i x_i^2 = N$, which gives the second moment, and then the fourth moment is $3N^2 - 2\sum_i E(x_i^4)$. Now by applying the second formula to the i-th row of U, which has norm 1, we obtain $E(x_i^4) = 3 - 2\sum_j U_{ij}^4$, and this gives the result. □

The program `glow.py` checks this formula by exact enumeration, for the 2 matrices of the Fano plane, and for random orthogonal matrices. As a consequence, the fourth cumulant of the glow is $-6N + 4||U||_4^4$, and the first invariant of U which is seen by the Ising array, at high temperature, is the 4-norm. By the Hölder inequality we have $||U||_4^4 \geq 1$ on O_N, with equality precisely for the rescaled Hadamard matrices [3], so we recover the cumulant $-6N + 4$ from [49], and in general we are led to the almost Hadamard matrix problematics for the exponent $p = 4$, studied in [3], [45], [46]. For the design matrices U_+ the 4-norm is easy to compute, and the values are given in the table from Section 3: for the Hadamard designs these are close to 1, while for the projective planes they grow with the order.

Regarding now the higher cumulants, in the Hadamard case their leading terms are universal, by Theorem 1.1. The proof there uses the orthogonality of the coupling matrix, and the fact that its entries have the same absolute value, and the second ingredient can be weakened:

Proposition 4.5. *Let $U_N \in O_N$ be orthogonal matrices, with $N \to \infty$ along some sequence, such that the entries of the matrices $\sqrt{N}U_N$ are bounded by a constant C. Then the cumulants of the glow are given by the formula*

$$\kappa_{2k} = (-1)^{k-1}(2k-1)!\, Cat_{k-1} N + O(1)$$

with $Cat_j = \binom{2j}{j}/(j+1)$ the Catalan numbers, and so $\frac{1}{N}\log E(e^{\beta\Omega}) \to \frac{1}{2}\Phi_0(\beta^2)$ coefficientwise.

Proof. We follow [49]. With $A = \sqrt{N}U$, the cumulant of order $2k$ of $< Ab, a >$ is a sum over the connected bipartite multigraphs with $2k$ edges, coming from pairs of partitions, of certain weights, which do not depend on A, multiplied by the contraction of A along the graph, with a free label in $\{1, \ldots, N\}$ at each vertex. Since $AA^t = A^tA = N$, a vertex of degree 2 can be removed, with a factor N. A graph which reduces in this way to a point contributes with N^{k+1}. Otherwise, after $k-s$ reductions we are left with $2s$ edges and with $v \leq s$ vertices, all of them having degree at least 4, and the contraction is bounded by $N^{k-s} \cdot N^v C^{2s} \leq C^{2k} N^k$. The total weight of the graphs which reduce to a point was computed in [49], by comparing with a Haar random matrix, and is $(-1)^{k-1}(2k-1)!\, Cat_{k-1}$. With $\Omega =< Ab, a > /\sqrt{N}$, this gives the result. □

As a first observation, at $k = 2$ we recover the leading term $-6N$ of the above cumulant, the 4-norm being bounded by C^4. Figure 19 shows the glow of the 2 Fano matrices, computed by `pictures.py`. The 2^{14} states are distributed over 52 energy levels, and the 2 densities of states are rather different, although their first moments are close to each other, the moment of order 2 being 7 in both cases, and the moments of order 4 being 109.82 for U_+ and 112.59 for U_-, against 147 for the Gaussian law. In both cases the top level $\Omega = 7$ consists of the 2 crystalline states, and the second levels are $(9 + 24\sqrt{2})/7 = 6.1344$ for U_+, with 42 states, and $(1 + 30\sqrt{2})/7 = 6.2038$ for U_-, with 56 states.

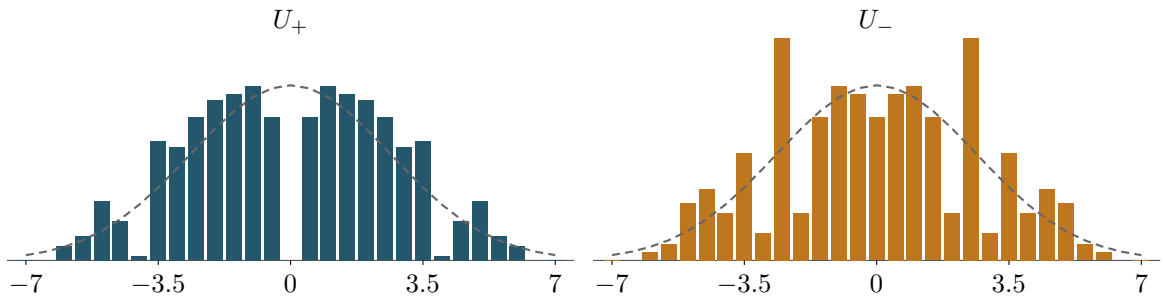

Figure 19: The densities of states of the 2 Fano arrays, in bins of width 1/2 and in units of 400 states, for U_+ on the left, and for U_- on the right. The dashed curve is the Gaussian law of variance 7.

Summarizing, at high temperature an Ising array is described by the strengths of its junctions, by the 4-norm of the coupling matrix and, when the entries are bounded, by the universal free energy. For the matrices coming from designs, the situation is as follows:

Theorem 4.6. *For the Ising arrays of the matrices $U_\pm$ of a symmetric (v, k, λ) design:*

1. *There are vk ferromagnetic junctions, of strength $(v - k \mp \sqrt{n})/(v\sqrt{n})$, and $v(v-k)$ antiferromagnetic junctions, of strength $(k \pm \sqrt{n})/(v\sqrt{n})$.*
2. *The cumulants of order 2 and 4 of the glow are v and $-6v + 4||U_\pm||_4^4$.*
3. *For the Hadamard designs the entries of $\sqrt{v}\, U_\pm$ are bounded by $3/2$, and so with $n \to \infty$ the free energy at high temperature converges coefficientwise to that of the Hadamard arrays, and of the random orthogonal model.*

Proof. (1) This is the formula of the entries of $U_\pm$, from Proposition 3.3.

(2) This follows from Proposition 4.4.

(3) For $v = 4n-1$ and $k = 2n-1$ the biggest entry of $\sqrt{v}\,U_\pm$, in absolute value, is the positive entry of $\sqrt{v}\,U_-$, which is $(2n+\sqrt{n})/\sqrt{n(4n-1)}$. The square of this number is at most $9/4$ precisely when $5n \geq 4\sqrt{n} + 13/4$, which holds for $n \geq 2$. Thus Proposition 4.5 applies, and the limiting free energy is the one from Theorem 1.1. □

For the projective planes of order q the positive entries of $\sqrt{v}\,U_\pm$ are of order $\sqrt{q}$, and the above argument does not apply as such. The 4-norms in the table from Section 3 grow accordingly, with $||U_+||_4^4$ being of order q, which is small with respect to $v \simeq q^2$, so the leading term of the fourth cumulant is still universal, and the higher orders are not known.

5 Design arrays and their crystals

We discuss now the Ising arrays at low temperature, where the phenomenon to be understood is the crystallization, in the sense of [49]. We keep the notations from the previous section, with $U \in O_N$ being the coupling matrix, and with $\Omega =< Ub, a >$.

Let us begin with the ground states. We have here the following result:

Proposition 5.1. *For any $U \in O_N$ we have $\Omega \leq N$, with equality precisely when $Ub = a$, and the partition function is given by $Z(\beta) = \sum_b \prod_i 2\cosh(\beta(Ub)_i)$.*

Proof. We have $\Omega \leq ||Ub||_1 \leq \sqrt{N}||Ub||_2 = N$, with equality in the first inequality when a is the sign vector of Ub, and in the second one when the entries of Ub have absolute value 1. As for the formula of $Z(\beta) = \sum_{ab} e^{\beta\Omega(a,b)}$, this follows by summing over a. □

As in [49], we call crystalline the states with $\Omega = N$, which correspond to the sign vectors b mapped by U to sign vectors. In the Hadamard case such states may or may not exist, and their number controls the crystallization of the array, the prediction from [49] for the crystallization temperature $T_c = 1/\beta$ being as follows, with c the number of crystalline states:

$$\beta + \frac{\log c}{N} = 2\log 2 + \frac{1}{2}\left(\sqrt{1+4\beta^2} - 1 - \log\frac{1+\sqrt{1+4\beta^2}}{2}\right)$$

Here on the left we have the free energy of the crystal, per row wire, and on the right we have the paramagnetic free energy, namely the one from Theorem 1.1, which applies as well to the Hadamard designs with $n \to \infty$, by Theorem 4.6. For the other designs, and at small orders, we use this formula as a heuristic.

The formula of $Z(\beta)$ in Proposition 5.1 involves only 2^N terms, so the Ising arrays can be solved exactly, at small N. The program `arrays.py` does this for the matrices U_+ of the designs from Section 3 with $v \leq 23$. It computes the number c of crystalline states, the above temperature T_c, and the maxima of the specific heat per row wire, $C = \beta^2 Var(\Omega)/N$. We obtain:

design	c	T_c	sharp maximum	broad maximum
$(7,3,1)$	2	0.219	$C = 0.83$ at $T = 0.220$	–
$(11,5,2)$	2	0.203	$C = 0.84$ at $T = 0.180$	$C = 0.44$ at $T = 0.414$
$(13,4,1)$	2	0.199	$C = 1.16$ at $T = 0.188$	$C = 0.40$ at $T = 0.480$
$(15,7,3)$	338	0.409	$C = 1.01$ at $T = 0.414$	–
$(19,9,4)$	2	0.192	$C = 1.71$ at $T = 0.194$	$C = 0.38$ at $T = 0.440$
$(21,5,1)$	898	0.355	$C = 1.35$ at $T = 0.354$	–
$(23,11,5)$	2	0.189	$C = 1.60$ at $T = 0.184$	plateau, $C \simeq 0.42$

We can see that the sharp maximum of the specific heat is close to the predicted crystallization temperature, the agreement being within 0.006, except for the designs $(11, 5, 2)$ and $(13, 4, 1)$, where the difference is about 0.02 and 0.01. The arrays having only 2 crystalline states have in addition a broad maximum, of height about 0.4, which becomes a plateau at $v = 23$, and which is similar to the one found in [49] for the Hadamard arrays having no crystalline states, which freeze smoothly. Observe also that with $c = 2$ and $N \to \infty$ the above equation gives $T_c \to 0.1776$. Figure 20 shows the specific heat of 4 of these arrays, as computed by `pictures.py`.

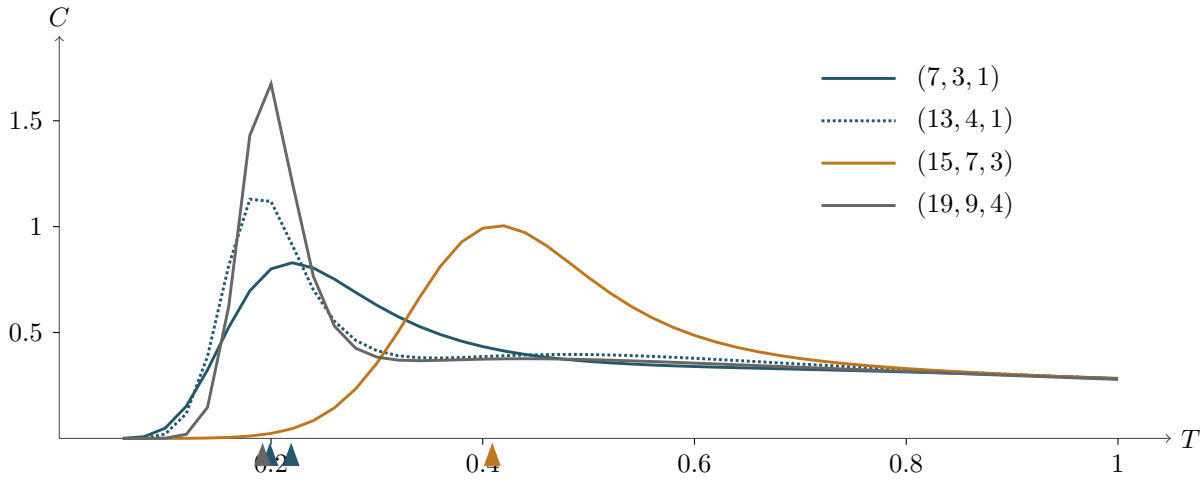

Figure 20: The specific heat per row wire of the arrays of 4 design matrices U_+, against the temperature. The triangles mark the predicted crystallization temperatures T_c. The designs with 2 crystalline states crystallize near $T = 0.2$, and the design $(15, 7, 3)$, which has 338 such states, near $T = 0.4$.

The same crystallization can be seen on the mean energy, divided by its lower bound $-N$, which is shown in Figure 21, together with the paramagnetic prediction $m = (\sqrt{1 + 4\beta^2} - 1)/(2\beta)$ coming from Theorem 4.6. At high temperature all the 4 curves follow this prediction quite closely, including the one of the projective plane of order 3, which is not covered by Theorem 4.6.

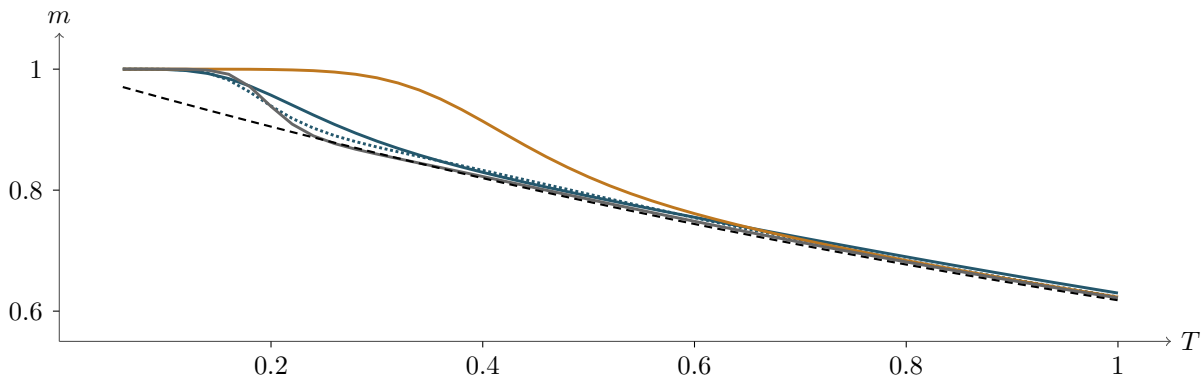

Figure 21: The mean energy of the same 4 arrays, divided by its lower bound, with the same colors as in Figure 20. The dashed curve is the paramagnetic prediction, which is followed down to the crystallization, where the energy jumps to 1.

The numbers of crystalline states in the above table can be understood in terms of the geometry of the design. Any sign vector can be written as $b = \xi - 2\chi_T$, with ξ being as usual

the all-one vector, and with χ_T being the indicator vector of a set of points T. We have:

Proposition 5.2. *Consider the matrices $U_\pm$ of a symmetric (v,k,λ) design, set $c_\pm = (k \pm \sqrt{n})/v$, and let $b = \xi - 2\chi_T$, with T being a set of t points.*

1. *U_+b is a sign vector precisely when each block meets T in c_+t or in $c_+t - \sqrt{n}$ points.*

2. *U_-b is a sign vector precisely when each block meets T in c_-t or in $c_-t + \sqrt{n}$ points.*

Proof. Let x_i be the number of points of T lying on the i-th block. The sum of the entries of b over this block is $k - 2x_i$, and the sum of all the entries of b is $v - 2t$. Since the entries of $U_\pm$ are $(1 - c_\pm)/\sqrt{n}$ on the blocks and $-c_\pm/\sqrt{n}$ outside, by using $c_\pm v = k \pm \sqrt{n}$ we obtain:

$$(U_\pm b)_i = \frac{k - 2x_i - c_\pm(v - 2t)}{\sqrt{n}} = \frac{2(c_\pm t - x_i)}{\sqrt{n}} \mp 1$$

This number is ± 1 precisely when x_i is as in the statement. □

Thus the crystalline states correspond to the sets of points having only 2 intersection numbers with the blocks, which must differ by $\sqrt{n}$. Observe also that, since each point lies on k blocks, we have $\sum_i x_i = kt$, and this shows that the second intersection number in the above statement is attained by exactly t blocks. Thus $a = U_\pm b$ is of the form $a = \mp(\xi - 2\chi_{T'})$, with T' being a set of t blocks, and since $b = U_\pm^t a$, this set T' has the same property, with respect to the dual design. Such sets T are classical objects in finite geometry, see [13], [31], and for the 2 designs of order 4 from Section 3, which are projective spaces, we obtain in this way remarkable configurations. The program `crystals.py` enumerates the crystalline states of these 2 designs, for both U_+ and U_-, and records the corresponding sets T and their intersection numbers.

The empty set and the set of all the points always have the above property, and correspond to the aligned states. In general, we have the following result, illustrated in Figure 22:

Theorem 5.3. *The crystalline states of the arrays of the design matrices $U_\pm$ are as follows, with each set T below producing the 2 states given by $b = \pm(\xi - 2\chi_T)$:*

1. *For any design we have the aligned states, coming from $T = \emptyset$, with $a = -b$ for U_+, and $a = b$ for U_-. When n is not a square, there are no other crystalline states.*

2. *For the projective space $PG(3,2)$, with parameters $(15,7,3)$, the other states come from the 168 ovoids, for U_+, and from the 35 lines and the 280 pairs of skew lines, for U_-.*

3. *For the projective plane $PG(2,4)$, with parameters $(21,5,1)$, the other states come from the 168 hyperovals and the 280 unitals, for U_+, and from the 360 Baer subplanes, for U_-.*

Proof. We use Proposition 5.2. Observe first that a set T and its complement produce the same 2 states, so we can restrict the attention to the sets having $t < v/2$ points.

(1) With $T = \emptyset$ the intersection numbers are 0, and we obtain $b = \xi$, with $U_\pm\xi = \mp\xi$. Assume now that $\sqrt{n}$ is irrational. Since the numbers x_i are integers, for U_+ we must have either $x_i = c_+t$, which gives $t = 0$, or $x_i = c_+t - \sqrt{n}$, which gives $t = v$, and similarly for U_-.

(2) Here $c_+ = 3/5$ and $c_- = 1/3$. For U_+ the number t must be a multiple of 5, and at $t = 5$ we obtain the sets of 5 points meeting each plane in 1 or 3 points, which are the ovoids. For U_- the number t must be a multiple of 3. At $t = 3$ we obtain the sets of 3 points meeting each plane in 1 or 3 points, and the lines have this property. At $t = 6$ we obtain the sets of 6 points meeting each plane in 2 or 4 points, and the unions of 2 skew lines have this property, because a plane cannot contain 2 skew lines. The program `crystals.py` finds 168 sets at $t = 5$, then 35 sets at $t = 3$, which are therefore the lines, and 280 sets at $t = 6$, which are therefore the pairs of skew lines, each line being skew to 16 others.

(3) Here $c_+ = 1/3$ and $c_- = 1/7$. For U_+ the number t must be a multiple of 3. At $t = 3$ each line should meet T in exactly one point, which is impossible. At $t = 6$ we obtain the sets of 6 points meeting each line in 0 or 2 points, which are the hyperovals, and at $t = 9$ we obtain the sets of 9 points meeting each line in 1 or 3 points, which are the unitals. For U_- we must have $t = 7$, and we obtain the sets of 7 points meeting each line in 1 or 3 points, and the Baer subplanes, which are the copies of the Fano plane inside our plane, have this property. The program finds 168 sets at $t = 6$ and 280 sets at $t = 9$, then 360 sets at $t = 7$, which are therefore the Baer subplanes, their number being well-known to be 360, see [31]. □

In particular we recover the numbers $2 + 2 \cdot 168 = 338$ and $2 + 2(168 + 280) = 898$ from the above table, and for U_- the numbers of crystalline states are 632 and 722. As for the sets of blocks T' found after Proposition 5.2, for an ovoid we obtain its 5 tangent planes, and for a hyperoval, its 6 exterior lines. In the cyclic models of Figure 22 many of these configurations are regular polygons: the multiples of 3 in $\mathbb{Z}_{15}$ form an ovoid, the multiples of 5 form a line, and the multiples of 3 in $\mathbb{Z}_{21}$ form a Baer subplane, the examples being chosen by `pictures.py`.

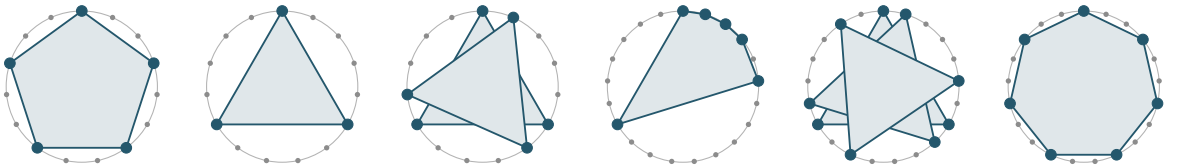

Figure 22: Crystals as point sets, in the cyclic models of $PG(3, 2)$, with points in $\mathbb{Z}_{15}$, for the first 3 pictures, and of $PG(2, 4)$, with points in $\mathbb{Z}_{21}$, for the last 3. The spins in blue are reversed.

The cyclic model hides the geometry, so here is a second picture. The projective space $PG(3, 2)$ has 15 points, namely the nonzero vectors of $\mathbb{F}_2^4$, and these can be placed on a tetrahedron: the 4 vertices, the 6 midpoints of the edges, the 4 centers of the faces, and the center, according to the number of nonzero coordinates. There are 35 lines, each having 3 points, and these are the lines of the celebrated problem of the 15 schoolgirls of Kirkman, see [52]. In this picture, shown in Figure 23, the 4 vertices and the center form an ovoid, each edge, taken with its midpoint, is a line, and 2 opposite edges are skew lines, as verified by `portraits.py`. Thus the array of U_+ has a crystal where the spins of the vertices and of the center are reversed, and the array of U_- has crystals where the spins of an edge, or of 2 opposite edges, are reversed.

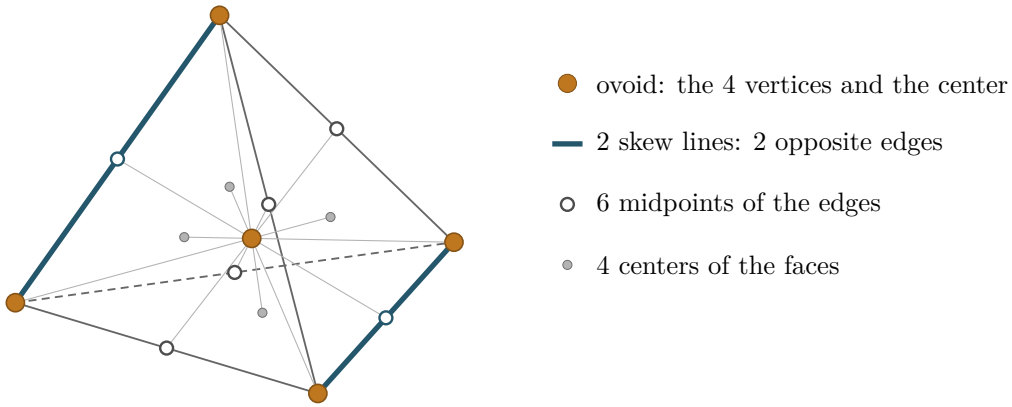

Figure 23: The 15 points of the projective space $PG(3, 2)$, placed on a tetrahedron. The thin lines are 7 of the 35 lines, passing through the center. The points in gold form an ovoid, and the 2 edges in blue, each taken with its midpoint, are 2 skew lines.

As for the projective plane $PG(2, 4)$, its crystals are the ingredients of one of the most

beautiful constructions in combinatorics, that of the Witt design, see [34]. The 168 hyperovals fall into 3 classes of 56, with 2 hyperovals being in the same class when they meet in an even number of points, and the 360 Baer subplanes fall into 3 classes of 120, with 2 subplanes being in the same class when they meet in an odd number of points, as verified by `portraits.py`. By adding 3 new points to the 21 points of the plane one obtains in this way $21+168+360+210 = 759$ sets of 8 points, coming from the lines, the hyperovals, the Baer subplanes and the pairs of lines, such that any 5 of the 24 points lie in exactly one of these sets. The automorphism group of this system is the Mathieu group M_{24}.

The numbers of crystals found above can be understood by using the symmetries. The collineation groups of $PG(3,2)$ and $PG(2,4)$ have orders 20160 and 120960, and act transitively on each of our types of configurations [31], so the number of configurations of a given type is the index of the stabilizer of one of them. The picture is as follows:

space	configuration	points	number	stabilizer
$PG(3,2)$	ovoid	5	168	120
$PG(3,2)$	line	3	35	576
$PG(3,2)$	2 skew lines	6	280	72
$PG(2,4)$	hyperoval	6	168	720
$PG(2,4)$	unital	9	280	432
$PG(2,4)$	Baer subplane	7	360	336

As an illustration, on the tetrahedron an ovoid consists of a basis of $\mathbb{F}_2^4$ and of the sum of its 4 vectors, any 4 of the 5 points being a basis. The stabilizer is therefore the symmetric group S_5, permuting the 5 points, and we obtain $20160/120 = 168$ ovoids. Also, each line meets $3 \cdot 6 = 18$ other lines, so it is skew to 16 lines, and there are $35 \cdot 16/2 = 280$ pairs of skew lines.

There is one more design with $n = 4$ in this paper, namely the Kummer configuration on the 4×4 board, where $\sqrt{v}\,U_+$ is a Hadamard matrix. Here the crystals can be drawn on the board itself:

Proposition 5.4. *The array of the matrix U_+ of the design on the 4×4 board has 896 crystalline states, which up to a global sign change are as follows:*

1. *The aligned state, with no spin reversed.*
2. *60 states with 4 reversed spins: the 36 squares, formed by 2 rows and 2 columns, and the 24 placements of 4 rooks, with no 2 of them on the same row or column.*
3. *192 states with 6 reversed spins, and $390/2 = 195$ states with 8 reversed spins, among which the 6 ones coming from 2 rows, or from 2 columns.*

Proof. This follows from an enumeration of the 2^{16} states, performed by `detours.py`. By Proposition 5.2 the crystals with t reversed spins correspond to the sets of t cells meeting each block in $t/2$ or $t/2-2$ cells, and for the squares and for the rooks this is clear, the intersections being 0 or 2. □

The number 896 is familiar: this is the number of bent functions of 4 variables. This is not a coincidence, because for the Walsh matrix W_N the crystalline states, which are the solutions of $W_N b = \sqrt{N}a$, are by definition the bent functions, and our Hadamard matrix is equivalent to the Walsh matrix of order 16, as explained in Section 3. As for the matrix U_-, which is a local maximizer here, but not a strict one, its array has 552 crystalline states.

The crystals found above, in the spaces $PG(3,2)$ and $PG(2,4)$, are the first instances of 2 infinite families. For any prime power q, the points and planes of $PG(3,q)$ form a symmetric design with parameters $(q^3+q^2+q+1, q^2+q+1, q+1)$, the points and lines of $PG(2,q^2)$

form a symmetric design with parameters $(q^4+q^2+1, q^2+1, 1)$, and in both cases $n=q^2$ is a square. Recall that an ovoid of $PG(3,q)$ is a set of q^2+1 points meeting each plane in 1 or $q+1$ points, such as an elliptic quadric, and that a partial spread is a set of pairwise skew lines. Also, a unital of $PG(2,q^2)$ is a set of q^3+1 points meeting each line in 1 or $q+1$ points, such as a Hermitian curve, a maximal arc of degree d is a set of points meeting each line in 0 or d points, and a Baer subplane is a copy of $PG(2,q)$ inside $PG(2,q^2)$. See [31]. We have:

Theorem 5.5. *For any prime power q, the following sets of points produce crystalline states of the design arrays, via $b=\pm(\xi-2\chi_T)$:*

1. *For $PG(3,q)$, with the planes as blocks: the ovoids, for the array of U_+, and the partial spreads, and in particular the lines, for the array of U_-.*

2. *For $PG(2,q^2)$: the unitals and the maximal arcs of degree q, for the array of U_+, and the Baer subplanes, for the array of U_-.*

Proof. We use Proposition 5.2, with t standing for the number of points of T.

(1) Here $v=(q+1)(q^2+1)$ and $k=q^2+q+1$, so $c_+=(q+1)/(q^2+1)$ and $c_-=1/(q+1)$. For an ovoid we have $c_+t=q+1$ and $c_+t-q=1$, as needed. For a partial spread with s lines we have $t=s(q+1)$, so $c_-t=s$. A plane contains at most one of our lines, because 2 lines in a plane meet, and meets the other lines at one point, so it meets T in s or $s+q$ points.

(2) Here $v=(q^2+q+1)(q^2-q+1)$ and $k=q^2+1$, so $c_\pm=1/(q^2\mp q+1)$. For a unital we have $c_+t=q+1$ and $c_+t-q=1$. A maximal arc of degree q has $t=1+(q^2+1)(q-1)=q(q^2-q+1)$ points, as one can see by counting on the lines through one of its points, so $c_+t=q$ and $c_+t-q=0$. Finally, a Baer subplane has $t=q^2+q+1$ points, and meets each line in 1 or $q+1$ points, and here $c_-t=1$ and $c_-t+q=q+1$. □

At $q=2$ we recover the configurations from Theorem 5.3, the hyperovals of $PG(2,4)$ being its maximal arcs of degree 2. In general, the maximal arcs of degree q exist in $PG(2,q^2)$ when q is even, by a construction of Denniston [31], and do not exist when q is odd [1]. The program `detours.py` verifies the above result at $q=3$, with an elliptic quadric and with partial spreads having $1,2,\ldots,10$ lines in $PG(3,3)$, and with a Hermitian curve and a Baer subplane in $PG(2,9)$. As for the numbers of crystals, these grow quickly with q. By dividing the orders of the collineation groups by those of the stabilizers [31], the space $PG(3,q)$ has $q^4(q^2-1)(q^3-1)/2$ elliptic quadrics and $(q^2+1)(q^2+q+1)$ lines, and the plane $PG(2,q^2)$ has $q^3(q^2+1)(q^3-1)$ Hermitian curves and $q^3(q^3+1)(q^2+1)$ Baer subplanes. At $q=2$ these are the numbers $168, 35, 280, 360$ found before, and at $q=3$ we obtain $8424, 130, 7020, 7560$.

As a conclusion, the Ising arrays with design couplings behave like the Hadamard arrays from [49], with a crystallization which is controlled by the number of crystalline states. The difference is that the crystal is always there, the aligned state being crystalline for any design, with no divisibility condition on the order, and with the crystallization temperature being the lowest possible one, when n is not a square. In the aligned crystal the 2 layers are aligned against each other for U_+, and with each other for U_-, as announced in Section 4, and for the Fano plane this is the picture of the 2 magnets from Figure 16. When n is a square the other crystals are the above configurations, with the spins of an ovoid, or of a hyperoval, being reversed.

6 Moving matrices, heating and cooling

We discuss now the second model from the Introduction, where the matrix itself moves on the orthogonal group, with energy $-||U||_1$. This is the hard matrix model of [23], which is defined on SO_N, the choice of the connected component being irrelevant, because the 1-norm is invariant under the sign change of a row, which exchanges the 2 components of O_N. The model was

studied in [23] for $N \in 4\mathbb{N}$, where the ground states are the rescaled Hadamard matrices, called crystals there, with the conclusion that a cooling misses the crystals, and produces a glass. An important role is played there by the matrices having a zero entry, called rubicons, which are the walls between the regions where the sign matrix is constant, and the energy linear.

At infinite temperature, the matrix is distributed according to the Haar measure of O_N. Since each entry is then a coordinate of a random point on the unit sphere of $\mathbb{R}^N$, we obtain:

$$E(||U||_1) = \frac{N^2\,\Gamma(N/2)}{\sqrt{\pi}\,\Gamma((N+1)/2)} \simeq \sqrt{\frac{2}{\pi}}\,N^{3/2}$$

Thus $||U||_1/N^{3/2}$ is slightly above 0.8 for a hot matrix, and is 1 for a Hadamard matrix. Our purpose here is to understand what happens in between, at the orders where there is no Hadamard matrix, and where the crystals of the model, in the sense of the ground states, are by definition the optimal almost Hadamard matrices. Let us begin with:

Proposition 6.1. *For any $U \in O_N$ and any sign matrix $S \in M_N(\pm 1)$ we have*

$$\Phi(U,S) \leq ||U||_1 \quad , \quad \Phi(U,S) \leq Tr|S|$$

with equality when S is a sign matrix of U, respectively when U is a polar part of S. In particular the 1-norm increases under the operation $U \to Pol(sgn(U))$.

Proof. The first inequality is clear from $\Phi(U,S) = \sum_{ij} U_{ij}S_{ij}$. The second one is the well-known fact that the maximum of $Tr(S^tU)$ over the orthogonal group is the sum of the singular values of S, and is attained when S^tU is positive. Here by sign matrix we mean any matrix with $S_{ij} = sgn(U_{ij})$ when $U_{ij} \neq 0$, and by polar part, any orthogonal matrix U such that S^tU is positive. Finally, the last assertion follows from:

$$||U||_1 = \Phi(U, sgn(U)) \leq Tr|sgn(U)| = \Phi(Pol(sgn(U)), sgn(U)) \leq ||Pol(sgn(U))||_1$$

Thus, we are led to the conclusions in the statement. □

We have therefore 2 ways of cooling a matrix, at zero temperature. The first one is the gradient ascent for the 1-norm, which follows the curves $t \to Ue^{tA}$, with $A = (X^t - X)/2$ and $X = S^tU$, and stays on the connected component of U. By Theorem 2.6 this can stop at plain, neutral and twisted local maximizers. The second one is the polar iteration from Proposition 6.1, which jumps, and which can stop at plain and neutral local maximizers, but not at twisted ones. The program `ascent.py` runs both procedures from Haar random matrices, with 3000 runs for the polar iteration, and 1000 runs for the gradient ascent. We obtain the following values of $||U||_1/N^{3/2}$, the hot column being the Haar average, and the last one the number of distinct end values of the polar iteration:

N	hot	ascent, mean	polar, mean	polar, best	end values
5	0.8385	0.9553	0.9557	0.9839	5
6	0.8317	0.9528	0.9498	0.9747	22
7	0.8268	0.9461	0.9462	0.9703	77
8	0.8231	0.9445	0.9437	1	515
9	0.8203	0.9433	0.9416	0.9822	1863
10	0.8180	0.9410	0.9403	0.9794	2862
11	0.8162	0.9395	0.9394	0.9723	2991
12	0.8147	0.9392	0.9383	0.9676	2984
13	0.8134	0.9391	0.9380	0.9661	2987

We can see that the 2 procedures end at about the same level, close to 0.94, and that the number of end states grows very quickly with N. All the 1000 gradient ascents end at plain local maximizers, with the exception of 2 runs at each of $N = 5, 6, 7$, which end at neutral ones. No twisted maximizer was reached. As for the crystals, at $N = 7$ the Fano matrix is found 21 times by the polar iteration, and 6 times by the gradient ascent, while at $N = 11, 13$ the matrices of the Paley biplane and of the projective plane of order 3, having values 0.9769 and 0.9935, are never found. The same happens with the Hadamard matrices, which are found 17 times at $N = 8$, by the polar iteration, and never at $N = 12$, in agreement with the findings in [23]. Figure 24, computed by `pictures.py`, shows what the 3 kinds of matrices look like at $N = 7$: a Haar random matrix, the end state of its polar iteration, and the Fano matrix.

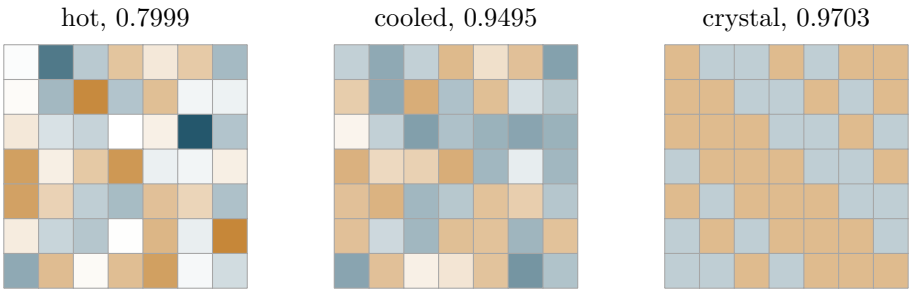

Figure 24: A hot matrix, the glassy matrix obtained from it by the polar iteration, and the crystal, at $N = 7$, with the values of $||U||_1/N^{3/2}$. The positive entries are in blue, the negative ones in gold, and the color is proportional to the absolute value: the cooling makes the entries more equal in absolute value, and the crystal has only 2 kinds of entries.

Figure 25 shows the distribution of the end values of the polar iteration at $N = 7$ and $N = 13$, for a second sample of 3000 runs, made by `pictures.py`, where the Fano matrix is found 28 times.

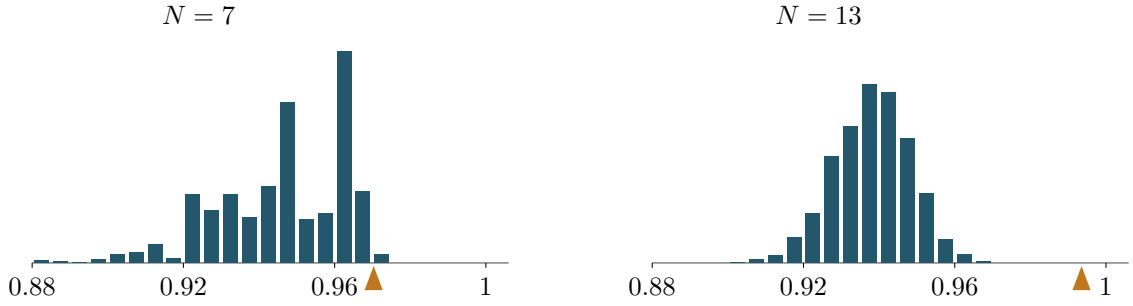

Figure 25: The end values of $||U||_1/N^{3/2}$ for 3000 polar iterations starting from Haar random matrices, in bins of width 0.005 and in units of 200 runs. The triangles mark the matrices of the Fano plane, reached by 28 runs, and of the projective plane of order 3, which is never reached.

We can see that the end values are spread over a band, with the crystal being at the upper end of this band at $N = 7$, and far above it at $N = 13$. Figure 26 summarizes the situation, with the best values being those from Section 7 below: the cooling brings the matrix from the hot level to a glassy level, which decreases slowly with N, and which stays well below the best level. In numbers, the hot level decreases from 0.8385 at $N = 5$ to 0.8134 at $N = 13$, towards its limit $\sqrt{2/\pi} = 0.798$, the glassy level decreases from 0.9557 to 0.9380, and the best level oscillates between 0.9703, at $N = 7$, and 1, at $N = 8, 12$. Thus the cooling recovers a fraction of the gap between the hot level and the best one which goes from about 0.8, at $N = 5, 6, 7$, down to 0.67, at $N = 12$.

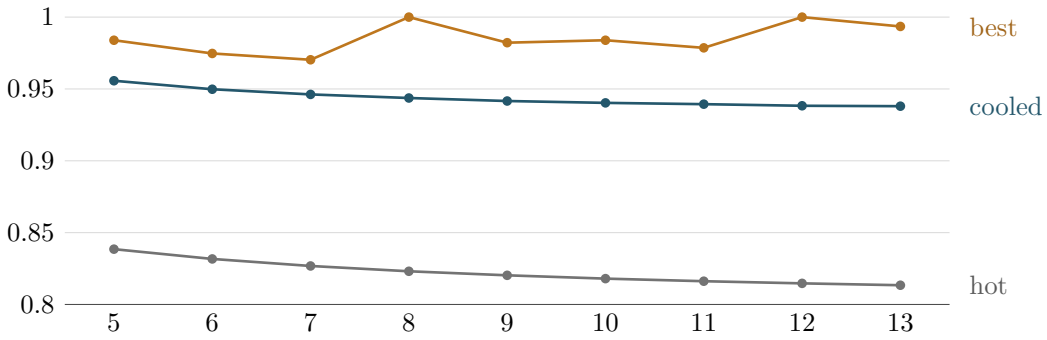

Figure 26: The 3 levels of the hard matrix model, as values of $||U||_1/N^{3/2}$ against N: the average over the Haar measure, the average end value of the polar iteration, and the best value that we know, which is 1 when there is a Hadamard matrix.

In order to conclude our study, let us go back to the polar iteration, which jumps from one sign region to another, without caring about the walls, and which produced the glassy matrices from Figure 24 and Figure 25. Its relation with the 3 types of local maximizers from Section 2 is as follows:

Theorem 6.2. *The polar iteration $U \to Pol(sgn(U))$, which is defined on the orthogonal matrices having nonzero entries and invertible sign matrix, has the following properties:*

1. *The 1-norm increases at each step.*
2. *The fixed points are precisely the plain local maximizers of the 1-norm.*
3. *A twisted local maximizer U is not a fixed point, and after one step its 1-norm increases by at least $2\sigma_N$, where σ_N is the smallest singular value of $sgn(U)$.*

Proof. (1) This is the last assertion of Proposition 6.1.

(2) If U is a fixed point then with $S = sgn(U)$ we have $U = Pol(S)$, so the matrix $X = S^tU = |S|$ is positive definite, and U is plain. Conversely, a plain local maximizer is the polar part of its sign matrix, by Proposition 2.5.

(3) By Proposition 2.5 we have $||U||_1 = \sigma_1 + \ldots + \sigma_{N-1} - \sigma_N$, with $\sigma_N > 0$, and the matrix $V = Pol(S)$ satisfies $||V||_1 \geq \Phi(V, S) = Tr|S| = ||U||_1 + 2\sigma_N$, by Proposition 6.1. □

Thus the twisted maximizers are invisible to the polar iteration, which jumps over the walls, while a continuous dynamics, such as the gradient ascent, or the Langevin dynamics at low temperature, can be trapped by them. For the matrix U_- of a Hadamard design the first step of the polar iteration leads to U_+, the gain being exactly 2. In terms of the sign matrices, the fixed points of the polar iteration are the almost Hadamard sign patterns from [5], that we will meet again in the next section.

7 Sign matrices, the optimal crystals

We have seen in the previous section that a cooling of the hard matrix model misses the crystals, and ends in a glassy state. In order to find the crystals, which are by definition the optimal almost Hadamard matrices, the efficient way is to use the dual variables, namely the sign matrices, where exhaustive searches and annealing are possible. We have:

Proposition 7.1. *The maximum of the 1-norm on O_N equals the maximum of $Tr|S|$ over the sign matrices $S \in M_N(\pm 1)$, and the maximizers correspond to each other, with S being the sign matrix of U, and with U being a polar part of S. Thus the optimal almost Hadamard matrices correspond to the ground states of the Ising model having N^2 spins S_{ij}, and energy $-Tr|S|$.*

Proof. Both maxima are equal to the maximum of $\Phi(U,S)$, by Proposition 6.1. If U is a maximizer of the 1-norm then its entries are nonzero, by Theorem 2.6, and with $S = sgn(U)$ we have $Tr|S| \geq \Phi(U,S) = ||U||_1$, so S is a maximizer of $Tr|S|$, and U is a polar part of it, by the equality case in Proposition 6.1. Conversely, if S is a maximizer of $Tr|S|$ and U is a polar part of S, then $||U||_1 \geq \Phi(U,S) = Tr|S|$, so U is a maximizer of the 1-norm, with nonzero entries, and the equality case in $\Phi(U,S) \leq ||U||_1$ gives $S = sgn(U)$. □

The quantity $Tr|S|$ is the energy of the matrix S, in the sense of spectral graph theory, where the maximal energy problem has been much studied, see [38], [48]. The above result is closely related to the work of Holbrook, Johnston and Schoch [32], where the maximum of the 1-norm on O_N is computed in terms of Schur norms, by semidefinite programming, with the exact values 11, $8+2\sqrt{10}$ and $1+12\sqrt{2}$ at $N = 5, 6, 7$, and with lower bounds up to $N = 24$. We will recover these 3 values by an exhaustive search, which gives the whole energy landscape. The above model has a gauge invariance, the energy being invariant under the sign changes and the permutations of the rows and columns. For $N \leq 6$ an exhaustive search, modulo the sign changes, is possible, and is done by `census.py`. At $N = 7$ the search modulo the sign changes involves 2^{36} matrices, and can be done by using the permutations of the rows as well. This is what the program `seven.py` does: with the first row and column being positive, the other 6 rows form a multiset of vectors in $\{\pm 1\}^6$, and there are $\binom{69}{6} = 119877472$ such multisets, to be counted with their multiplicities. The top of the spectrum of $Tr|S|$, as found by `census.py` and `seven.py`, is as follows, the numbers of matrices being modulo the sign changes of the rows and columns:

N	top level	matrices	second level	matrices
5	11	120	$5+4\sqrt{2}$	2400
6	$8+2\sqrt{10}$	7200	$10\sqrt{2}$	21600
7	$1+12\sqrt{2}$	151200	$11+4\sqrt{3}$	1058400

At $N = 7$ the top level is that of the Fano plane, and the second level, which is very close, is that of a sign matrix S with SS^t having eigenvalues $12, 12, 9, 4, 4, 4, 4$, given in `optimal.py`, which is the sign matrix of its polar part too. With the exhaustive data in hand we can compute the thermodynamics of the model with energy $-Tr|S|$ at temperature T. The whole densities of states, and the corresponding specific heat, are shown in Figure 27, computed by `pictures.py`.

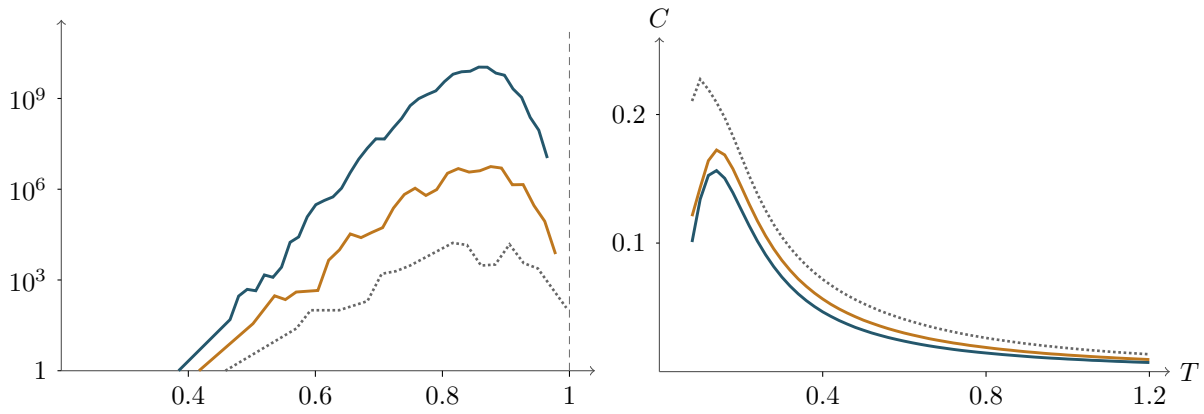

Figure 27: On the left, the number of sign matrices in bins of width 1/4 of the energy $Tr|S|$, modulo the sign changes of the rows and columns, on a logarithmic scale, against $Tr|S|/N^{3/2}$, at $N = 5$ (dotted), $N = 6$ (gold) and $N = 7$ (blue), the dashed line being the Hadamard bound. On the right, the specific heat per spin of the Ising model with energy $-Tr|S|$, with $(N-1)^2$ free spins, against the temperature, computed from the exact levels at $N = 5, 6$, and from bins of width 0.01 at $N = 7$.

On this figure we can see that the levels which are close to the Hadamard bound are rare: at $N = 7$ there are about 10^5 matrices on the top level, out of $7 \cdot 10^{10}$, the mean value of $Tr|S|/N^{3/2}$ being 0.851. As for the specific heat, this has a single maximum, near $T = 0.10$ at $N = 5$, and near $T = 0.14$ at $N = 6, 7$.

For bigger N the program `anneal.py` performs a simulated annealing with single spin flips [37], with 4 runs of 300000 steps for each N, followed by the polar iteration. All 4 runs end at the same value, for each N, and the results are as follows, with the exact values coming from `optimal.py`, which contains the sign matrices at $N = 6, 7, 9, 11$, and computes the characteristic polynomials of SS^t over the integers, and from `bounds.py` at $N = 14$:

N	best value of $Tr\|S\|$	numeric	divided by $N^{3/2}$	comment
5	11	11.0000	0.9839	optimal, K_5
6	$8 + 2\sqrt{10}$	14.3246	0.9747	optimal
7	$1 + 12\sqrt{2}$	17.9706	0.9703	optimal, Fano plane
9	$2 + 12\sqrt{2} + \sqrt{57}$	26.5204	0.9822	
10	$22\sqrt{2}$	31.1127	0.9839	optimal, $K_5 \otimes H_2$
11	see below	35.7007	0.9786	new
13	$5 + 24\sqrt{3}$	46.5692	0.9935	optimal, plane of order 3
14	$24\sqrt{3} + 2\sqrt{26}$	51.7673	0.9882	optimal

Here the optimality at $N = 10, 13, 14$ will be proved in the next section. These values are to be compared with those in the table from [6], which lists the best matrices known there up to $N = 13$, and with those from [32], up to $N = 24$. At $N = 5, 7, 10, 13$ we recover the matrices from [6], at $N = 6, 9, 14$ we recover the values from [32], with closed forms at $N = 9, 14$, and at $N = 11$ we obtain a better matrix. At $N = 6$ the value $8+2\sqrt{10}$, found in [32], is above the value $10\sqrt{2} = 14.1421$ from [6], and the sign matrix of the optimal matrix, and the optimal matrix $U_6 = Pol(S_6)$ itself, are as follows, with $a = 1/\sqrt{10}$, $b = 1/3+1/(3\sqrt{10})$ and $c = 2/3-1/(3\sqrt{10})$, that is, $a = 0.316$, $b = 0.439$, $c = 0.561$, as computed by `pictures.py`:

$$S_6 = \begin{pmatrix} + & + & + & + & + & + \\ + & - & - & - & + & + \\ + & - & - & + & - & + \\ + & - & - & + & + & - \\ + & - & + & - & - & - \\ + & + & - & - & - & - \end{pmatrix} \qquad U_6 = \begin{pmatrix} c & b & b & a & a & a \\ a & -a & -a & -c & b & b \\ a & -a & -a & b & -c & b \\ a & -a & -a & b & b & -c \\ b & -b & c & -a & -a & -a \\ b & c & -b & -a & -a & -a \end{pmatrix}$$

We have $Tr|S_6| = 8 + 2\sqrt{10}$, the singular values being $\sqrt{10}$, with multiplicity 2, and 2, with multiplicity 4. At $N = 7$ the top level is that of the Fano plane, as explained above, and the second level, $11 + 4\sqrt{3}$, is that of the matrix S_7' below. At $N = 9$ the best matrix that we know is S_9 below, the eigenvalues of $S_9 S_9^t$ being 8, with multiplicity 6, then $(29 \pm \sqrt{57})/2$, and 4:

$$S_7' = \begin{pmatrix} + & + & + & + & + & + & + \\ + & - & - & - & - & - & + \\ + & - & + & - & - & + & - \\ + & + & - & - & - & + & - \\ + & - & - & + & + & - & - \\ + & + & + & - & + & - & - \\ + & + & + & + & - & - & - \end{pmatrix} \qquad S_9 = \begin{pmatrix} + & - & - & - & + & + & + & - & - \\ + & + & - & + & + & + & - & - & + \\ + & + & - & - & - & - & + & + & + \\ + & - & + & + & + & + & + & + & + \\ - & + & - & + & + & + & + & + & - \\ + & + & + & - & - & + & - & + & - \\ - & + & + & - & + & + & + & - & + \\ - & - & - & + & - & + & + & - & + \\ + & + & + & + & - & - & + & - & - \end{pmatrix}$$

Both these matrices are the sign matrices of their polar parts, as verified by `optimal.py`. At $N = 11$ the matrix of the Paley biplane has 1-norm $1 + 20\sqrt{3} = 35.6410$, the best previous

value is 35.6991, from [32], and the sign matrix found by the annealing is as follows:

$$S_{11} = \begin{pmatrix} + & + & + & + & + & - & - & + & + & - & - \\ + & + & + & - & + & + & + & + & + & + & - \\ - & - & + & - & + & + & - & + & + & + & + \\ + & - & + & - & + & - & - & - & - & + & - \\ + & + & + & - & - & + & - & + & - & - & + \\ - & - & - & + & + & + & + & + & - & - & - \\ - & + & + & - & + & - & + & - & - & - & + \\ + & - & + & + & + & + & + & - & + & - & + \\ + & - & - & - & + & - & + & + & + & - & + \\ - & - & + & - & - & - & + & + & + & - & - \\ - & + & - & - & + & + & - & - & + & - & - \end{pmatrix}$$

The eigenvalues of $S_{11}S_{11}^t$ are 12, with multiplicity 4, then $12 \pm 4\sqrt{2}$, each with multiplicity 2, then $(21 \pm \sqrt{41})/2$, and 4, and this gives the following formula:

$$Tr|S_{11}| = 2 + 8\sqrt{3} + \sqrt{41} + 4\sqrt{6 + 2\sqrt{7}} = 35.7006\ldots$$

The upper bounds from the next section are 26.7505 at $N = 9$ and 36.2054 at $N = 11$, so S_9 and S_{11} are within 0.9% and 1.4% of them. We do not know if these 2 matrices are optimal.

In the language of the switching game from Section 1, the dual model is a game for the designer of the board, who chooses which lamps are lit, the goal being to maximize the energy $Tr|S|$ of the board. Figure 28 shows the boards of S_6, of the Paley biplane, and of S_{11}.

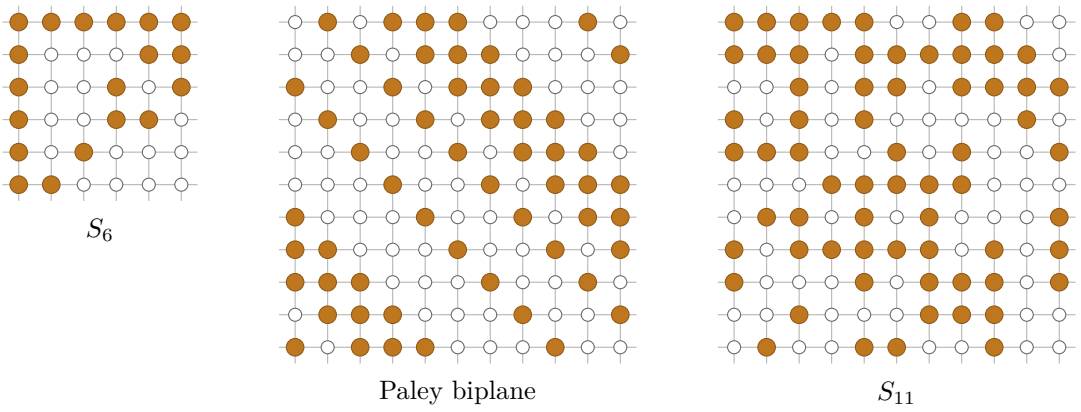

Figure 28: The boards of the sign matrix S_6, which maximizes $Tr|S|$, of the Paley biplane, and of S_{11}, whose energy is higher than that of the Paley biplane. The lamps are lit at the entries 1.

Summarizing, the dual model gives the exact maxima up to $N = 7$, and lower bounds afterwards. We have the following result, the first 2 assertions being known from [32], in terms of Schur norms, and the last one improving the bound 35.6991 from there:

Theorem 7.2. *The maximum m_N of the 1-norm on O_N is as follows:*

1. *$m_5 = 11$, $m_6 = 8 + 2\sqrt{10}$ and $m_7 = 1 + 12\sqrt{2}$, by exhaustive search.*
2. *At $N = 7$ any maximizer is obtained from the matrix U_+ of the Fano plane by permuting the rows and columns, and changing their signs.*
3. *$m_9 \geq 2 + 12\sqrt{2} + \sqrt{57}$, and $m_{11} \geq 35.7006$, the Paley biplane giving $1 + 20\sqrt{3} = 35.6410$.*

Proof. (1,3) This follows from Proposition 7.1 and from the above computations, the sign matrices at $N = 6, 7, 9, 11$ being indeed the sign matrices of their polar parts.

(2) By Proposition 7.1 it is enough to show that the maximizers of $Tr|S|$ are the sign matrices obtained from $S = 2M - \mathbb{I}$, with M being the incidence matrix of the Fano plane, by permuting the rows and columns, and changing their signs. All these matrices are maximizers. In order to count them, assume $PSQ = S$, with P, Q being signed permutation matrices. Then P commutes with $SS^t = 8 - \mathbb{I}$, so $P\xi = \pm\xi$, and similarly $Q\xi = \pm\xi$. Thus, up to a common sign, P, Q are permutation matrices, which must form an automorphism of the Fano plane. Since there are 168 such automorphisms, the number of matrices in question, modulo the sign changes, is $(7!)^2/168 = 151200$. But this is precisely the number of maximizers found by `seven.py`, and we are done. □

Thus the Fano plane is the crystal of the hard matrix model at $N = 7$, which is unique, up to the symmetries of the model.

The energy levels found above have a common explanation, coming from the submatrices of the Hadamard matrices. Consider a Hadamard matrix of order $N = r + d$, with $r \leq d$, written in block form, with square blocks $A \in M_r(\pm 1)$ and $D \in M_d(\pm 1)$ on the diagonal:

$$H = \begin{pmatrix} A & B \\ C & D \end{pmatrix}$$

The matrices A, D are called complementary, and they are related by the following result, due to Szöllősi [57] for the first assertion, and coming from [5] for the other ones:

Theorem 7.3. *With the above notations, the following hold:*

1. *The singular values of D are those of A, and $\sqrt{N}$ with multiplicity $d - r$. In particular we have $Tr|D| = Tr|A| + (d - r)\sqrt{N}$ and $|\det D| = N^{(d-r)/2}|\det A|$.*
2. *When A is invertible, $\sqrt{N}\, Pol(D) = D - E$, where $E = C(\sqrt{N} + |A|)^{-1} Pol(A)^t B$.*
3. *When the entries of E are smaller than 1 in absolute value, which is the case for $r \leq 3$, and for A Hadamard with $N > r(r-1)^2$, the matrix D is the sign matrix of its polar part, which is a plain local maximizer of the 1-norm on O_d.*

Proof. (1) The orthogonality of the rows and of the columns of H gives $AA^t + BB^t = N$ and $B^tB + D^tD = N$, and the result follows from the fact that BB^t and B^tB have the same eigenvalues, up to $d - r$ values of 0.

(2) By using the other orthogonality relations, the singular value decompositions of the 4 blocks can be chosen in a compatible way, with only 4 orthogonal matrices involved, and the formula follows by multiplying. See [5], and [60] for the complex case.

(3) Here $Pol(D)$ has the same signs as D, and since $D^tPol(D) = |D|$ is positive, Theorem 6.2 applies. As for the estimates, with $||.||_\infty$ being the biggest absolute value of the entries, we have $||E||_\infty \leq r^2||(\sqrt{N} + |A|)^{-1} Pol(A)^t||_\infty$, which is $r\sqrt{r}/(\sqrt{r} + \sqrt{N})$ when A is Hadamard, and at $r \leq 3$ the matrix E can be computed explicitly [5]. □

At $r = 1$, with H normalized as to have 1 entries on its first row and column, the matrix D is the core of H. This is the sign matrix $S = 2M - \mathbb{I}$ of a Hadamard design, with $v = N - 1$, and any Hadamard design appears in this way [56]. Here $A = (1)$ and $E = \mathbb{I}/(1 + \sqrt{N})$, so we recover the matrices U_+ of the Hadamard designs, in the form $\sqrt{N}\, U_+ = S - \mathbb{I}/(1 + \sqrt{N})$, and with $Tr|D| = 1 + (N - 2)\sqrt{N}$. In general, the program `detours.py` goes through the complements of the small submatrices of the Hadamard matrices of order 8 and 12, which are unique up to equivalence, with the following results:

order	inside	r	A	$Tr\|D\|$	numeric	comment
5	H_8	3	invertible	$5+4\sqrt{2}$	10.6569	second level
6	H_8	2	Hadamard	$10\sqrt{2}$	14.1421	second level
7	H_8	1	(1)	$1+12\sqrt{2}$	17.9706	top level, Fano plane
7	H_{12}	5	optimal	$11+4\sqrt{3}$	17.9282	second level, S_7'
9	H_{12}	3	invertible	$5+12\sqrt{3}$	25.7846	below S_9
10	H_{12}	2	Hadamard	$2\sqrt{2}+16\sqrt{3}$	30.5412	below $K_5 \otimes H_2$
11	H_{12}	1	(1)	$1+20\sqrt{3}$	35.6410	Paley biplane

Thus all the second levels found by the exhaustive searches come from complements. The case of S_7' is particularly interesting: this matrix is equivalent to the complement, inside H_{12}, of the optimal matrix of order 5, whose energy is $m_5 = 11$, and whose determinant is 48. By (1) its determinant is $12 \cdot 48 = 576$, which is the maximal determinant at order 7, and we will come back to this in the next section. This is an instance of the embedding of the maximal determinant matrices into the Hadamard matrices, studied in [54], with the minors of the Hadamard matrices themselves being computed in [39], [55].

As a last comment, the smallness assumption in (3) is needed. As shown in [5], the Walsh matrix of order 8 has a 4×4 submatrix whose polar part has a zero entry, lying therefore on a wall, and H_{12} has 7×7 submatrices which are not the sign matrices of their polar parts. The program `detours.py` finds that this latter phenomenon is not rare: among the complements of the invertible 5×5 submatrices of H_{12}, about one third are not the sign matrices of their polar parts.

8 Conference matrices, the upper bounds

We have seen that the dual model gives the optimal matrices up to $N = 7$. In this section we go beyond this, with upper bounds for the 1-norm, which are attained at $N = 5, 6, 10, 13, 14$. Let us start with the orders $N = 6, 10, 14$, where a second construction of Paley is available [50]. For a prime power $q = 1(4)$ the Paley graph has as vertices the elements of $\mathbb{F}_q$, with 2 vertices being joined when their difference is a square. With A being the adjacency matrix of this graph, and with $\bar{A}$ being that of the complementary graph, the matrix $A - \bar{A}$, bordered with a first row and a first column of 1 entries, and with 0 on the diagonal, is a conference matrix: it has order $N = q + 1$, and it satisfies $CC^t = q$. The Paley graphs are strongly regular, with parameters $(q, (q-1)/2, (q-5)/4, (q-1)/4)$, as mentioned in Section 3. Figure 29 shows the Paley graphs of order $5, 9, 13$.

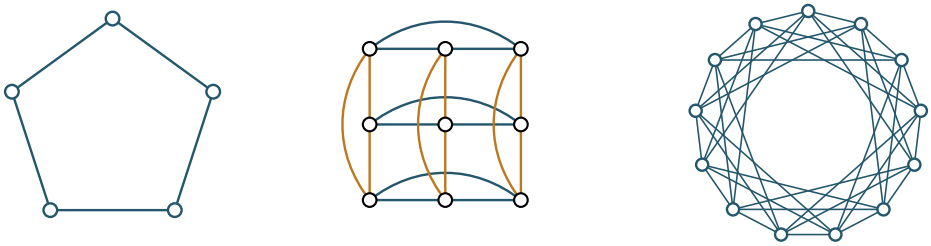

order 5 order 9 order 13

Figure 29: The Paley graphs of order $5, 9, 13$: the pentagon, the graph of the moves of a rook on a 3×3 board, where each row and each column is a triangle, and the graph on $\mathbb{Z}_{13}$ where i, j are joined when $i - j = \pm 1, \pm 3, \pm 4$.

The matrix $U = C/\sqrt{q}$ is orthogonal, but has N zero entries, so it is not almost Hadamard. In the language of Section 6, this matrix lies on N walls at the same time, and here is what the

1-norm does around it:

Proposition 8.1. *Let C be a symmetric conference matrix of order $N = q + 1$, and set $U = C/\sqrt{q}$.*

1. *We have $||U||_1 = N\sqrt{N-1}$.*
2. *For any antisymmetric matrix A we have $||Ue^{tA}||_1 = N\sqrt{N-1} + |t| \sum_i |(UA)_{ii}| + O(t^2)$.*

In particular the 1-norm increases, linearly, in any direction which is transverse to the walls.

Proof. (1) is clear, U having $N^2 - N$ nonzero entries, equal to $\pm 1/\sqrt{q}$. As for (2), the entries of Ue^{tA} are $U_{ij} + t(UA)_{ij} + O(t^2)$. The off-diagonal ones contribute to the 1-norm with $|U_{ij}| + t\, C_{ij}(UA)_{ij}$, and since $C_{ii} = 0$, the sum of the terms of order 1 is $t\, Tr(C^t UA) = t\sqrt{q}\, Tr(A) = 0$. The diagonal entries contribute with $|t||(UA)_{ii}|$, and this gives the result. □

Thus U is the bottom of a funnel, surrounded by 2^N sign regions, which correspond to the sign matrices $S = C + D$ obtained by filling the diagonal of C with signs. For the pentagon the conference matrix, and its best filling, which is the one with $D = diag(1, 1, 1, -1, -1, -1)$, are as follows:

$$C_6 = \begin{pmatrix} 0 & + & + & + & + & + \\ + & 0 & + & - & - & + \\ + & + & 0 & + & - & - \\ + & - & + & 0 & + & - \\ + & - & - & + & 0 & + \\ + & + & - & - & + & 0 \end{pmatrix} \qquad S_6' = \begin{pmatrix} + & + & + & + & + & + \\ + & + & + & - & - & + \\ + & + & + & + & - & - \\ + & - & + & - & + & - \\ + & - & - & + & - & + \\ + & + & - & - & + & - \end{pmatrix}$$

The program `portraits.py` finds that $Tr|S_6'| = 8 + 2\sqrt{10}$, the eigenvalues of $S_6' S_6'^t$ being 10, with multiplicity 2, and 4, with multiplicity 4, as for the matrix S_6. Thus the optimal matrix at $N = 6$ comes from the pentagon. In general, the fillings can be estimated as follows:

Proposition 8.2. *Let C be a symmetric conference matrix of order N, and let D be a diagonal sign matrix, of trace τ. Then, with the remainder being bounded independently of N, D, we have*

$$Tr|C + D| = N\sqrt{N} - \left(1 + \frac{\tau^2}{N^2}\right)\frac{\sqrt{N}}{4} + O(1)$$

so all the fillings with $\tau = o(N)$ have the same deficit, namely $\sqrt{N}/4$, at this order.

Proof. With $S = C + D$ we have $S^2 = N + E$, where $E = CD + DC$, and so $Tr|S| = \sqrt{N}\, Tr\sqrt{1 + E/N}$. Since the eigenvalues of E/N are at most $2/\sqrt{N}$ in absolute value, the Taylor formula for the square root gives, with a remainder as in the statement:

$$Tr|S| = N\sqrt{N} + \frac{Tr(E)}{2\sqrt{N}} - \frac{Tr(E^2)}{8N\sqrt{N}} + O(1)$$

Now $Tr(E) = 2\, Tr(CD) = 0$, and $Tr(E^2) = 2\, Tr(CDCD) + 2\, Tr(C^2) = 2(\tau^2 - N) + 2N(N - 1)$, because $Tr(CDCD) = \sum_{i \neq j} D_{ii} D_{jj}$. This gives the formula in the statement. □

Thus a balanced filling halves the deficit of the conference matrix, which is of $\sqrt{N}/2$. The program `detours.py` goes through all the fillings at $N = 6, 10, 14$, with the following results:

N	fillings	values of $Tr\|S\|$	smallest	largest	best fillings	local maximizers
6	64	5	13.4164	14.3246	10	62
10	1024	11	30.0000	30.9756	90	1022
14	16384	30	50.4777	51.5940	78	16382

Here the last column counts the fillings which are the sign matrices of their polar parts, these polar parts being then plain local maximizers of the 1-norm, by Theorem 6.2. This happens for all the fillings, except for $D = \pm 1$, where the polar part is U itself, and where $Tr|S| = N\sqrt{N-1}$ is the smallest value in the table. Thus the funnel is surrounded by $2^N - 2$ local maximizers, one in each of the neighboring sign regions.

It is instructive to compare these fillings with the complements from Theorem 7.3, at $r = 2$. At $N = 6, 10, 14$ these complements, taken inside the Hadamard matrices of order $8, 12, 16$, have energy $(N-2)\sqrt{N+2} + 2\sqrt{2}$, which is 14.1421, 30.5412 and 50.8284 respectively, and in each case this is below the energy of the best filling, in agreement with Proposition 8.2, which gives a deficit of $\sqrt{N}/4$ for the fillings, against a deficit of $\sqrt{N}$ for the complements. Thus at $N = 2(4)$ the conference matrices are a better starting point than the Hadamard matrices, the point being that a conference matrix is only N entries away from a sign matrix of the same order.

However, the fillings are not optimal either. At $N = 10, 14$ the best fillings give $Tr|S|/N^{3/2} = 0.9795$ and 0.9849, which is less than what the annealing finds, namely the value $22\sqrt{2}$ at $N = 10$, with ratio 0.9839, and the following matrix at $N = 14$, with ratio 0.9882, the eigenvalues of $S_{14}S_{14}^t$ being 26, with multiplicity 2, and 12, with multiplicity 12:

$$S_{14} = \begin{pmatrix}
+ & - & + & + & + & - & - & + & - & - & + & - & - & - \\
- & - & + & - & - & + & + & - & - & - & - & - & - & + \\
- & + & - & + & + & - & + & - & - & - & - & - & + & - \\
+ & + & + & - & - & - & + & + & + & - & - & + & - & - \\
+ & + & - & - & - & + & + & + & - & - & + & - & + & + \\
+ & - & + & + & + & + & + & + & - & + & - & + & + & - \\
- & - & - & - & + & - & - & + & - & - & - & + & + & + \\
+ & - & - & - & - & - & - & - & - & + & - & - & + & - \\
+ & + & + & - & + & + & - & - & + & - & - & - & + & + \\
+ & + & + & - & + & - & + & - & - & + & + & + & - & + \\
- & - & + & - & + & - & + & + & + & + & + & - & + & - \\
- & + & + & + & - & - & - & + & - & + & - & - & + & + \\
- & + & + & - & - & + & - & - & - & - & + & + & + & - \\
- & + & - & - & + & + & - & + & - & + & - & - & - & - \\
\end{pmatrix}$$

The eigenvalues found at $N = 6, 10, 14$, namely $2N-2$, with multiplicity 2, and $N-2$, with multiplicity $N-2$, and those of the design matrices at $N = 5, 13$, namely $2N-1$, and $N-1$ with multiplicity $N-1$, are familiar from the maximal determinant problem of Hadamard, where they correspond to the upper bounds of Barba [7] and of Ehlich and Wojtas [24], [61]. See [12]. As we will show now, the same happens for the trace norm. We start with:

Proposition 8.3. *Let $G \in M_m(\mathbb{R})$ be a positive matrix having all its diagonal entries equal to N, and whose off-diagonal entries satisfy $|G_{ij}| \geq c$, where $0 < c < N$. Then*

$$Tr\sqrt{G} \leq (m-1)\sqrt{N-c} + \sqrt{N+(m-1)c}$$

with equality precisely when the eigenvalues of G are $N+(m-1)c$, and $N-c$ with multiplicity $m-1$.

Proof. Set $a = N - c$ and $b = N + (m-1)c$, and let $\lambda_1 \geq \ldots \geq \lambda_m \geq 0$ be the eigenvalues of G. By computing the traces of G and G^2 we obtain:

$$\sum_i \lambda_i = mN = (m-1)a + b \quad , \quad \sum_i \lambda_i^2 = \sum_{ij} G_{ij}^2 \geq mN^2 + m(m-1)c^2 = (m-1)a^2 + b^2$$

Assume first $\lambda_1 \geq b$. The Cauchy-Schwarz inequality, applied to the other eigenvalues, gives $Tr\sqrt{G} \leq \varphi(\lambda_1)$, where $\varphi(t) = \sqrt{t} + \sqrt{(m-1)(mN-t)}$. This function is decreasing on $[N, mN]$, and since $b \geq N$, we obtain $Tr\sqrt{G} \leq \varphi(b) = \sqrt{b} + (m-1)\sqrt{a}$, as desired.

Assume now $\lambda_1 \leq b$, and let q be the polynomial of degree 2 satisfying $q(a) = \sqrt{a}$, $q'(a) = 1/(2\sqrt{a})$ and $q(b) = \sqrt{b}$. By the formula of the remainder in the Hermite interpolation, for any $x > 0$ there is a number $\xi > 0$ such that:

$$\sqrt{x} - q(x) = \frac{1}{16}\,\xi^{-5/2}(x-a)^2(x-b)$$

Thus $\sqrt{x} \leq q(x)$ on $[0, b]$, and so $Tr\sqrt{G} \leq \sum_i q(\lambda_i)$. Now since the square root is strictly concave, the coefficient of x^2 in q is negative, so the quantity $\sum_i q(\lambda_i)$, which depends only on $\sum_i \lambda_i$ and $\sum_i \lambda_i^2$, decreases when $\sum_i \lambda_i^2$ increases. Thus this quantity is at most the value that it takes when the eigenvalues are b, and a with multiplicity $m-1$, which is $(m-1)q(a)+q(b) = (m-1)\sqrt{a}+\sqrt{b}$. Finally, the equality case is clear from the above, because in the first case we must have $\lambda_1 = b$ and $\lambda_2 = \ldots = \lambda_m$, and in the second case we must have $\lambda_i \in \{a, b\}$ for any i, with the value b appearing once, because the sum of the eigenvalues is $(m-1)a + b$. □

With this in hand, we can prove the analogues of the bounds of Barba and of Ehlich and Wojtas, for the trace norm, and so for the almost Hadamard matrices. As for the determinant, the point is that the entries of SS^t are subject to parity constraints:

Theorem 8.4. *The maximum m_N of the 1-norm on O_N is subject to the following bounds:*

1. $m_N \leq (N-1)\sqrt{N-1} + \sqrt{2N-1}$, *for N odd.*
2. $m_N \leq (N-2)\sqrt{N-2} + 2\sqrt{2N-2}$, *for $N = 2(4)$.*
3. *We have equality at $N = 5, 13$ and at $N = 6, 10, 14$. Thus $m_{10} = 22\sqrt{2}$, then $m_{13} = 5 + 24\sqrt{3}$, the matrix of the projective plane of order 3 being optimal, and $m_{14} = 24\sqrt{3} + 2\sqrt{26}$.*

Proof. By Proposition 7.1 we have to bound the quantity $Tr|S| = Tr\sqrt{G}$, where $S \in M_N(\pm 1)$ and $G = SS^t$. The diagonal entries of G are equal to N.

(1) When N is odd the off-diagonal entries of G are odd numbers, and the result follows from Proposition 8.3, applied with $m = N$ and $c = 1$, the case $N = 1$ being trivial.

(2) At $N = 2$ the bound is $2\sqrt{2}$, which is the 1-norm of the rescaled Hadamard matrix. Assume now $N = 2(4)$ with $N \geq 6$, and let w_i be the number of -1 entries on the i-th row of S. The rows i, j differ at d_{ij} places, with $d_{ij} = w_i + w_j(2)$, and we have $G_{ij} = N - 2d_{ij}$. Thus, if we put first the rows with w_i even, and then those with w_i odd, the 2 diagonal blocks G', G'' of G that we obtain, of sizes $n' + n'' = N$, have off-diagonal entries equal to 2 modulo 4. Now observe that the matrix having G', G'' as diagonal blocks, and 0 elsewhere, is the average of G and VGV, where $V = diag(1, \ldots, 1, -1, \ldots, -1)$. Since the function $X \to Tr\sqrt{X}$ is concave on the positive matrices [10], by using Proposition 8.3 with $c = 2$ we obtain:

$$Tr\sqrt{G} \leq Tr\sqrt{G'} + Tr\sqrt{G''} \leq (N-2)\sqrt{N-2} + \sqrt{N-2+2n'} + \sqrt{N-2+2n''}$$

Here we have used the fact that the bound in Proposition 8.3 holds as well, trivially, for the matrices of size $m = 0, 1$. Since the square root is concave, the sum of the last 2 terms is at most $2\sqrt{2N-2}$, and this gives the result.

(3) At $N = 5, 13$ the bound is attained by the sign matrices of the trivial design and of the projective plane of order 3, by Proposition 3.3. At $N = 6, 10, 14$ it is attained by the matrix S_6, by the sign matrix of $K_5 \otimes H_2$, and by the above matrix S_{14}. The program `bounds.py` checks all this in exact arithmetic. □

As a first comment, the equality cases are the same as for the determinant. In (1) the eigenvalues of SS^t must be $2N-1$, and $N-1$ with multiplicity $N-1$, so $2N-1$ must be a square, and up to sign changes of the rows we must have $SS^t = N - 1 + \mathbb{I}$, which is the equality case in the bound of Barba. In (2) the matrices G', G'' must be of size $N/2$, and of the form

$N-2+2\mathbb{I}$, up to sign changes, with G vanishing outside these 2 blocks, the function $X \to Tr\sqrt{X}$ being strictly concave, which is the equality case in the bound of Ehlich and Wojtas, and which requires $2N-2$ to be a sum of 2 squares. Thus our bounds are attained precisely when the determinant bounds are, for instance at $N = 25$, or at $N = 18, 26$, see [12]. In general, however, the 2 problems are different. At $N = 7$ the maximal determinant is 576, and `bounds.py` finds that this is the determinant of the matrix S'_7, lying on the second level of our model, while the sign matrix of the Fano plane has determinant 512.

In terms of the previous work on the subject, the above result shows that the best matrices known at $N = 10, 13, 14$, from [6], [32], are optimal, and the same will happen at $N = 18$, in the next section. The sign matrices appearing in the equality cases are well-known in statistics too, as chemical balance weighing designs, and they are shown there to be optimal with respect to large classes of spectral criteria, see Cheng [17] and Jacroux, Wong and Masaro [36]. What we have here is a short proof for the trace norm, with bounds which hold at any order, including those where they are not attained, and with the translation in terms of almost Hadamard matrices.

In the odd case we can go further, and find all the matrices attaining the bound, at any N, because the equality case leads to a design, with very special parameters:

Theorem 8.5. *The bound $m_N \leq (N-1)\sqrt{N-1} + \sqrt{2N-1}$ at $N > 1$ odd has the following properties:*

1. *It is attained precisely when $N = 2q^2+2q+1$ for some $q \geq 1$, and there exists a symmetric design with parameters $(N, q^2, q(q-1)/2)$.*

2. *In this case the sign matrices maximizing $Tr|S|$ are the matrices $S = 2M - \mathbb{I}$ coming from such designs, up to permutations and sign changes of the rows and columns, and the optimal almost Hadamard matrices are the corresponding matrices U_+.*

3. *At $N = 5, 13$ the design is unique, and the number of maximizers, modulo the sign changes, is $(5!)^2/120 = 120$, respectively $(13!)^2/5616$.*

Proof. (1,2) Let S be a matrix attaining the bound. By the equality case in Proposition 8.3, and by its proof, the matrix $G = SS^t$ has eigenvalues $2N-1$, and $N-1$ with multiplicity $N-1$, and its off-diagonal entries are ± 1. Thus $G-(N-1)$ is a positive matrix of rank one, with 1 on the diagonal, so it is of the form ww^t with $w \in \{\pm 1\}^N$, and by changing the signs of the rows we can assume $SS^t = N-1+\mathbb{I}$. The same applies to the matrix S^tS, which has the same eigenvalues, so by changing the signs of the columns we can assume $S^tS = N-1+\mathbb{I}$ too. Now $S(S^tS) = (SS^t)S$ gives $S\mathbb{I} = \mathbb{I}S$, so all the row and column sums of S are equal to a number r, with $r^2 = 2N-1$, coming from $SS^t\xi = r^2\xi$. Thus $2N-1$ is a square, and by changing the sign of S we can assume $r = -(2q+1)$ with $q \geq 1$, so that $N = 2q^2+2q+1$. With $S = 2M - \mathbb{I}$ the matrix M has $(N+r)/2 = q^2$ entries equal to 1 on each row and column, and we obtain:

$$MM^t = \frac{N-1}{4} + \frac{N+1+2r}{4}\,\mathbb{I} = \frac{q(q+1)}{2} + \frac{q(q-1)}{2}\,\mathbb{I}$$

Thus M is the incidence matrix of a design as in the statement. Conversely, for such a design we have $n = q(q+1)/2$ and $v-2k = 2q+1$, so Theorem 3.4 gives $||U_+||_1 = 2(N-1)\sqrt{n}+2q+1$, and this is the bound, because $4n = N-1$ and $(2q+1)^2 = 2N-1$.

(3) At $q = 1$ the matrix M is a permutation matrix, and at $q = 2$ we obtain the projective plane of order 3, which is known to be unique, up to isomorphism [31]. As in the proof of Theorem 7.2, the number of matrices is $(N!)^2$ divided by the order of the automorphism group of the design, which is 120, respectively 5616, by `portraits.py`. □

In particular the crystal of the hard matrix model at $N = 13$ is unique, up to the symmetries of the model. The designs in the above statement are known to exist when q is an odd prime

power, by a construction of Brouwer, and at $q = 2, 4$ as well, see [12]. Thus the optimal almost Hadamard matrices are design matrices at infinitely many orders, starting with $N = 5, 13, 25, 41, 61$, where $m_{25} = 7 + 48\sqrt{6}$, then $m_{41} = 9 + 80\sqrt{10}$, and $m_{61} = 11 + 120\sqrt{15}$. The first open case is $q = 6$, where $N = 85$. A similar discussion applies at $N = 2(4)$, where the matrices attaining the bound are those from the determinant theory, and we will construct such matrices in the next section.

At $N = 5$ we recover in this way the number of maximizers found by the exhaustive search, and at $N = 13$ the number of maximizers is 6904520663040000. In order to see where we stand at the other orders, let us write $Tr|S| = N\sqrt{N} - \delta\sqrt{N} + O(1)$. The values of δ, computed by `detours.py`, are as follows:

matrices	order	δ
upper bound	N odd	$3/2 - \sqrt{2} = 0.0858$
upper bound	$N = 2(4)$	$3 - 2\sqrt{2} = 0.1716$
balanced fillings	$N = q + 1$	$1/4$
conference matrices	$N = q + 1$	$1/2$
Hadamard designs	$N = 4n - 1$	$1/2$
complements, $r = 2$	$N = 4n - 2$	1
complements, $r = 3$	$N = 4n - 3$	$3/2$

Thus at $N = 2(4)$ the fillings of the Paley conference matrices reach $\delta = 1/4$, which is not far from the upper bound, and the gap is closed at the orders where the bound of Ehlich and Wojtas is attained. At $N = 3(4)$ the Hadamard designs give $\delta = 1/2$, and the upper bound for N odd applies, but can never be attained, because $2N - 1$ is not a square there. As for $N = 1(4)$, here Theorem 7.3 gives $m_N \geq 5 + (N - 3)\sqrt{N + 3}$ whenever there is a Hadamard matrix of order $N + 3$, the energy of an invertible sign matrix of order 3 being 5, and this corresponds to $\delta = 3/2$.

Question 8.6. What are the values of m_9 and m_{11}, where the above bounds, 26.7505 and 36.2054, are not attained? In general, what is the analogue of the bound of Ehlich at $N = 3(4)$?

At $N = 9$ and $N = 11$ we only know that $m_9 \geq 2+12\sqrt{2}+\sqrt{57} = 26.5204$ and $m_{11} \geq 35.7006$, by Theorem 7.2. As for an exhaustive search at $N = 9$, of the type of the one done at $N = 7$, this would involve the multisets of 8 vectors in $\{\pm 1\}^8$, which are about $5.1 \cdot 10^{14}$ in number, and is out of reach for our programs.

As a conclusion, here is where we stand at the orders $N \leq 24$ where the maximum m_N is not known, taking into account Theorem 9.7 below, which deals with $N = 18$. The lower bounds are those from [32], except at $N = 11$, the values at $N = 9, 17$ being $2 + 12\sqrt{2} + \sqrt{57}$ and $60 + \sqrt{89}$, and the upper bounds are those from Theorem 8.4:

N	lower bound	from	upper bound	gap
9	26.5204	[32]	26.7505	0.86%
11	35.7006	Theorem 7.2	36.2054	1.39%
15	57.1522	[32]	57.7684	1.07%
17	69.4340	[32]	69.7446	0.45%
19	81.8353	[32]	82.4503	0.75%
21	95.6206	[32]	95.8458	0.24%
22	102.3127	[32]	102.4042	0.09%
23	109.0784	[32]	109.8974	0.75%

Thus the gap between what is known and what is possible is everywhere below 1.4%, and at $N = 22$ it is below 0.1%. At the orders $N \leq 24$ which are not in this table, the maximum m_N is known.

9 Circulant matrices, the spin chains

In the theory of the almost Hadamard matrices from [3], [6], the matrices coming from the block designs stand next to the circulant ones. In fact, the 8 designs from Section 3 come from cyclic difference sets, so their matrices $U_\pm$ are circulant. We discuss here the circulant case, which has its own physics. A circulant sign matrix is the same thing as a sequence of N spins $s_0, \ldots, s_{N-1}$, placed on a ring, with the matrix being $S = (s_{j-i})_{ij}$, with the indices taken modulo N. The dual model becomes in this way a spin chain, whose energy is best understood in terms of the Fourier transform $\widehat{s}_k = \sum_j s_j w^{jk}$, where $w = e^{2\pi i/N}$:

Proposition 9.1. *Let S be the circulant matrix of a sequence of signs $s_0, \ldots, s_{N-1}$.*

1. *The singular values of S are the numbers $|\widehat{s}_k|$, and so $Tr|S| = \sum_k |\widehat{s}_k|$.*
2. *We have $N \leq Tr|S| \leq N\sqrt{N}$, with equality at left when the sequence is constant, or alternating with N even, and at right when S is a circulant Hadamard matrix.*
3. *When the numbers $\widehat{s}_k$ are nonzero, $Pol(S)$ is the circulant matrix of the sequence given by $\gamma_j = \frac{1}{N}\sum_k \varphi_k w^{-jk}$, where $\varphi_k = \widehat{s}_k/|\widehat{s}_k|$.*

Proof. The vectors $(w^{jk})_j$ are eigenvectors of S, with eigenvalues $\widehat{s}_k$, and since these vectors are pairwise orthogonal, S is normal, which gives (1) and (3). As for (2), we have $\sum_k |\widehat{s}_k|^2 = N^2$ and $|\widehat{s}_k| \leq N$. Thus $\sum_k |\widehat{s}_k| \geq \sum_k |\widehat{s}_k|^2/N = N$, with equality when the Fourier transform is supported at one point, and $\sum_k |\widehat{s}_k| \leq N\sqrt{N}$ by Cauchy-Schwarz, with equality when $|\widehat{s}_k| = \sqrt{N}$ for any k. □

Thus we have a chain of N Ising spins, with energy $-\sum_k |\widehat{s}_k|$, whose ground states are the sequences having the flattest possible Fourier transform. This is a close relative of the low autocorrelation model of Bernasconi [9], studied in [41], [42] as a basic example of a system which is glassy without having any disorder: there the energy is $\sum_k |\widehat{s}_k|^4$, up to a constant, and flat spectra are favored too. Observe the unusual feature of such models: the ordered states, such as the ferromagnet, are those of highest energy. Figure 30 shows 3 chains at $N = 11$, with their spectra.

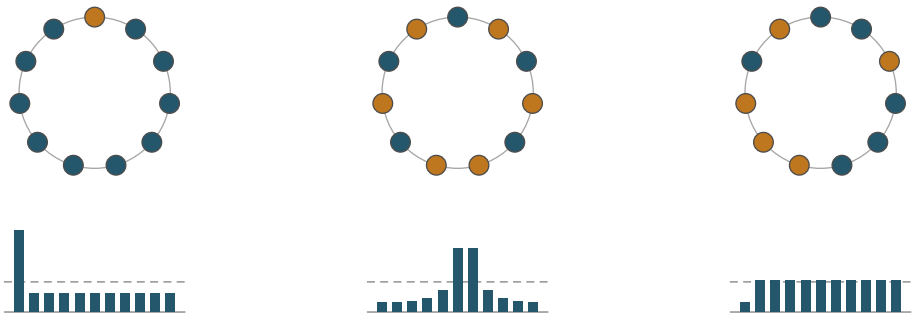

one flipped spin, 29 | alternating chain, 27.38 | Legendre sequence, 35.64

Figure 30: 3 spin chains at $N = 11$, with the spins $+1$ in blue and -1 in gold, and with their energies $Tr|S|$. Below each chain, the absolute values $|\widehat{s}_k|$ of its Fourier transform, for $k = 0, \ldots, 10$, the dashed line being the flat level $\sqrt{N}$. The energy is the total height of the bars, and it is maximal when the spectrum is flat.

The first 2 chains in the figure are well-known in the theory of the almost Hadamard matrices. The first one gives the basic matrix $K_N/\sqrt{N}$, that we met in Section 3 as the matrix U_+ of the trivial design, up to a sign, and the second one gives the circulant matrix found in [6]. With K_N and L_N being the rescaled versions of these matrices, the result is as follows:

Theorem 9.2. *The following sequences are such that S is the sign matrix of $U = Pol(S)$, which is therefore a plain local maximizer of the 1-norm on O_N:*

1. *One flipped spin, at $N \geq 3$. Here $Tr|S| = 3N - 4$, and $U = K_N/\sqrt{N} = 2\mathbb{I}/N - 1$.*
2. *The alternating chain $s_j = (-1)^{\min(j,N-j)}$, at N odd. Here $Tr|S| = \sum_k 1/|\cos(\pi k/N)|$, and $U = L_N/\sqrt{N}$ is the circulant matrix of the sequence $\gamma_j = (-1)^j/(N\cos(\pi j/N))$.*

Proof. This is from [6], the idea being as follows. In the first case we have $\hat{s}_0 = N - 2$ and $\hat{s}_k = -2$ for $k \neq 0$, so $Tr|S| = 3N - 4$, and Proposition 9.1 gives $\gamma_j = 2/N - \delta_{j0}$. In the second case the sequence is a shift of $((-1)^j)_j$, whose Fourier transform is $2/(1 + w^k)$, of absolute value $1/|\cos(\pi k/N)|$, and a similar computation gives γ. In both cases the signs of γ are those of s, so S is the sign matrix of U, and Theorem 6.2 applies. □

The energy of the alternating chain is of order $N \log N$, so both these families are far from the bound $N\sqrt{N}$ when N is big. As an illustration for (2), at $N = 5$ we have $1/\cos(\pi/5) = \sqrt{5} - 1$ and $1/\cos(2\pi/5) = \sqrt{5} + 1$, and so with $x = 1 + \sqrt{5}$ and $y = 1 - \sqrt{5}$ the matrix is:

$$\frac{L_5}{\sqrt{5}} = \frac{1}{5}\begin{pmatrix} 1 & y & x & x & y \\ y & 1 & y & x & x \\ x & y & 1 & y & x \\ x & x & y & 1 & y \\ y & x & x & y & 1 \end{pmatrix}$$

In order to reach flat spectra, we need arithmetics. The third chain in Figure 30 is the Legendre sequence, which is the standard example of a sequence having good correlation properties, and which behaves as follows:

Proposition 9.3. *Let p be an odd prime, with quadratic character χ, and consider the Legendre sequence, $s_0 = 1$ and $s_j = \chi(j)$ for $j \neq 0$, so that $S = 1 + Q$, where $Q = (\chi(j - i))_{ij}$.*

1. *When $p = 3(4)$ we have $Tr|S| = 1 + (p - 1)\sqrt{p + 1}$, and S is, up to a sign and a transposition, the sign matrix of the Paley design.*
2. *When $p = 1(4)$ we have $Tr|S| = 1 + (p - 1)\sqrt{p}$, and $Pol(S) = (\mathbb{I} + \sqrt{p}\,Q)/p$.*

In both cases S is the sign matrix of $Pol(S)$, which is a plain local maximizer of the 1-norm.

Proof. The Gauss sum formula gives $\hat{s}_k = 1 + \chi(k)g$ for $k \neq 0$, where $g = \sqrt{p}$ when $p = 1(4)$, and $g = i\sqrt{p}$ when $p = 3(4)$, and we have $\hat{s}_0 = 1$.

(1) Here $|\hat{s}_k| = \sqrt{p + 1}$ for $k \neq 0$, which gives the formula of $Tr|S|$. Since Q is antisymmetric, and the sign matrix of the Paley design is $Q - 1$, we have the second assertion too.

(2) Here $|\hat{s}_k| = \sqrt{p} + \chi(k)$ for $k \neq 0$, and by summing we obtain the formula of $Tr|S|$. The phases are $\varphi_k = \chi(k)$ for $k \neq 0$, and $\varphi_0 = 1$, so Proposition 9.1 gives, again by using the Gauss sum, $\gamma_0 = 1/p$ and $\gamma_j = (1 + \chi(j)\sqrt{p})/p$ for $j \neq 0$. Since $\sqrt{p} > 1$, the signs are those of S. □

Observe that in (2) the matrix S does not come from a design, the Paley graph having $\lambda = \mu - 1$, so that Proposition 3.5 does not apply. The same computation works for any prime power $q = 1(4)$, with $Q = A - \bar{A}$ coming from the Paley graph, as in Section 8, the matrix $(\mathbb{I} + \sqrt{q}\,Q)/q$ being a plain local maximizer, with 1-norm $1 + (q - 1)\sqrt{q}$, as verified by `chains.py` at $q = 9$. In terms of the table from Section 8 these matrices have $\delta = 1$, which is better than the value $\delta = 3/2$ coming from the complements, at the orders $N = 1(4)$ which are prime powers. At $p = 5$ the Legendre sequence is obtained from the alternating chain by the substitution $j \to 2j$, and we recover the above matrix L_5, with x and y interchanged. Figure 31 shows the polar parts for our 3 chains.

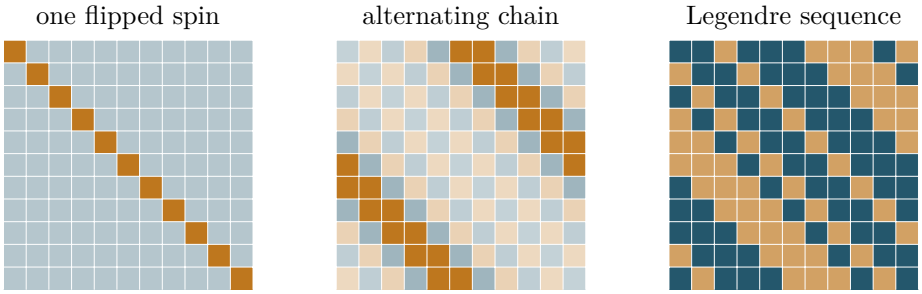

Figure 31: The polar parts of the circulant matrices of the 3 chains from Figure 30, with the positive entries in blue, the negative ones in gold, and the color being proportional to the absolute value. The ordered chains produce matrices concentrated near the diagonal, or near the antidiagonal directions, while the matrix of the Legendre sequence is much flatter.

Let us go now for the ground states. Since there are only 2^N chains, an exhaustive search is possible at orders which are far beyond those from Section 7. The program `chains.py` goes through all the sequences for $N \leq 30$, and its faster version `shamrock.c`, written in C, and using the Gray code, reaches $N = 40$, with $N = 41$ being done by its copy `lamotta.c`. For $N \leq 24$ these maxima were computed in [32], in the form of the Schur norms c_N/N, and our values agree with those found there. The results are as follows, where the energy is the biggest value of $Tr|S|$, the ratio is this value divided by $N\sqrt{N}$, and the last number counts the ground states:

N	energy	ratio	states	N	energy	ratio	states	N	energy	ratio	states
3	5.0000	0.9623	6	16	62.2107	0.9720	256	29	153.8954	0.9854	1624
4	8.0000	1.0000	8	17	68.3489	0.9751	544	30	161.8512	0.9850	960
5	11.0000	0.9839	10	18	74.2765	0.9726	1296	31	170.9639	0.9905	1240
6	14.0000	0.9526	24	19	81.7951	0.9876	684	32	179.1418	0.9896	2048
7	17.9706	0.9703	28	20	88.0000	0.9839	200	33	188.1430	0.9925	1320
8	21.8564	0.9659	32	21	94.7490	0.9846	84	34	195.6605	0.9869	2176
9	25.6851	0.9513	108	22	100.9621	0.9784	880	35	205.3052	0.9915	1680
10	29.7136	0.9396	160	23	108.7775	0.9862	92	36	214.7387	0.9942	3456
11	35.6410	0.9769	44	24	116.7366	0.9929	768	37	223.1908	0.9917	2664
12	40.9706	0.9856	96	25	123.2405	0.9859	1000	38	231.5549	0.9885	2736
13	46.5692	0.9935	104	26	130.4727	0.9841	1248	39	241.9228	0.9933	624
14	50.9706	0.9730	112	27	138.6161	0.9880	1944	40	251.3340	0.9935	2560
15	57.1016	0.9829	480	28	145.9114	0.9848	2688	41	260.4314	0.9920	3280

In all cases the ground states are the sign matrices of their polar parts, and so produce plain local maximizers of the 1-norm. The ratios are between 0.9396, at $N = 10$, and 0.9942, at $N = 36$, if we exclude the circulant Hadamard matrix at $N = 4$. Our main conclusions are:

Theorem 9.4. *The biggest value c_N of the energy $Tr|S|$ over the circulant sign matrices of order N, with $N \leq 41$, has the following properties:*

1. *$c_N = m_N$ at $N = 3, 4, 5, 7, 13$, where the optimal almost Hadamard matrices are circulant.*
2. *At $N = 7, 11, 23$ the ground states are the $4N$ Legendre sequences, from Proposition 9.3.*
3. *At $N = 15, 19$ the cyclic Hadamard designs are not ground states: we have $c_{15} > 57.1015$ and $c_{19} > 81.7950$, the designs having energy 57 and $1 + 18\sqrt{20} = 81.4984$.*
4. *We have $c_N < N\sqrt{N}$ for $4 < N \leq 41$.*

Proof. All this follows from the above table, and from Theorem 7.2 and Theorem 8.4, which give the values of m_N, with $m_3 = 5$ and $m_4 = 8$ being elementary. For (2), the Legendre sequences

are taken here with $s_0 = \pm 1$, and with their opposites and their shifts, so there are $4N$ of them, and Proposition 9.3 and its proof show that they have energy $1 + (N-1)\sqrt{N+1}$, which is the value in the table. □

The last assertion is a verification of the circulant Hadamard conjecture, which states that there is no circulant Hadamard matrix at $N > 4$, see [53]. In our terms, the conjecture says that the spin chain has no perfect crystal, apart from the one at $N = 4$. The conjecture itself is known to hold for much bigger values of N, by arithmetic methods, and what the table brings is quantitative information, on how close to perfection one can get. At $N = 29, 37, 41$ the Legendre sequences have energy 151.7846, 219.9795 and 257.1250, and are not ground states either, and at $N = 9, 11$ the ground states are below the matrices S_9, S_{11} from Section 7, which are not circulant. The same happens at $N = 15, 19$, where the best values known, namely 57.1522 and 81.8353, are those from [32]. Finally, at $N = 25, 41$, where the bound from Theorem 8.5 is attained, we have $c_N < m_N$, the values being 123.2405 against $7 + 48\sqrt{6} = 124.5755$, and 260.4314 against $9 + 80\sqrt{10} = 261.9822$, so the optimal almost Hadamard matrices are not circulant there. At $N = 31$ the Legendre sequence, coming from the Paley design, has energy $1 + 30\sqrt{32} = 170.7056$, and is not a ground state, the biggest energy being 170.9639.

Question 9.5. Do we have $c_N/N\sqrt{N} \to 1$ with $N \to \infty$? Is the convergence monotone along some natural sequences of orders, such as the primes $p = 3(4)$?

Regarding now the thermodynamics, the situation is quite different from the one of the design arrays from Section 5. A random chain has $|\widehat{s}_k|^2$ of mean N, and by the central limit theorem the mean of $Tr|S|/N^{3/2}$ is close to $\sqrt{\pi}/2 = 0.886$, the exact value at $N = 23$ being 0.887. This is higher than the hot level $\sqrt{2/\pi} = 0.798$ of the hard matrix model. Figure 32 shows the density of states at $N = 23$, and the specific heat, computed from the densities of states, in bins of width 0.02 of the energy.

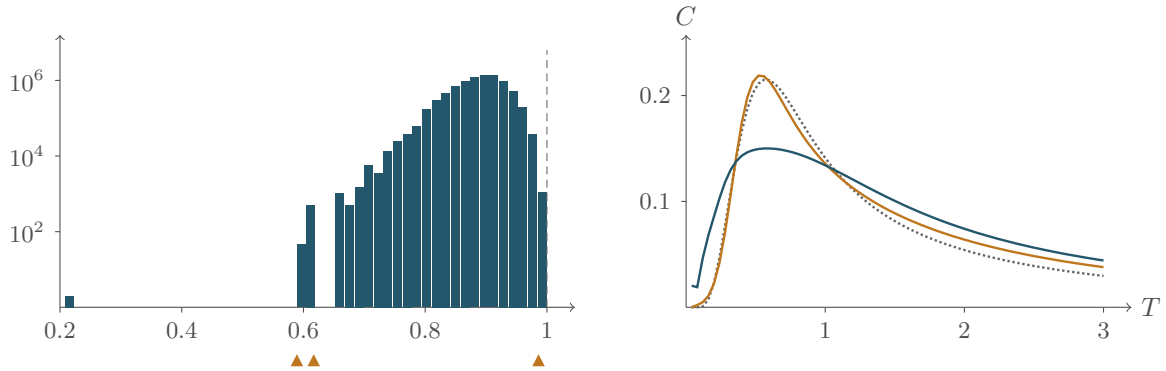

Figure 32: On the left, the number of chains of $N = 23$ spins, in 50 bins of the energy $Tr|S|$, on a logarithmic scale, against $Tr|S|/N^{3/2}$. The empty bins at left are genuine gaps between the first energy levels. The triangles mark the chain with one flipped spin, the alternating chain, and the Legendre sequence, which is the ground state. On the right, the specific heat per spin at $N = 13$ (dotted), $N = 19$ (gold) and $N = 23$ (blue), against the temperature.

The specific heat has a single broad maximum, near $T = 0.6$, of height 0.22, 0.22, 0.15 at $N = 13, 19, 23$, which does not sharpen with N in this range, so there is no sign of crystallization: the $4N$ ground states are simply the end of a smooth distribution. As for the ordered chains, these are isolated on the left, and Theorem 9.2 shows that they are nevertheless local maximizers of the 1-norm, that is, metastable states of the hard matrix model.

Let us discuss now the orders $N = 2(4)$, where the ground states of the chain are far below the bound from Theorem 8.4. Here the solution, which goes back to Ehlich [24], and which

appears as well in [6], is to use 2 circulant blocks. Given 2 sequences of signs a, b of length $N/2$, with circulant matrices A, B, consider the following sign matrix, of order N:

$$S = \begin{pmatrix} A & B \\ -B^t & A^t \end{pmatrix}$$

The energy of such a matrix can be computed as for the chains, and we have:

Proposition 9.6. *For the above matrix, built from 2 sequences a, b of length $n = N/2$:*

1. $Tr|S| = 2\sum_k \sqrt{|\widehat{a}_k|^2 + |\widehat{b}_k|^2}$.
2. *The bound $(N-2)\sqrt{N-2} + 2\sqrt{2N-2}$ from Theorem 8.4 is attained precisely when the periodic autocorrelations of a and b sum up to 2, at any nonzero shift.*

Proof. Since the circulant matrices commute, SS^t has diagonal blocks $AA^t + BB^t$, and vanishes outside these blocks. This matrix $AA^t + BB^t$ is circulant, with eigenvalues $|\widehat{a}_k|^2 + |\widehat{b}_k|^2$, which gives (1). As for (2), by the discussion following Theorem 8.4, the bound is attained precisely when the eigenvalues of SS^t are $2N-2$, with multiplicity 2, and $N-2$. In our case this means that the circulant matrix $AA^t + BB^t - (N-2)$, which is positive, with 2 on the diagonal, has rank one, so it equals $2\mathbb{I}$, the size $N/2$ being odd. Since the entries of $AA^t + BB^t$ are the sums of the autocorrelations of a and b, this gives the result. □

The program `chains.py` goes through all the pairs of sequences at $N \leq 26$, which is an easy task, there being at most 2^{26} such pairs, with the following results, where a, b is a pair of sequences maximizing the energy, and where the upper bound is the one from Theorem 8.4:

N	a	b	$Tr\|S\|$	upper bound	equality
6	+++	++-	14.3246	14.3246	yes
10	++++-	+++-+	31.1127	31.1127	yes
14	++++++-	+++-+-	51.7673	51.7673	yes
18	+++++++-	+++-++-+-	75.6619	75.6619	yes
22	++++++-+--	++++-++-+-	102.2100	102.4042	no
26	+++++++++-++-	++++-+-+-+-	131.7176	131.7176	yes
30	+-+++-+-------	+-+-+-++-++++	163.3936	163.3936	yes
38	+-+-+-++-++++++++	+-+-+++-+-+++-+++	233.2047	233.2047	yes
42	+--+++-++-+++++++++	+-+-++-+-+-+-+-+++	271.0930	271.0930	yes
46	+--+++-++-++++++++++	+-++-+-++-+-++-+-+-++	310.8366	310.8366	yes
50	+--+-+++-+-++-++++++++	+-+-++-+++-+-+-+++-++++	352.3527	352.3527	yes

At $N = 6, 10, 14$ we recover the optimal values from Theorem 8.4, the matrices being now of a simple form. As an illustration, here is the optimal matrix at $N = 10$, built from the sequences in the table, which has energy $22\sqrt{2}$, as the matrix $K_5 \otimes H_2$ from Section 7:

$$\left(\begin{array}{ccccc|ccccc} + & + & + & + & - & + & + & + & - & + \\ - & + & + & + & + & + & + & + & + & - \\ + & - & + & + & + & - & + & + & + & + \\ + & + & - & + & + & + & - & + & + & + \\ + & + & + & - & + & + & + & - & + & + \\ \hline - & - & + & - & - & + & - & + & + & + \\ - & - & - & + & - & + & + & - & + & + \\ - & - & - & - & + & + & + & + & - & + \\ + & - & - & - & - & + & + & + & + & - \\ - & + & - & - & - & - & + & + & + & + \end{array}\right)$$

The other orders are new, with respect to what we know so far. At $N = 18, 26$ the bound is attained, as expected from the determinant theory, where such matrices are well-known, the

value at $N = 18$ being the one found in [32], and at $N = 22$ our value is below the lower bound $m_{22} \geq 102.3127$ from there. The last 5 lines of the table come from a different computation: here `chains.py` looks directly for the equality case, by matching the autocorrelations of a with those of b, at the orders $N \leq 50$ where $2N-2$ is a sum of 2 squares. Summarizing, we have the following result:

Theorem 9.7. *The bound $m_N \leq (N-2)\sqrt{N-2}+2\sqrt{2N-2}$ at $N = 2(4)$ is attained by matrices made of 2 circulant blocks at any $6 \leq N \leq 50$ such that $2N-2$ is a sum of 2 squares, namely at $N = 6, 10, 14, 18, 26, 30, 38, 42, 46, 50$. In particular $m_{18} = 64 + 2\sqrt{34}$, $m_{26} = 48\sqrt{6} + 10\sqrt{2}$, $m_{30} = 56\sqrt{7} + 2\sqrt{58}$, and so on. At $N = 22$ the biggest energy of such matrices is $\simeq 102.2100$.*

Proof. This follows from Proposition 9.6, and from the above table. Observe that at $N = 22$ the bound cannot be attained, by any sign matrix, because $2N - 2 = 42$ is not a sum of 2 squares, as explained in Section 8. □

10 Complex matrices, the dual model

We discuss now the complex case, where the orthogonal group O_N is replaced by the unitary group U_N, and the sign matrices by the matrices having entries of modulus 1, which form a torus $M_N(\mathbb{T})$. The complex Hadamard matrices are the matrices $H \in M_N(\mathbb{T})$ whose rows are pairwise orthogonal, and exist at any N, the basic example being the Fourier matrix. We refer to [58] for the general theory of such matrices. As in the real case, for $U \in U_N$ we have $||U||_1 \leq N\sqrt{N}$, with equality precisely when $H = \sqrt{N}U$ is a complex Hadamard matrix. The complex almost Hadamard matrices were introduced in [4] in analogy with the real ones, by using the local maximizers of the 1-norm on U_N, with the following conjectural conclusion: any such local maximizer is a global one. This is the almost Hadamard conjecture, which is proved at $N \leq 3$, with a number of further results at $N = 4$, and with evidence at $N = 4, 5$ coming from long numerical searches. See [4], [15]. We will come back to it at the end of this section, with a computer-assisted proof for the existence of a counterexample at $N = 16$.

In order to discuss this, let us go back to the pairing from the Introduction, whose complex version is as follows, with $U \in U_N$ and $S \in M_N(\mathbb{T})$:

$$\Phi(U, S) = Re\, Tr(S^*U) = \sum_{ij} Re(\bar{S}_{ij}U_{ij})$$

We call phase matrix of a matrix U having nonzero entries the matrix $S_{ij} = U_{ij}/|U_{ij}|$, and we denote as usual by $|S| = \sqrt{S^*S}$ the modulus of a matrix, and by $Pol(S) = S|S|^{-1}$ the polar part of an invertible matrix. With these conventions, we have:

Proposition 10.1. *The functions $L(U) = ||U||_1$ on U_N and $M(S) = Tr|S|$ on $M_N(\mathbb{T})$ are the partial maxima of Φ, with respect to S and U respectively. For U with nonzero entries the first maximum is attained only at the phase matrix of U, and for S invertible the second maximum is attained only at $U = Pol(S)$. Moreover, we have $M(S) \leq N\sqrt{N}$, with equality precisely when S is a complex Hadamard matrix.*

Proof. The first assertion is clear, and the second one is the standard fact that the maximum of $Re\, Tr(S^*U)$ over the unitary group is the sum of the singular values of S, and is attained when S^*U is positive. As for the last assertion, this follows from the Cauchy-Schwarz inequality, $Tr|S| \leq \sqrt{N}\, Tr(S^*S)^{1/2} = N\sqrt{N}$, with equality when $|S| = \sqrt{N}$. □

Thus we have a dual model, with N^2 planar rotators S_{ij} and with energy $-Tr|S|$, whose ground states are the complex Hadamard matrices. In physical terms, the rotators live on the edges of the complete bipartite graph $K_{N,N}$, and the energy is invariant under the gauge

transformations $S_{ij} \to \alpha_i S_{ij} \beta_j$, with $\alpha_i, \beta_j \in \mathbb{T}$. By using these transformations we can always assume that the first row and column of S consist of 1 entries, as for the dephased complex Hadamard matrices, and we are left with $(N-1)^2$ angles. The quantities $Tr((S^*S)^p)$ are sums of Wilson loops of length $2p$, the simplest one being $Tr((S^*S)^2) \geq N^3$, which is the plaquette action, and which is minimal precisely for the complex Hadamard matrices too. Figure 33 illustrates this.

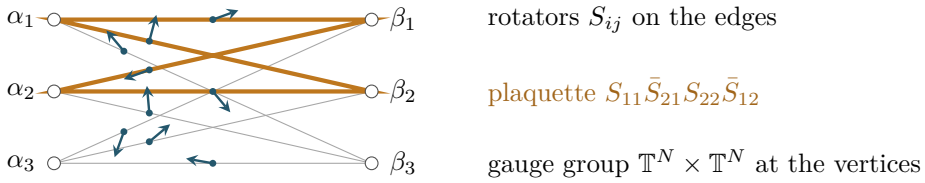

Figure 33: The dual model at $N = 3$: a planar rotator on each edge of $K_{3,3}$, and gauge transformations at the vertices. The energy is a function of the Wilson loops, such as the plaquette in gold.

Before going further, observe that the complementation formula from Theorem 7.3 holds in the complex case too, for the submatrices of the complex Hadamard matrices [60]. However, the last assertion there has no complex analogue. For the Fourier matrix $F_N = (w^{ij})$ with $w = e^{2\pi i/N}$, at $r = 1$ we obtain $\sqrt{N}\, Pol(D) = D - \mathbb{I}/(1+\sqrt{N})$, and since the correction is real, the entries of this matrix do not have the phases of the entries of D, unless these are ± 1. Thus D is not the phase matrix of its polar part, in agreement with the above conjecture, and as verified by `detours.py` at $N = 5, 7$.

In order to compare the 2 models, we need the second variation of Φ. We consider curves of type $t \to (Ue^{itB}, S_t)$, with B self-adjoint, and with $S_t = (S_{ij}e^{it\theta_{ij}})$, where $\theta \in M_N(\mathbb{R})$.

Proposition 10.2. *Let $U \in U_N$ have nonzero entries, with phase matrix S, and assume that $X = S^*U$ is self-adjoint. Then (U, S) is a critical point of Φ, and the second derivative of Φ at $t = 0$ along the above curves is the quadratic form*

$$Q(B, \theta) = -Tr(XB^2) + 2\sum_{ij} \theta_{ij} R_{ij} - \sum_{ij} \theta_{ij}^2 |U_{ij}|$$

where $R_{ij} = Re(\bar{S}_{ij}(UB)_{ij})$.

Proof. The function to be differentiated is $\sum_{ij} Re(\bar{S}_{ij}e^{-it\theta_{ij}}(Ue^{itB})_{ij})$. The first derivative at $t = 0$ is $\sum_{ij} \theta_{ij} Im(\bar{S}_{ij}U_{ij}) - Im\, Tr(XB)$, and both terms vanish, because $\bar{S}_{ij}U_{ij} = |U_{ij}|$ is real, and because X is self-adjoint. As for the second derivative, this is the sum of the following 3 terms, coming from differentiating twice $e^{-it\theta_{ij}}$, then once each factor, and then twice e^{itB}, which give the formula in the statement:

$$-\sum_{ij} \theta_{ij}^2 |U_{ij}| \quad , \quad 2\sum_{ij} \theta_{ij} Re(\bar{S}_{ij}(UB)_{ij}) \quad , \quad -Re\, Tr(S^*UB^2)$$

Thus, we are led to the conclusion in the statement. □

By maximizing over θ we obtain the Hessian of L, namely $\sum_{ij} R_{ij}^2/|U_{ij}| - Tr(XB^2)$, which is the formula from [4], [15]. The program `inertia.py` computes the inertia of this Hessian, and of the Hessian of M, computed independently, via the perturbation theory of the singular values. For all the matrices that we tried, the 2 inertias coincide, and for the real local maximizers from Section 3, regarded as unitary matrices, the results are as follows, with the last row being the number of positive eigenvalues, that is, the number of independent directions in U_N along which the 1-norm increases:

matrix	K_3	K_5	K_6	K_7	$(7,3,1)$	$(11,5,2)$	$(13,4,1)$	$(15,7,3)$
escape directions	1	5	9	14	7	35	53	35

Here K_N stands for the matrix $1-2P$ from Section 3, and the designs for their matrices U_+. In all these cases the kernel of the Hessian has dimension $2N-1$, coming from the gauge transformations. Thus the real almost Hadamard matrices coming from designs are saddles on U_N, in agreement with the results in [4], where the matrices K_N with $N \neq 4$, and those of the projective planes and of the Paley biplane, are shown not to be complex almost Hadamard.

The program also treats 2 remarkable matrices of order 4, which are as follows, with $q \in \mathbb{T}$ for the first one, and with $c = \cos(\pi/8)$, $s = \sin(\pi/8)$ for the second one:

$$F_4^q = \frac{1}{2}\begin{pmatrix} 1 & 1 & 1 & 1 \\ 1 & q & -1 & -q \\ 1 & -1 & 1 & -1 \\ 1 & -q & -1 & q \end{pmatrix} \qquad Z_4 = \frac{1}{\sqrt{2}}\begin{pmatrix} c & s & c & s \\ c & -s & -s & -c \\ s & c & -c & s \\ s & -c & -s & c \end{pmatrix}$$

The matrices F_4^q are the rescaled complex Hadamard matrices of order 4, which form a 1-parameter family, and at a generic value of q the Hessian is negative, with a kernel of dimension 8, one more than the dimension $2N-1$ coming from the gauge transformations. As for the matrix Z_4, from [15], this is a real orthogonal matrix, which is a plain local maximizer of the 1-norm on O_4, of norm $8\cos(\pi/8) = 7.391$, and which is a saddle on U_4, with 3 escape directions.

As a second experiment, the program `cooling.py` runs the alternating maximization of Φ, namely $S \to U = Pol(S) \to S$, with S being at the end the phase matrix of U, from 300 random sign matrices, and from 100 random matrices in $M_N(\mathbb{T})$, for each N. In the real case this is the polar iteration from Section 6. The results are as follows, with the mean end value of $Tr|S|/N^{3/2}$ in the real case, and with the lowest end value in the complex case, after at most 20000 steps:

N	4	5	6	7	8	9	10	11	12
real	0.933	0.948	0.944	0.944	0.943	0.942	0.942	0.941	0.939
complex	1	1	1	1	1	1	0.99999	0.99998	0.99999

The difference between the 2 cases is striking, and is best seen on individual runs. Figure 34, computed by `pictures.py`, shows 3 runs of each type at $N = 7$, on logarithmic scales.

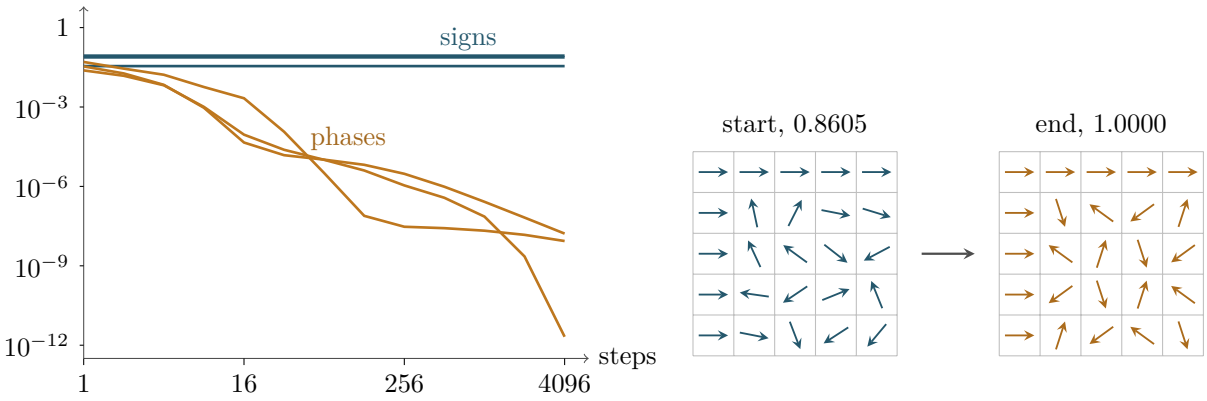

Figure 34: On the left, the distance $1-Tr|S|/N^{3/2}$ to the Hadamard bound, along the alternating maximization at $N = 7$, on logarithmic scales: from random signs, in blue, where the runs freeze after one step, and from random phases, in gold, where they converge to complex Hadamard matrices. On the right, the rotators S_{ij} at the start and at the end of such a run at $N = 5$, with the first row and column rotated to 1, and with the values of $Tr|S|/N^{3/2}$.

The same figure shows the rotators themselves, at the start and at the end of such a run, at $N = 5$. At the end all the angles are multiples of $72°$, and we have reached the Fourier matrix F_5, with its columns permuted.

Let us go back now to the circulant matrices from Section 9, in the complex case. Here the chain consists of N planar rotators $s_j \in \mathbb{T}$, and Proposition 9.1 holds, with the same proof: we have $N \leq Tr|S| = \sum_k |\widehat{s}_k| \leq N\sqrt{N}$, with equality at left for the characters of $\mathbb{Z}_N$, multiplied by scalars, and with equality at right when S is a circulant complex Hadamard matrix. The point now is that such matrices exist at any N. Indeed, the quadratic chains, given by $s_j = w^{j^2}$ with $w = e^{2\pi i/N}$ when N is odd, and by $s_j = e^{\pi i j^2/N}$ when N is even, have Fourier transforms of constant absolute value $\sqrt{N}$, by the Gauss sum computation. Thus the chain of rotators has perfect crystals at any N, in contrast with the spin chain. The perfect chains correspond to the cyclic N-roots, studied by Björck and Haagerup [11], [28].

The question is whether a cooled chain always reaches a perfect crystal, which would be a circulant version of the almost Hadamard conjecture. The program `chains.py` runs the alternating maximization, which for the chains is the map taking s to the phases of the inverse Fourier transform of the phases of $\widehat{s}$, from random chains. Procedures of this type are used for finding biunimodular vectors, see [27]. At $3 \leq N \leq 10$ all the 400 runs end at perfect chains, up to 10^{-9} in $Tr|S|/N^{3/2}$. At bigger orders the program finds other limits, and iterates until the derivatives of the energy are below 10^{-9}, with the following results, for 1500 runs at each $N \leq 18$:

N	levels	classes	ratios	escape directions	no escape
12	1	1	0.9963575	12	0
14	1	1	0.9999246	4	0
15	6	8	0.9970394 – 0.9999700	6 – 16	0
16	15	21	0.9968086 – 0.9999908	0 – 19	1
17	7	9	0.9972459 – 0.9999997	0 – 20	2
18	67	118	0.9977215 – 0.9999998	0 – 26	6

Here we count the chains found which are local maximizers of the energy on the torus $\mathbb{T}^N$, the Hessian being negative, apart from the direction of the global phase, and which are not perfect, with their ratios $Tr|S|/N^{3/2}$. The levels are the values of the energy, and the classes are spectral: they put together the chains having the same numbers $|\widehat{s}_k|$, up to their order. This multiset is invariant under the symmetries of the energy, namely the global phases, the shifts, the multiplications by characters, the conjugation, and the maps $j \to aj$ with a invertible modulo N, so chains in different classes are not equivalent, while chains in the same class might not be equivalent either. A level can contain several classes, as for instance that of s and that of the chain formed by the phases of $\widehat{s}$, which is a critical point having the same energy. All the classes are recorded in the output of the program. Our runs found no such chains at $N = 11, 13$. Thus the chain of rotators has metastable states, the first ones found being at $N = 12$.

The last 2 columns of the table concern the matrix $U = Pol(S)$, which is a critical point of the 1-norm on U_N, the matrix S being its phase matrix. As in the program `inertia.py`, we compute the Hessian of the 1-norm on the full unitary group, which has $2N - 1$ zero directions, coming from the gauge group, and we count its positive eigenvalues, which are the escape directions. At $N \leq 15$ there are always such directions, so these matrices are saddles of the 1-norm, in agreement with the almost Hadamard conjecture. At $N = 16, 17, 18$, however, the program finds classes having no escape direction at all. The one at $N = 16$, which was reached by 24 runs, is as follows, with $s_j = e^{i\theta_j}$, with the normalization $\theta_0 = 0$, coming from the global phase, and with the absolute values $r_j = |U_{0j}|$ of the entries of $U = Pol(S)$, so that $U_{ij} = r_{j-i}e^{i\theta_{j-i}}$, with the indices taken modulo 16:

j	θ_j	r_j	j	θ_j	r_j
0	0.000000000000	0.249112	8	5.389932745529	0.250877
1	6.240306560271	0.250021	9	3.194231298411	0.249227
2	2.868822117139	0.249272	10	4.386957422709	0.249769
3	2.389181994234	0.249706	11	5.151415954210	0.248750
4	0.732512772865	0.249690	12	2.131057143608	0.251005
5	4.623096445795	0.250876	13	5.024113455286	0.252894
6	4.554149641546	0.249059	14	1.946536126847	0.251075
7	5.351695847842	0.248717	15	5.434630538975	0.249914

For this chain $Tr|S| = 63.9994133344$, which is below $N\sqrt{N} = 64$, the numbers $|\widehat{s}_k|$ being between 3.9753 and 4.0346, and the entries of $U = Pol(S)$ having absolute values between 0.2487 and 0.2529. The program `chains.py` computes the Hessian of the 1-norm at U, on U_{16}, in 3 different ways: with the 2 formulae from `inertia.py`, and by finite differences, over an orthonormal basis of the Lie algebra. In all 3 cases there are 31 zero eigenvalues, coming from the gauge group, and 225 negative ones, the largest one being -0.0035. Also, the alternating maximization on U_{16}, started at 6 points at distance 0.02 from U, comes back to the same 1-norm, up to 10^{-13}. Figure 35 shows this chain, next to the quadratic one.

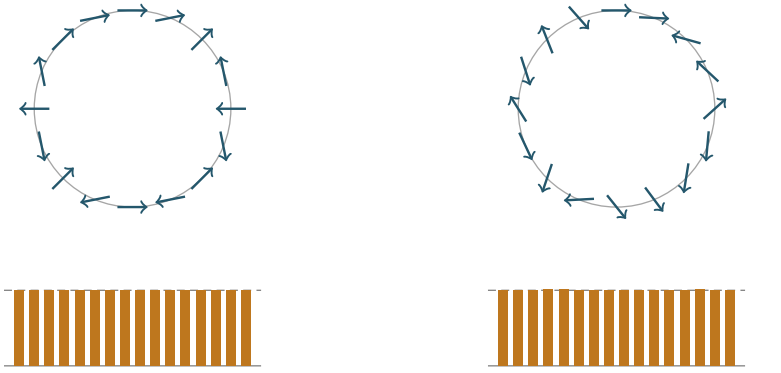

quadratic chain, ratio 1 the chain s, ratio 0.99999083

Figure 35: 2 chains of $N = 16$ planar rotators, and below them the absolute values of their Fourier transforms, the dashed line being the flat level $\sqrt{N} = 4$. The quadratic chain is a perfect crystal. The chain on the right is the one from the above table: its spectrum is flat only up to 1%, but the chain cannot be improved by small moves, even when leaving the circulant matrices.

The same checks were done for the 2 classes with no escape direction found at $N = 17$, and for the 6 classes found at $N = 18$. The 9 classes are as follows, with the numbers of runs which reached them, and with the largest eigenvalue of the Hessian, transversally to the gauge group:

N	$Tr\|S\|$	$N\sqrt{N} - Tr\|S\|$	runs	largest eigenvalue
16	63.99941333	0.00058667	24	−0.003479
17	70.09277589	0.00001975	8	−0.000059
17	70.09277589	0.00001975	9	−0.002657
18	76.36588901	0.00164335	2	−0.009803
18	76.36676265	0.00076972	8	−0.001830
18	76.36676265	0.00076972	6	−0.000486
18	76.36744750	0.00008486	9	−0.000904
18	76.36750802	0.00002435	1	−0.001338
18	76.36750867	0.00002370	4	−0.004169

These floating point computations are not a proof, but since the Hessians are nondegenerate, transversally to the gauge directions, a computer-assisted proof is possible. It is based on the following principle, with h being the Hessian from the comments after Proposition 10.2:

Proposition 10.3. *Let $U \in U_N$ have nonzero entries, with phase matrix S, such that $X = S^*U$ is positive, and let K be the span of the matrices E_{jj} and $U^*E_{jj}U$. If $h(B) \leq -c||B||_2^2$ for any self-adjoint matrix $B \perp K$, with $c > 0$, then U is a local maximizer of the 1-norm on U_N.*

Proof. Since X is self-adjoint, U is a critical point of L. The 1-norm is invariant under the gauge group $\mathbb{T}^N \times \mathbb{T}^N$, acting by $U \to DUD'$ with D, D' diagonal, and in the parametrization Ue^{iB}, with B self-adjoint, the tangent space of the orbit of U is K. The map $(g, B) \to g \cdot Ue^{iB}$, from the gauge group times $K^\perp$, has a surjective differential at $(1, 0)$, so its image contains a neighborhood of U. Since $L(g \cdot Ue^{iB}) = L(Ue^{iB}) \leq L(U) - c||B||_2^2/2 + o(||B||_2^2)$, this gives the result. □

Thus, in order to have a counterexample, we need an exact critical point, which is not Hadamard, and the above negativity of the Hessian, and all this can be checked on a small box around a numerical solution. The program `certify.py` redoes everything in interval arithmetic, with 60 digits and outward rounding, and with the Krawczyk operator [40], [47] for the critical points, starting from the chains found by `chains.py`, with their angles rounded to 12 digits, which are recorded in `certify.json`, and which at $N = 16$ are those in the above table. We have:

Theorem 10.4. *The almost Hadamard conjecture fails at $N = 16, 17, 18$. More precisely, for each of the 9 chains recorded in `certify.json`, there is an exact chain $s \in \mathbb{T}^N$, with $\theta_0 = 0$ and with the other angles within 10^{-11} of the recorded ones, whose circulant matrix S has the following properties:*

1. *S is the phase matrix of $U = Pol(S)$, which is a local maximizer of the 1-norm on U_N.*
2. *$||U||_1 = Tr|S| < N\sqrt{N}$, so that $\sqrt{N}U$ is not a complex Hadamard matrix.*

Proof. We use Proposition 10.3, whose assumptions are checked by `certify.py`. It works with intervals of decimal numbers with 60 digits, rounded outwards, so that each operation returns an interval containing its exact result, and any formula evaluated in this way over a box returns an interval containing the exact values of this formula on the whole box. The other ingredients are enclosures for π, by the formula of Machin, for cos and sin, by Taylor series with the Lagrange remainder, and for the square roots, checked by squaring back. All the conclusions below hold on whole boxes, and so apply to the exact chain, which is not explicitly known:

(1) Let $\theta_0 = 0$, and $F_j = Im(\bar{s}_j\gamma_j)$, with γ as in Proposition 9.1, which is $1/N$ times the derivative of the energy with respect to θ_j. Consider the map $T(\theta) = \theta - YF(\theta)$, with Y an approximate inverse of the Jacobian of $(F_1, \ldots, F_{N-1})$, which can be any matrix. On the box of radius 10^{-11} around the recorded angles $\theta_1, \ldots, \theta_{N-1}$ the program encloses T, by using the mean value theorem, and shows that T maps the box into itself, and that the enclosure of $1 - YF'$ over the box has norm less than 1. Thus T is a contraction of the box, and Y is invertible, so the equations $F_1 = \ldots = F_{N-1} = 0$ have a unique solution in this box. Since $\sum_j F_j = Im \sum_k |\widehat{s}_k|/N = 0$, we have $F_0 = 0$ too. The same test on the box of radius 10^{-30} around a refined center, lying in the first box, locates this solution within 10^{-30}, and the next steps use this smaller box.

(2) For this exact chain the numbers $\bar{s}_j\gamma_j$, which are real, are enclosed in intervals of positive numbers. Thus S is the phase matrix of $U = Pol(S)$, which is the circulant matrix of γ, and $X = S^*U = |S|$ is positive. Also, the energy $Tr|S| = \sum_k |\widehat{s}_k|$ is enclosed in an interval lying below $N\sqrt{N}$.

(3) The program computes the Hessian h in the orthonormal basis E_{jj}, $(E_{jk}+E_{kj})/\sqrt{2}$, $i(E_{jk}-E_{kj})/\sqrt{2}$ of the self-adjoint matrices, and the coordinates of the vectors k_p spanning K, and an interval Cholesky decomposition shows that the matrix $\sum_p k_p k_p^t - h - c$ is positive definite, with $c = 0.003$ at $N = 16$, and with c between $3 \cdot 10^{-5}$ and 0.005 in the other cases. Indeed, when the Cholesky decomposition of an interval matrix can be carried out with positive pivots, all the symmetric matrices with entries in these intervals are positive definite, because their Cholesky decompositions stay inside the intervals. Thus $h(B) \leq -c||B||_2^2$ for $B \perp K$, as desired.

Finally, the data used by the program, namely the matrix Y and the refined centers, are proposed by floating point computations, and a wrong proposal could only make a test fail. □

At $N = 16$ the exact chain is the one in the above table, up to 10^{-11}, and $||U||_1 = 63.9994133344048634413828 2\ldots$ The same program with more digits would locate the exact chains to any desired precision, their Jacobians being invertible. The computation takes about 3 minutes, with output in `certify.log`, and it stops with an error if a check fails, or if a chain is missing. As a test, at $N = 16$ the program refuses the margin $c = 0.0036$, above the true value 0.00348, and the chain formed by the phases of $\widehat{s}$, which has 2 escape directions. For the 9 chains, the certified values are as follows, with the deficit $N\sqrt{N} - Tr|S|$, the margin c, the smallest pivot of the interval Cholesky decomposition, and the radius of the image of the box of radius 10^{-30} under T:

N	$N\sqrt{N} - Tr\|S\|$	c	smallest pivot	image radius
16	0.00058666559513...	0.003	0.069398	$9.9 \cdot 10^{-41}$
17	0.00001974749006...	0.00003	0.002095	$1.1 \cdot 10^{-39}$
17	0.00001974749006...	0.001	0.061633	$7.9 \cdot 10^{-40}$
18	0.00164335469779...	0.005	0.210347	$7.6 \cdot 10^{-41}$
18	0.00076971891625...	0.0009	0.073657	$9.9 \cdot 10^{-41}$
18	0.00076971891625...	0.0002	0.020058	$1.3 \cdot 10^{-40}$
18	0.00008486347250...	0.0005	0.023564	$1.4 \cdot 10^{-40}$
18	0.00002435010528...	0.0007	0.031938	$3.1 \cdot 10^{-40}$
18	0.00002369603932...	0.002	0.088390	$4.7 \cdot 10^{-40}$

The exact angles are algebraic numbers. Indeed, with the numbers $\sigma_k = |\widehat{s}_k|$ added as new unknowns, subject to $\sigma_k^2 = |\widehat{s}_k|^2$ and $\sigma_k > 0$, the critical point equations become polynomial, with algebraic coefficients, and by (1) our solutions are isolated, so their coordinates are algebraic. We know however nothing about their degrees, and the counterexamples are not explicit.

An independent verification of the 9 cases was done by GPT, with a different program, using exact integer arithmetic instead of decimals, the dual model $M(S) = Tr|S|$ on the torus of phase matrices, with the first row and column fixed, instead of the unitary group, and a different formula for the Hessian. The passage to U_N is then via $L(W) \leq M(S') \leq M(S) = L(U)$, for W close to U, with S' being the phase matrix of W. All 9 cases pass this second test too, and at $N = 16$ the second program locates the exact chain within $2 \cdot 10^{-38}$, with the same deficit as above.

Question 10.5. What is the smallest N where the 1-norm on U_N has a local maximizer which is not a rescaled complex Hadamard matrix? Is it $N = 16$?

At $N \leq 15$ our runs found no circulant counterexamples, the metastable chains found at $N = 12, 14, 15$ having escape directions on the unitary group. Observe also that the above counterexamples would have been hard to find by a search on the full unitary group, as in [15], their 1-norms being within 0.1% of the Hadamard bound.

Summarizing, in the real case the cooling ends in the glassy states from Section 6, while in the complex case all the 900 runs on the unitary group converge to complex Hadamard matrices,

up to 10^{-6} in $Tr|S|/N^{3/2}$ for $N \leq 9$, and with a number of runs still slowly increasing when stopped, for $N \geq 10$, in agreement with the numerical evidence from [15], obtained at $N = 4, 5$ with far more starting points. Our general results are as follows:

Theorem 10.6. *Let $L(U) = ||U||_1$ on U_N, and $M(S) = Tr|S|$ on $M_N(\mathbb{T})$.*

1. *If U is a local maximizer of L then its phase matrix S is an invertible local maximizer of M, with $Pol(S) = U$. Conversely, if S is an invertible local maximizer of M, whose polar part U has nonzero entries, then U is a local maximizer of L.*

2. *At a critical point U of L with nonzero entries, such that $S^*U > 0$, the Hessians of L at U and of M at S have the same inertia.*

3. *At a given order N, all the local maximizers of L are rescaled complex Hadamard matrices if and only if all the invertible local maximizers of M, whose polar parts have nonzero entries, are complex Hadamard matrices.*

Proof. (1) Let U be a local maximizer of L. Then U has nonzero entries, by [4], and with $X = S^*U$ we have $X \geq 1/N$, by [15]. Thus $S = UX$ is invertible, with $|S| = X$ and $Pol(S) = U$. Now since the polar part is continuous on the invertible matrices, for S' close to S the matrix $U' = Pol(S')$ is close to U, and by using Proposition 10.1 we obtain:

$$M(S') = \Phi(U', S') \leq L(U') \leq L(U) = \Phi(U, S) = M(S)$$

Conversely, let S be an invertible local maximizer of M, with $U = Pol(S)$ having nonzero entries. For S' close to S we have $\Phi(U, S') \leq M(S') \leq M(S) = \Phi(U, S)$, so S is a local maximizer of the function $S' \to \Phi(U, S') = \sum_{ij} Re(\bar{S}'_{ij} U_{ij})$, and this shows that S is the phase matrix of U. Now for U' close to U the phase matrix S' of U' is close to S, and so:

$$L(U') = \Phi(U', S') \leq M(S') \leq M(S) = \Phi(U, S) = L(U)$$

(2) We use Proposition 10.2. The restrictions of the quadratic form Q to the variables B and θ are both negative definite, because $Tr(XB^2) = Tr(BXB) > 0$ for $B \neq 0$, and because the entries of U are nonzero. Thus the 2 partial maxima of Φ are nondegenerate, and their Hessians are the corresponding Schur complements of Q. By the Haynsworth inertia additivity formula [29], the inertia of Q is the sum of the inertia of each of these Schur complements and of that of a negative definite form in N^2 variables, and this gives the result.

(3) If all the local maximizers of L are rescaled complex Hadamard matrices, and S is as in the statement, then $U = Pol(S)$ is a local maximizer of L, by (1), so $\sqrt{N}U$ is a complex Hadamard matrix, and so is S, because S is the phase matrix of U. Conversely, if the statement about M holds and U is a local maximizer of L, then its phase matrix S is a complex Hadamard matrix, by (1), and so $U = Pol(S) = S/\sqrt{N}$ is a rescaled complex Hadamard matrix. □

As a first comment, at a complex Hadamard matrix the kernel of the Hessian of M has dimension $2N - 1 + d$, where d is the defect of Tadej and Zyczkowski [59], as a consequence of (2) and of the results in [4]. In general, the interest in the dual formulation comes from the fact that the unitarity constraint has disappeared, the function M being simply the restriction of a norm to a product of circles. Models of this type, with rotators or with spins on higher spheres, appear in the theory of the Kuramoto model, where the absence of spurious local maxima is known in a number of situations, and is proved by plugging well-chosen tangent vectors into the Hessian, see [19], [43]. This is the method from [4], and the hope is that the dual form, with its free angles, could make the choice of the tangent vectors easier. Observe also that in the dual picture the difference between the real and the complex case becomes transparent: the real model has Ising spins, and no infinitesimal moves at all, while the complex model has rotators, which can go around the walls where an entry of U vanishes.

References

[1] S. Ball, A. Blokhuis and F. Mazzocca, Maximal arcs in Desarguesian planes of odd order do not exist, *Combinatorica* **17** (1997), 31–41.

[2] T. Banica, B. Collins and J.M. Schlenker, On orthogonal matrices maximizing the 1-norm, *Indiana Univ. Math. J.* **59** (2010), 839–856.

[3] T. Banica and I. Nechita, Almost Hadamard matrices: the case of arbitrary exponents, *Discrete Appl. Math.* **161** (2013), 2367–2379.

[4] T. Banica and I. Nechita, Almost Hadamard matrices with complex entries, *Adv. Oper. Theory* **3** (2018), 137–177.

[5] T. Banica, I. Nechita and J.M. Schlenker, Submatrices of Hadamard matrices: complementation results, *Electron. J. Linear Algebra* **27** (2014), 197–212.

[6] T. Banica, I. Nechita and K. Zyczkowski, Almost Hadamard matrices: general theory and examples, *Open Syst. Inf. Dyn.* **19** (2012), 1–26.

[7] G. Barba, Intorno al teorema di Hadamard sui determinanti a valore massimo, *Giorn. Mat. Battaglini* **71** (1933), 70–86.

[8] J. Bernal and J. Lawrence, Characterization and computation of matrices of maximal trace over rotations, *J. Geom. Symmetry Phys.* **53** (2019), 21–53.

[9] J. Bernasconi, Low autocorrelation binary sequences: statistical mechanics and configuration space analysis, *J. Physique* **48** (1987), 559–567.

[10] R. Bhatia, Matrix analysis, Springer (1997).

[11] G. Björck, Functions of modulus 1 on $\mathbb{Z}_n$ whose Fourier transforms have constant modulus, and cyclic n-roots, in "Recent advances in Fourier analysis and its applications", Kluwer (1990), 131–140.

[12] P. Browne, R. Egan, F. Hegarty and P. Ó Catháin, A survey of the Hadamard maximal determinant problem, *Electron. J. Combin.* **28** (2021), 1–35.

[13] R. Calderbank and W.M. Kantor, The geometry of two-weight codes, *Bull. London Math. Soc.* **18** (1986), 97–122.

[14] P. Chandra, L.B. Ioffe and D. Sherrington, Possible glassiness in a periodic long-range Josephson array, *Phys. Rev. Lett.* **75** (1995), 713–716.

[15] Chat, Grok and Teo, Numerical evidence for the almost Hadamard conjecture, zenodo:24357392 (2026).

[16] Chat, Opus and Teo, Planar rotators with Hadamard couplings, zenodo:24408089 (2026).

[17] C.S. Cheng, Optimality of some weighing and 2^n fractional factorial designs, *Ann. Statist.* **8** (1980), 436–446.

[18] C.J. Colbourn and J.H. Dinitz, Handbook of combinatorial designs, CRC Press (2007).

[19] C. Criscitiello, Q. Rebjock, A.D. McRae and N. Boumal, Synchronization on circles and spheres with nonlinear interactions, arXiv:2405.18273 (2024).

[20] L.F. Cugliandolo, J. Kurchan, G. Parisi and F. Ritort, Matrix models as solvable glass models, *Phys. Rev. Lett.* **74** (1995), 1012–1015.

[21] B. Derrida, Random-energy model: an exactly solvable model of disordered systems, *Phys. Rev. B* **24** (1981), 2613–2626.

[22] I. Dolgachev, Kummer surfaces: 200 years of study, *Notices Amer. Math. Soc.* **67** (2020), 1527–1533.

[23] J. Dong, V. Elser, G. Gyawali, K.Y. Jee, J. Kent-Dobias, A. Mandaiya, M. Renz and Y. Su, Glass phenomenology in the hard matrix model, *J. Stat. Mech. Theory Exp.* (2021).

[24] H. Ehlich, Determinantenabschätzungen für binäre Matrizen, *Math. Z.* **83** (1964), 123–132.

[25] E.E. Fenimore and T.M. Cannon, Coded aperture imaging with uniformly redundant arrays, *Appl. Opt.* **17** (1978), 337–347.

[26] P.C. Fishburn and N.J.A. Sloane, The solution to Berlekamp's switching game, *Discrete Math.* **74** (1989), 263–290.

[27] H. Führ and Z. Rzeszotnik, On biunimodular vectors for unitary matrices, *Linear Algebra Appl.* **484** (2015), 86–129.

[28] U. Haagerup, Cyclic p-roots of prime lengths p and related complex Hadamard matrices, arXiv:0803.2629 (2008).

[29] E.V. Haynsworth, Determination of the inertia of a partitioned Hermitian matrix, *Linear Algebra Appl.* **1** (1968), 73–81.

[30] P.J. Heawood, Map-colour theorem, *Quart. J. Pure Appl. Math.* **24** (1890), 332–338.

[31] J.W.P. Hirschfeld, Projective geometries over finite fields, Oxford Univ. Press (1998).

[32] J. Holbrook, N. Johnston and J.P. Schoch, Real Schur norms and Hadamard matrices, *Linear Multilinear Algebra* **72** (2024), 1967–1984.

[33] R.W.H.T. Hudson, Kummer's quartic surface, Cambridge Univ. Press (1905).

[34] D.R. Hughes and F.C. Piper, Design theory, Cambridge Univ. Press (1985).

[35] M. Idel and M.M. Wolf, Sinkhorn normal form for unitary matrices, *Linear Algebra Appl.* **471** (2015), 76–84.

[36] M. Jacroux, C.S. Wong and J.C. Masaro, On the optimality of chemical balance weighing designs, *J. Statist. Plann. Inference* **8** (1983), 231–240.

[37] S. Kirkpatrick, C.D. Gelatt and M.P. Vecchi, Optimization by simulated annealing, *Science* **220** (1983), 671–680.

[38] J.H. Koolen and V. Moulton, Maximal energy graphs, *Adv. Appl. Math.* **26** (2001), 47–52.

[39] C. Koukouvinos, M. Mitrouli and J. Seberry, An algorithm to find formulae and values of minors for Hadamard matrices, *Linear Algebra Appl.* **330** (2001), 129–147.

[40] R. Krawczyk, Newton-Algorithmen zur Bestimmung von Nullstellen mit Fehlerschranken, *Computing* **4** (1969), 187–201.

[41] E. Marinari, G. Parisi and F. Ritort, Replica field theory for deterministic models: binary sequences with low autocorrelation, *J. Phys. A* **27** (1994), 7615–7646.

[42] E. Marinari, G. Parisi and F. Ritort, Replica field theory for deterministic models II: a non-random spin glass with glassy behaviour, *J. Phys. A* **27** (1994), 7647–7668.

[43] J. Markdahl, J. Thunberg and J. Gonçalves, Almost global consensus on the n-sphere, *IEEE Trans. Automat. Control* **63** (2018), 1664–1675.

[44] M. Mézard, G. Parisi and M.A. Virasoro, Spin glass theory and beyond, World Scientific (1987).

[45] M.T. Mohan, On some p-almost Hadamard matrices, *Oper. Matrices* **13** (2019), 253–281.

[46] M.T. Mohan, p-almost Hadamard matrices and λ-planes, *J. Algebraic Combin.* **55** (2022), 89–108.

[47] R.E. Moore, A test for existence of solutions to nonlinear systems, *SIAM J. Numer. Anal.* **14** (1977), 611–615.

[48] V. Nikiforov, The energy of graphs and matrices, *J. Math. Anal. Appl.* **326** (2007), 1472–1475.

[49] Opus and Teo, Ising spins with Hadamard couplings, zenodo:24546490 (2026).

[50] R.E.A.C. Paley, On orthogonal matrices, *J. Math. Phys.* **12** (1933), 311–320.

[51] G. Parisi and M. Potters, Mean-field equations for spin models with orthogonal interaction matrices, *J. Phys. A* **28** (1995), 5267–5285.

[52] B. Polster, A geometrical picture book, Springer (1998).

[53] H.J. Ryser, Combinatorial mathematics, Math. Assoc. America (1963).

[54] J. Seberry and M. Mitrouli, Some remarks on Hadamard matrices, *Cryptogr. Commun.* **2** (2010), 293–306.

[55] J. Seberry, T. Xia, C. Koukouvinos and M. Mitrouli, The maximal determinant and subdeterminants of ±1 matrices, *Linear Algebra Appl.* **373** (2003), 297–310.

[56] D.R. Stinson, Combinatorial designs: constructions and analysis, Springer (2004).

[57] F. Szöllősi, Exotic complex Hadamard matrices and their equivalence, *Cryptogr. Commun.* **2** (2010), 187–198.

[58] W. Tadej and K. Zyczkowski, A concise guide to complex Hadamard matrices, *Open Syst. Inf. Dyn.* **13** (2006), 133–177.

[59] W. Tadej and K. Zyczkowski, Defect of a unitary matrix, *Linear Algebra Appl.* **429** (2008), 447–481.

[60] Teo B and Chat GPT, On Fourier and Hadamard matrices of prime order, zenodo:24061004 (2026).

[61] M. Wojtas, On Hadamard's inequality for the determinants of order non-divisible by 4, *Colloq. Math.* **12** (1964), 73–83.